

UNIVERSITÄTSKLINIKUM HAMBURG-EPPENDORF

Zentrum für Molekulare Neurobiologie Hamburg (ZMNH),
Institut für Entwicklungsneurophysiologie

Centrosome-dependent microtubule stabilization and somatic F-actin translocation into neurites affect neuronal polarization

Dissertation

zur Erlangung des Doktorgrades der Naturwissenschaften

an der Fakultät für Mathematik, Informatik, und Naturwissenschaften
Fachbereich Chemie der Universität Hamburg

von:

Hong Shuai
Beijing, China

Hamburg 2023

**Disputation von der
Fachbereich Chemie der Universität Hamburg am: 15th Dec.2023**

**Veröffentlicht mit Genehmigung der
Fachbereich Chemie der Universität Hamburg**

Evaluators der Dissertation:

Prof. Dr. rer. nat. Hartmut Schlüter

Dr. Froylan Calderón de Anda

The experimental part of this thesis was mainly carried out from October 2020 to October 2023 under the supervision of Dr. Froylan Calderón de Anda in the Institut für Entwicklungsneurophysiologie, Zentrum für Molekulare Neurobiologie Hamburg (ZMNH), Universitätsklinikum Hamburg-Eppendorf.

Contents

ZUSAMMENFASSUNG	1
ABSTRACT	3
1. INTRODUCTION	5
1.1 NEURONAL POLARITY	5
1.2 NEURONAL POLARIZATION PROCESS	7
1.2.1 Neuronal polarization in cultured hippocampal neurons.....	7
1.2.2 Neuronal polarization in vivo.....	9
1.3 POLARIZATION REGULATION AND THE NEURONAL CYTOSKELETON.....	11
1.3.1 Molecular regulators involved in neuronal polarization.....	12
1.3.2 The role of cytoskeleton in neuronal polarization	19
1.4 CENTROSOME BEHAVIOUR DURING NEURONAL POLARIZATION	26
1.5 OBJECTIVES OF THIS THESIS.....	28
2. RESULTS	30
2.1 CENTROSOME-DEPENDENT MICROTUBULE STABILIZATION SETS THE CONDITIONS FOR AXON FORMATION	30
2.1.1 Radial organization of acetylated microtubules in early developing neurons.....	30
2.1.2 An increase of somatic microtubule stability precedes axon formation.....	34
2.1.3 The centriolar protein Cep120 modulates MTs stability determining axon formation	38
2.2 SOMATIC F-ACTIN TRANSLOCATION ACTS AS AN INHIBITOR FOR NEURITE GROWTH.....	43
2.2.1 Somatic F-actin translocates into neurites to restrict cellular growth	43
2.2.2 Myosin II motors mediate somatic F-actin translocation into neurites.....	48
2.3 ACTIN PHOSPHORYLATION AT TYROSINE-53 IN NEURITES PROMOTES NEURITE ELONGATION .	54
2.3.1 Actin phosphorylation at tyrosine-53 in neurite shafts counteracts somatic F-actin translocation.....	54
2.3.2 Phosphorylation-induced actin instability in the neurite shaft promotes axon formation	58
2.3.3 Microtubule acetylation favours actin phosphorylation at tyrosine-53 in neurites to facilitate neuronal polarization	62
3. DISCUSSION	69
3.1 THE CENTROSOME ORGANIZES MT STABILIZATION FOR AXON SPECIFICATION.....	70
3.1.1 Axon-related radially arranged acetylated MTs invade neurites	70
3.1.2 Regulation of somatic MT stabilization promotes the formation of axons	71
3.1.3 The centrosome directs microtubule stability to initiate axon outgrowth	73
3.1.4 Somatic microtubule dynamics versus PTMs.....	75
3.2 ACTIN-Y53 PHOSPHORYLATION REGULATES SOMATIC F-ACTIN TRANSLOCATION TO PROMOTE NEURONAL POLARIZATION	77
3.2.1 Myosin II-mediated somatic F-actin translocation suppresses neurite growth.....	77

3.2.2 Actin-Y53 phosphorylation modulates somatic F-actin delivery	79
3.2.3 Actin-Y53 phosphorylation favours axon/neurite elongation	81
3.3 INTERPLAY OF MICROTUBULE ACETYLATION AND ACTIN-Y53 PHOSPHORYLATION PROMOTES NEURONAL POLARIZATION	83
4. OUTLOOK.....	84
5. MATERIAL AND METHOD.....	86
5.1 MATERIAL.....	86
5.1.1 Animal	86
5.1.2 Cell lines	86
5.1.3 Recombinant DNAs	86
5.1.4 Medium and reagents for primary cell culture	87
5.1.5 Antibodies	87
5.1.6 Other Dyes.....	89
5.1.7 Chemicals	89
5.1.8 Commercial Kits.....	89
5.1.9 Enzymes and DNA markers	90
5.1.10 Main equipments.....	90
5.2. METHOD.....	90
5.2.1 RNA interference and fluorescent protein constructs.....	90
5.2.2 Recombinant DNAs preparation	91
5.2.3 In utero electroporation (IUE)	92
5.2.4 Primary cell culture	93
5.2.5 Pharmacological treatment.....	95
5.2.6 Photoactivation experiments.....	95
5.2.7 Mouse cortical slices.....	97
5.2.8 Immunofluorescence.....	98
5.2.9 Western blotting.....	98
5.2.10 Image acquisition	99
5.2.11 Image analysis	101
5.2.12 Quantification and statistical analysis	102
5.2.13 Image processing.....	102
6. REFERENCES	102
7. APPENDIX	119
7.1 LIST OF ABBREVIATION.....	119
7.2 LIST OF HAZARDOUS SUBSTANCES	122
7.3 LIST OF PUBLICATIONS.....	123
ACKNOWLEDGEMENT	124
DECLARATION ON OATH.....	125

Zusammenfassung

Neuronen durchlaufen einen komplizierten Prozess, um ein Axon und mehrere Dendriten zu bilden, die den Informationsprozess ermöglichen. Dieser zelluläre Prozess ist stark stereotyp, wobei einer der Neuriten austritt und zum Axon wird und sich die weiteren Neuriten nacheinander zu Dendriten entwickelt. Die Bildung des Axons zeichnet sich durch einen dynamischen Wachstumskegel und stabilere Mikrotubuli aus. Kürzlich haben wir festgestellt, dass somatisches F-Aktin in die Zellperipherie transportiert wird, um das Verhalten der Wachstumskegel zu beeinflussen.

Meine Studie zeigt, dass die Zentrosom-abhängige Mikrotubuli-Stabilisierung die Bedingungen für die Axonbildung schafft. Insbesondere konnte ich durch Immunfärbung und Western-Blot-Analyse feststellen, dass acetylierte Mikrotubuli, die ursprünglich in der Nähe des Zentrosoms organisiert waren, sich radial ausbreiten, wenn der unpolarisierte Zustand aufgehoben wird, und sich schließlich in einem bestimmten Neuriten anreichern, dem mutmaßlichen Axon. Darüber hinaus habe ich beobachtet, dass Cep120, ein zentriolares Protein, den Grad der Mikrotubuli-Acetylierung moduliert, um folglich die Axonbildung über die Regulierung der Cep120-Expression zu steuern. Andererseits konnte ich durch Photoaktivierungsanalyse feststellen, dass somatisches F-Aktin bevorzugt in die kürzeren Neuriten verlagert wird, um deren Wachstum während der Axonbildung zu unterdrücken. Dementsprechend wird während des Dendritenwachstums die somatische F-Actin-Translokation aus allen Neuriten drastisch verringert, was darauf hindeutet, dass der somatische F-Actin-Fluss in wachsende Neuriten ein hemmendes Signal für das Zellwachstum ist. Mechanistisch konnte ich entdecken, dass Myosin-II-Motoren diese radiale somatische F-Aktin-Translokation vermitteln. Darüber hinaus deuten meine Daten darauf hin, dass die Aktinphosphorylierung an Tyrosin-53 in den Neuritenschäften diese

somatische F-Aktin-Translokation in Neuriten ausschließt/minimiert und dadurch das Neuritenwachstum erleichtert. Darüber hinaus zeigen meine Ergebnisse, dass die Akkumulation der Kinesin-1-Motordomäne, die der früheste Marker der axonalen Identität ist, selektiv im Neurit mit stärker phosphoryliertem Aktin erfolgt. Wichtig ist, dass die Mikrotubuli-Acetylierung und Aktin-Phosphorylierung an Tyrosin-53 im längsten Neurit, der als Axon wächst, gemeinsam angereichert sind. Die pharmakologische Verstärkung der Mikrotubuli-Acetylierung fördert die Aktinphosphorylierung, um die Etablierung der Polarität zu regulieren.

Meine Daten liefern mechanistische Einblicke in die Rolle des Zentrosoms, das die Stabilisierung der Mikrotubuli bei der Axonbildung organisiert. Darüber hinaus zeige ich einen zellulären Mechanismus, der aus der Translokation von somatischem F-Aktin in Neuriten besteht und das Neuritenwachstum hemmt. Schließlich stelle ich fest, dass dieser somatischen F-Aktin-Translokation in Neuriten durch Aktin-Phosphorylierung an Tyrosin-53 im Neuritenschaft entgegengewirkt wird; Dadurch wird die neuronale Polarisierung in Synergie mit der Acetylierung der Mikrotubuli gefördert.

Abstract

Neurons undergo an intricate process to generate an axon and several dendrites enabling information process. This cellular process is highly stereotyped during which one of the neurites outpaces the others to become the axon, while the rest sequentially develop into dendrites. The formation of the axon is featured with a dynamic growth cone and more stable microtubules. Recently, we identified that somatic F-actin is transported to the cell periphery to affect growth cone behavior.

My study unveiled that centrosome-dependent microtubule stabilization sets the conditions for axon formation. Specifically, by immunostaining and western blot analysis I could detect that acetylated microtubules initially organized near the centrosome spread out radially as the unpolarized state is broken, and are eventually enriched in one specific neurite which is the putative axon. Moreover, I have observed that Cep120, a centriolar protein, modulates the level of microtubule acetylation to consequently direct axon formation via the regulation of Cep120 expression. On the other hand, by photoactivation analysis I could ascertain that somatic F-actin is preferentially translocated into the shorter neurites to suppress their growth during axon formation. Accordingly, during dendrite outgrowth somatic F-actin translocation to all neurites is drastically diminished suggesting somatic F-actin flow into growing neurites is an inhibitory signal for cellular growth. Mechanistically, I could discover that myosin II motors mediate this radial somatic F-actin translocation. Furthermore, my data indicate that actin phosphorylation at tyrosine-53 in the neurite shaft excludes/minimizes this somatic F-actin translocation into neurites, thereby facilitating neurite growth. Additionally, my results unveil that the accumulation of the Kinesin-1 motor domain, which is the earliest marker of axonal identity, occurs selectively in the neurite with more phosphorylated actin. Importantly, microtubule acetylation and actin phosphorylation at tyrosine-53 are co-enriched in the

longest neurite that grows as an axon. Pharmacological enhancement of microtubule acetylation promotes actin phosphorylation to regulate the establishment of polarity.

My data provide mechanistic insights into the role of the centrosome organizing microtubule stabilization in axon formation. Moreover, I uncovered a cellular mechanism consisting of the translocation of somatic F-actin into neurites, which inhibits neurite growth. Finally, I identified that this somatic F-actin translocation into neurites is counteracted by actin phosphorylation at tyrosine-53 in the neurite shaft; thus, promoting neuronal polarization in synergy with microtubule acetylation.

1. Introduction

1.1 Neuronal polarity

Neurons are highly polarized cells typically bearing one single axon and multiple dendrites which lay the foundation to form proper connections in the nervous system. The establishment of neuronal polarity is described as the process of breaking cellular symmetry to create an asymmetric architecture with distinct axonal and dendritic domains (Dotti and Banker, 1987). In most vertebrate neurons, neuronal polarization generally begins with the formation of the axon followed by dendrite outgrowth (Barnes and Polleux, 2009; Donahoo and Richards, 2009). Once established, its polarity accompanies a neuron until the end of its life to maintain unidirectional signal propagation which is essential for neuronal activities involved in learning, memory, and emotion.

The polarized axonal and dendritic compartments are drastically different in their morphology, which in turn determines their distinct functions in signal transmission and reception, respectively (Horton and Ehlers, 2003). Axons grow into a long, slender process which generates action potentials at the initial segment (AIS), termed 'axon hillock' (Catterall, 2000). These action potentials (electrical signals) are conducted down to the axon presynaptic terminals where they will trigger the release of neurotransmitters, indicating that electrical signals convert into chemical signals which later are passed on to the postsynaptic cells (Figure1-1) (Bennett and Zukin, 2004; Cook et al., 2021). By contrast, dendrites develop into relatively shorter, but highly branched processes (Craig and Banker, 1994) fitted to receive input signals (Cook et al., 2021; Mannan et al., 2021). Receptors in the dendritic membrane capture the neurotransmitters released by the axon to evoke or regulate postsynaptic potentials (PSPs) (Südhof, 2008). These potentials are integrated in the dendrites and the cell body, stimulating a new action potential at the AIS

transmitting over a long distance to the next neuron thereby forming an information flow (Tang et al., 2019).

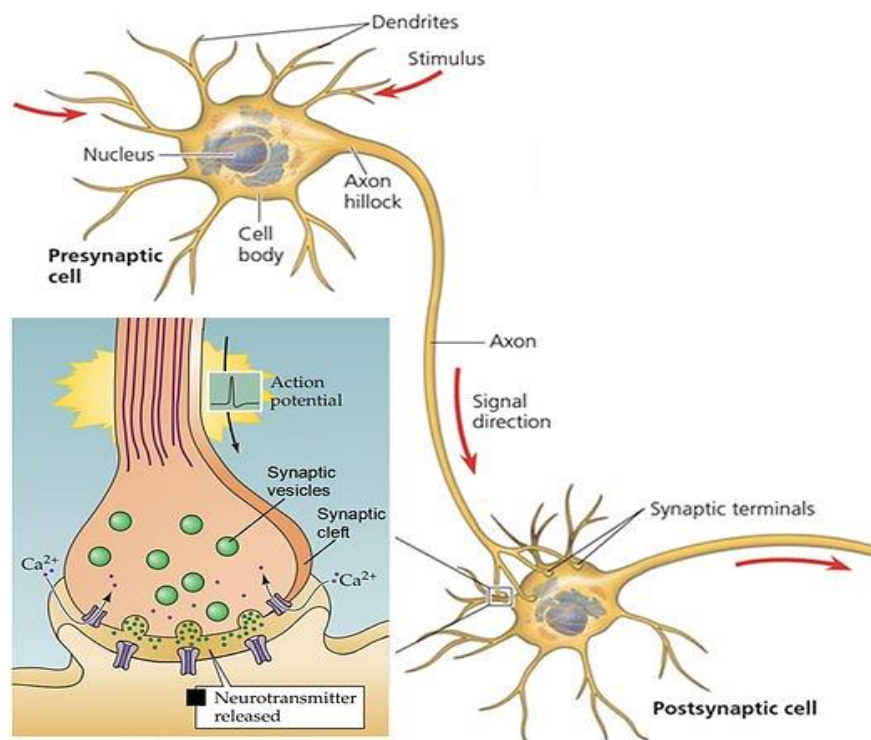


Figure 1-1: Neuronal polarity and signal transmission. Numerous dendrites detect stimuli or receive signals from other neurons and transfer the signals toward the cell body. A single axon (joined to the cell body by the axon hillock) transmits signals away from the cell body to other cells (neurons or effector cells). Figure from (Tang et al., 2019).

Moreover, the axonal and dendritic domains of a differentiated neuron also differ substantially in the segregation of membrane and cytoplasmic components, such as various cytoskeletal/-associated proteins, motor proteins, ion channels, and synaptic constituents (containing synaptic vesicle proteins and transmitter receptors) (Craig and Banker, 1994; Jan and Jan, 2003; Scott and Luo, 2001). Importantly, dendrites bear some mRNAs and organelles including late endosomes, ribosomes, endoplasmic reticulum (ER) and Golgi complex, which enables dendritic protein synthesis (Baillat et al., 2001; Gao, 1998; Huber et al., 2000; Pierce et al., 2001; Steward and Schuman, 2001; Wells et al., 2000). Such distinct molecular segregation can be mediated by multiple mechanisms: selective trafficking, membrane insertion, selective

retention after nonpolarized delivery, and dendrite-to-axon transcytosis by dendritic endosomes (Sampo et al., 2003; Song et al., 2009; Yap et al., 2008). In neurons, some motor proteins of the kinesin superfamily (KIFs), like KIF5 and KIF17, are reported to drive the polarized transport of axon- and dendrite-targeting cargos. Notably, a cytoplasmic filter at the AIS together with its plasma membrane diffusion barrier is found to facilitate exclusive trafficking and segregation of cellular components (Nakada et al., 2003; Song et al., 2009; Winckler et al., 1999) to promote and maintain neuronal polarity.

In summary, the morphological and molecular polarization of axon and dendrites underlies the ability of neurons to integrate and transmit signals unidirectionally.

1.2 Neuronal polarization process

Considering the importance of axon-dendrite polarity in information processing, great efforts have been made to characterize the process of neuronal polarization *in vitro* and *in vivo* to further understand the polarity principles.

1.2.1 Neuronal polarization in cultured hippocampal neurons

Hippocampal neurons dissociated from rat or mouse brains are a well-established and historically used system to study neuronal polarization *in vitro* (Banker, 2018; Craig and Banker, 1994; Dotti et al., 1988), possessing the following advantages: dissociated hippocampal cells are composed of almost exclusive neurons, which provides a homogeneous cell group to investigate the morphological dynamics of neurons undergoing polarization (Benson et al., 1994); Cultured hippocampal neurons successfully develop their morphological and functional polarity *in vitro* free of external cues existing *in vivo*. Hence, this system allows to study the cell-autonomous intracellular mechanism regulating polarity formation and the effects of specific external signals on neuronal polarization in a relatively isolated context (Kaech and Banker, 2006). Notably,

it is feasible to perform live-observation since cultured hippocampal neurons can be maintained for up to 3-5 weeks (Kaneko and Sankai, 2014) under appropriate conditions *in vitro*.

The polarization of cultured hippocampal neurons follows a typical developmental paradigm that is classified into five different stages (Figure 1-2) (Dotti et al., 1988). Newly plated cells appear symmetrically spherical, commence to form lamellipodia (stage 1). These lamellipodia transform into several short identical processes, termed “minor neurites” (stage 2; day 0.5–1.5). One of these minor neurites accumulates membrane, organelles as well as cytosolic proteins (Bradke and Dotti, 1997) to grow rapidly into the axon (stage 3; day 1.5–3), which is the crucial hallmark for neuronal polarization. The remaining minor neurites subsequently start to elongate and differentiate into dendrites, meanwhile, the axon continuously grows (stage 4; day 4–7). At this time, distinct molecules are polarized into axonal and dendritic compartments, respectively (Bradke and Dotti, 2000a). At stage 5 (>7 days in culture), neurons mature to establish synaptic connections and generate electric currents, which indicates polarizing functionally.

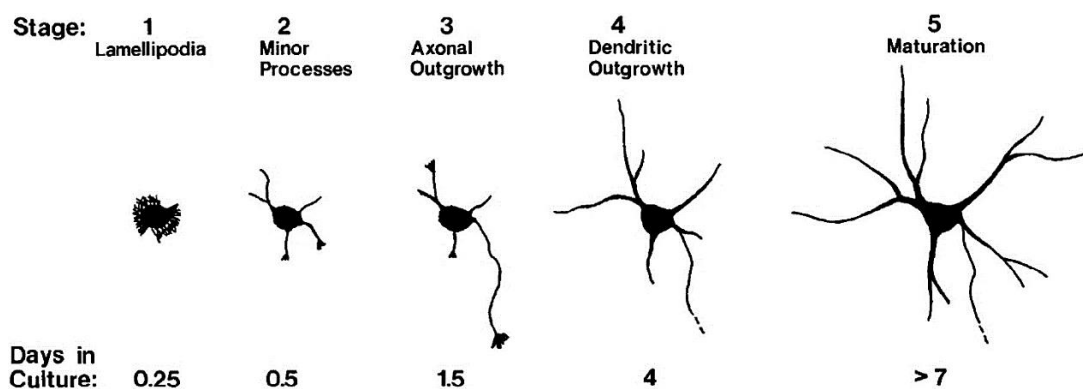


Figure 2-2: Development of hippocampal neurons *in vitro*. Stages of development of hippocampal neurons in culture. The approximate times when cells enter each of the stages are indicated. Figure from (Banker, 2018).

In this model, it is observed that one of the minor neurites preferentially elongates to become the axon. Furthermore, after transecting this growing

neurite experimentally, a new potential axon emerges *de novo* derived from a minor neurite (future dendrite), suggesting initial minor neurites share similar potential to differentiate into an axon *in vitro* (Dotti and Banker, 1987), as well implying that axon formation is preceded by stochastic selection. An alternative system to study neuronal polarity is cultured cerebellar granule neurons (CGNs) undergoing a similar sequence of developmental events (Kubota et al., 2013; Powell et al., 1997) by first extending a single long axon followed by the extension of several short dendrites.

1.2.2 Neuronal polarization *in vivo*

The establishment of neuronal polarity *in vivo* is commonly accomplished during migration. Nascent neurons exiting the cell cycle, migrate over a long distance to reach their destination, during which neurons form a leading and a trailing process that will become the axon or the dendrite depending on the neuronal type (Figure 1-3).

During development, neural progenitors *per se* exhibit an apico-basal polarity (Götz and Huttner, 2005). Hence, in *in vivo* studies, one vital question is whether newly born neurons inherit some level of polarity from their parent progenitors. Based on the investigation of the morphological transition between progenitors and post-mitotic neurons, retinal ganglion cells (RGCs), retinal bipolar neurons, and tegmental hindbrain nuclei neurons (Figure 1-3A, B) appear to inherit the parental apico-basal polarity, known as “inheritance of polarity” (Barnes and Polleux, 2009; Morgan et al., 2006; Zolessi et al., 2006). Moreover, retinal ganglion cells present inherited polarity in their appearance but also in the polarized distribution of intracellular components, including the centrosome and Golgi apparatus (Zolessi et al., 2006).

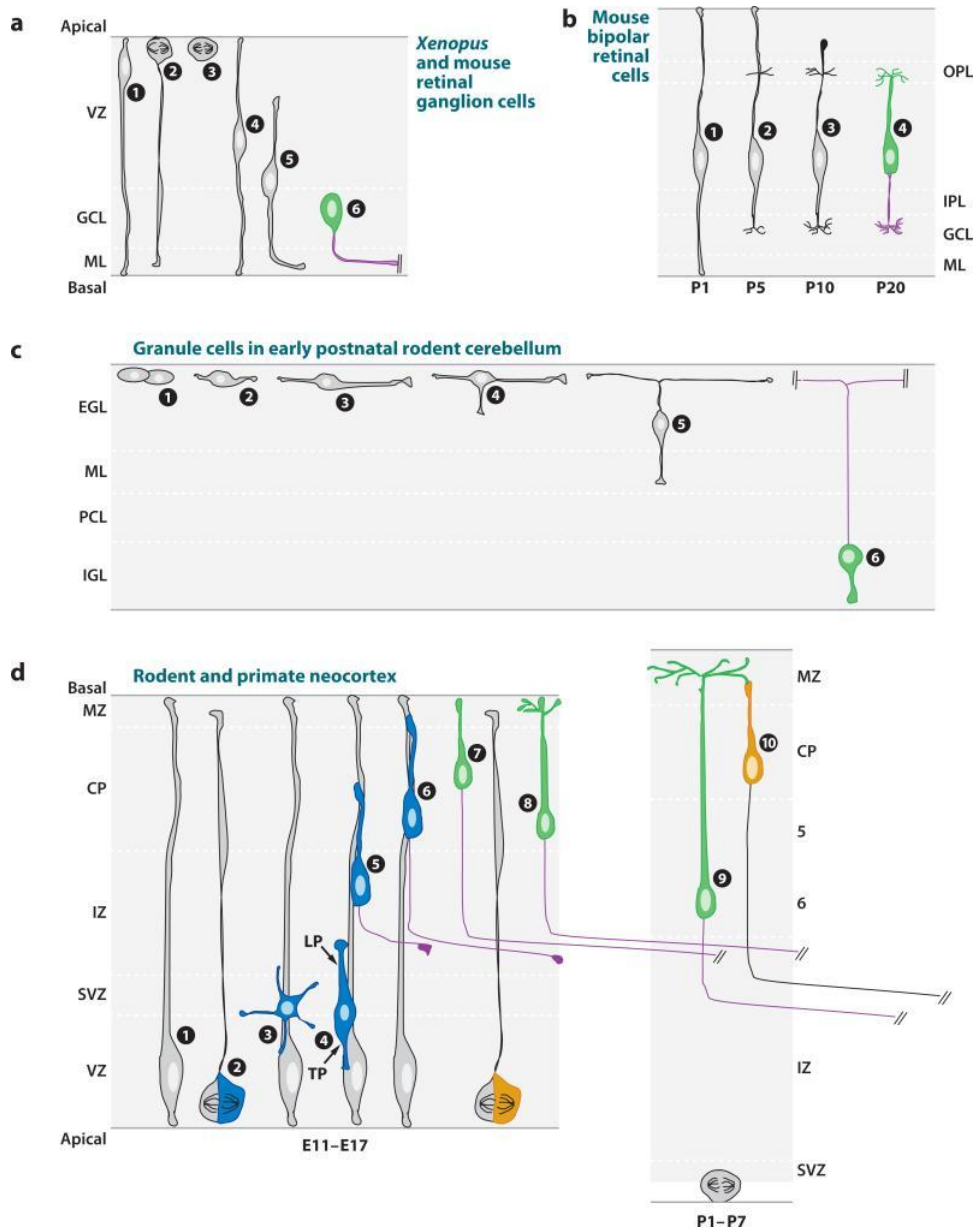


Figure 3-3: Schematic neuronal polarization models *in vivo*. Examples of the sequence of events leading to the polarized emergence of axon and dendrites in four distinct vertebrate neuronal cell types *in vivo*. The nascent axon is depicted in red and the somatodendritic domain in purple. Nascent axons are depicted in purple and dendrites/soma in green. (a) RGC precursors translocate the nucleus to the basal side and loses its apical attachment, while its basal process starts growing into the axon and the apical process into dendrite. (b) RBCs transform into bipolar cells by first losing the basal attachment while the apical process starts branching before losing attachment. The axon emerges from the basal process (red) and the dendrite emerges from the apical process. (c) Granule cell progenitors upon cell cycle exit start adopting a bipolar morphology before migrating tangentially with a leading and a trailing process. The trailing processes form a characteristic T-shaped axon (red in C6), whereas the leading process gives rise to the dendritic domain. (d) Pyramidal neurons in the mammalian neocortex are generated in the ventricular zone bearing a long basal (radial) process and a

short apical process, the post-mitotic neuron (blue) goes through a multipolar transition initiating radial translocation along a radial glial process. The leading process gives rise to the apical dendrite (purple in D7). Figure from (Barnes and Polleux, 2009).

On the other hand, other neurons, in which this inherited relationship is unclear, undergo stereotyped morphological changes leading to polarized outgrowth of the axon and dendrites, named as “establishment of polarity” (Barnes and Polleux, 2009; Namba et al., 2015) . This is the case for cerebellar granule neurons (CGNs), cortical and hippocampal pyramidal neurons (PNs) (Figure 1-3C, D) (Barnes and Polleux, 2009; Gao and Hatten, 1993; Noctor et al., 2004). Remarkably, these migrating post-mitotic neurons experience a transition from multipolar to bipolar by forming one trailing and one leading process. Here, polarity is defined by one of these two first-appearing neurites acquiring axonal identity, irrespective of how many other neurites are later established (Calderon de Anda et al., 2008).

To summarize, neuronal polarization follows a similar pattern of differentiation to grow an axon first and then dendrites *in vivo/in vitro*. Interestingly, *in vitro* studies demonstrate that axonal fate is defined by a stochastic selection of one of the multiple minor neurites for rapid outgrowth, while the axon-dendrite identity *in vivo* is acquired from the generation of leading/trailing processes.

1.3 Polarization regulation and the neuronal cytoskeleton

In vitro and *in vivo* studies indicate that the formation of the axon is the defining step of neuronal polarization, as it initiates the symmetry breakage during neuronal development. Later, dendrites extend to establish neuronal connections. Thus, one long-standing question in neurobiology is how developing neurons establish the axonal-dendritic polarity.

Accumulating work has identified that substantial regulators including intrinsic determinants within the neuron and extrinsic factors from its environment, are orchestrated to activate intrinsic signalling pathways which in turn regulate

cytoskeletal dynamics to initiate neuronal polarization (Arimura and Kaibuchi, 2007; Barnes et al., 2008; Hand et al., 2005).

1.3.1 Molecular regulators involved in neuronal polarization

1.3.1.1 Phosphatidylinositol 3-kinase directs polarization

A growing body of evidence indicates that lipid kinase phosphatidylinositol 3-kinase (PI3K) plays a central role in neuronal polarization (Ménager et al., 2004; Shi et al., 2003) (Figure 1-4). PI3K activation, which can be triggered by upstream regulators including Ras (Huang and Reichardt, 2003; Oinuma et al., 2007; Yoshimura et al., 2006) and insulin receptor substrate-1 (IRS-1) (Zheng and Wang, 2021), is required and decisive for axon specification. Additionally, Shootin1 and Singar1/2 can interact with PI3K to modulate its activity during polarity acquirement (Mori et al., 2007; Toriyama et al., 2006). Activated PI3K promotes the generation of phospholipid phosphatidylinositol-(3,4,5)-trisphosphate (PIP3) in specific membrane sites where PIP3 acts as a scaffold to recruit signalling molecules for neurite outgrowth and axon determination (Horiguchi et al., 2006; Ménager et al., 2004).

Specifically, molecules bearing pleckstrin homology domains present a high affinity with PIP3, such as phosphoinositide 3-dependent protein kinase 1 (PDK1), integrin-linked kinase (ILK) and their target Serine/threonine protein kinase (Akt, also known as protein kinase B, PKB). Therefore, they preferentially dock into these PIP3-enriched sites of the membrane produced by PI3K (Cantley, 2002; Lawlor and Alessi, 2001; Oinuma et al., 2007). Consequently, the accumulation of PDK1 and ILK can further facilitate phosphorylation-induced Akt/PKB activation. Activated Akt/PKB is able to phosphorylate/inactivate glycogen synthase kinase 3 β (GSK3 β) (Shi et al., 2003; Yoshimura et al., 2006) leading to a differential distribution of active GSK3 β in axons and dendrites to precede axon formation (Doble and Woodgett,

2003). Consistently, increasing the activity of GSK3 β can inhibit the axon formation, whereas reducing its activity induces multiple axons (Jiang et al., 2005). Moreover, ILK is also reported to inactivate GSK3 β activity via phosphorylation to promote the establishment of axons (Delcommenne et al., 1998; Guo et al., 2007).

On the contrary, active phosphatase and tensin homologue deleted on chromosome 10 (PTEN) acts opposite to PI3K activity by decreasing PIP3 levels (dephosphorylate PIP3 into PIP2) at the leading edge of neurites and negatively regulating the development of polarity (Barnes and Polleux, 2009; Jiang et al., 2005; Shi et al., 2003). PTEN knockdown leads to a multiple-axon phenotype (Jiang et al 2005). Interestingly, inactive GSK3 β could also activate PTEN to impede axon formation (Jang et al., 2021). These results suggest GSK3 β is a critical mediator in the neuronal polarity cascades.

1.3.1.2 Glycogen synthase kinase 3 β mediates polarization

GSK3 β is a multifunctional constitutively active serine/threonine kinase that can be inactivated through phosphorylation by multiple kinases, including Akt/PKB, ILK and atypical protein kinase C (aPKC) (Etienne-Manneville and Hall, 2003). The constitutively active form of GSK3 β suppresses the activity of its targets and needs to be inactivated/phosphorylated during neuronal polarization (Doble and Woodgett, 2003; Jiang et al., 2005; Yoshimura et al., 2005).

Moreover, several downstream targets of GSK3 β are identified to be potential polarity effectors (Kim et al., 2011). For instance, collapsin-response mediator protein 2 (CRMP2), which is enriched at the tip of the nascent axon, is phosphorylated/inactivated by GSK3 β resulting in disruption of tubulin assembly (Fukata et al., 2002). Upregulation of CRMP2 is sufficient to induce multiple axons, while truncated forms of CRMP2 can impair axon establishment (Inagaki et al., 2001; Yoshimura et al., 2005). Additionally, GSK3 β could

phosphorylate adenomatous polyposis coli (APC) thereby to block its ability of promoting microtubule stabilization (Zumbrunn et al., 2001). An early accumulation of APC at the tip of one neurite precedes fast axonal outgrowth, which depends on GSK3 β inhibition (Gärtner et al., 2006; Votin et al., 2005). However, a dominant-negative mutant of APC impedes the formation of axons (Shi et al., 2004; Zhou et al., 2004). Similarly, GSK3 β -mediated phosphorylation of microtubule associated protein 1b (MAP1b) and Tau appears to alter microtubule dynamics to spatially regulate axon outgrowth (Kim et al., 2011; Trivedi et al., 2005). Thus, GSK3 β seems to tune the regulation of axon determination by transducing upstream signalling to reorganize the axonal cytoskeleton, especially microtubules (Figure 1-4).

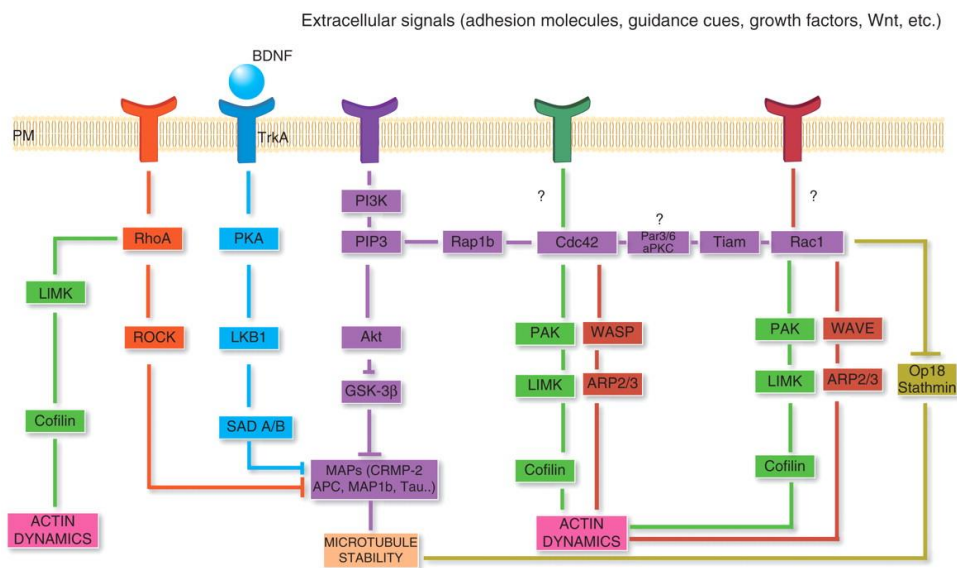


Figure 1-4: Coordination of extracellular and intracellular signaling regulates cytoskeletal dynamics and axon formation. Overview of selected signaling pathways that may initiate neuronal polarization and axon specification. BDNF signaling (blue) leads to activation of PKA/LKB1/SAD A/B signaling that regulates the stability of microtubules and induces axon formation. The PI3K/PIP3/Akt/GSK-3 β pathway (purple) regulates MAPs and the stability of microtubules. Another signaling branch activates Rap1b and the Rho GTPases Cdc42 and Rac1. Signals from both of these GTPases regulate actin dynamics via WASP/WAVE (red) or PAK-cofilin pathways (green). Rac1 may also regulate microtubules by regulating the microtubule destabilizer Op18/Stathmin. Apart from being downstream of PI3K signaling, Cdc42 and Rac1 may be activated by other signals (potential green and red plasma membrane receptors). Another molecule implicated in axon development is RhoA, which might

regulate actin via the LIMK/cofilin pathway (green) or microtubule dynamics via ROCK signaling to MAPs (orange). Figure from (Tahirovic and Bradke, 2009).

Notably, GSK3 β -APC were identified to modulate positioning of partitioning defective 3 (PAR3) which is another polarity protein (Shi et al., 2004). PAR3 is the core scaffold protein of the PAR3/6-aPKC complex which specifically localizes at the tip of the nascent axon to recruit multiple proteins including the small GTPase Cdc42 (Garrard et al., 2003), the guanine exchange factor Tiam1/STEF (Chen and Macara, 2005; Nishimura et al., 2005), and PTEN (Feng et al., 2008; von Stein et al., 2005). This PAR complex, which is identified to lie in the downstream of PI3K, is required for regulating asymmetric cell division and inducing axonal development (Shi et al., 2003).

1.3.1.3 Rho-family of small GTPases induce polarization

Rho GTPases and their effectors are another group of regulators implicated in breaking neuronal symmetry to confer axonal identity (Arimura and Kaibuchi, 2007; Govek et al., 2005), which is also well known to regulate the cellular cytoskeleton, membrane dynamics and vesicle transport (Etienne-Manneville and Hall, 2002; Govek et al., 2005). The activity of Rho GTPases is regulated by GTPase activating proteins (GAPs), guanine nucleotide-exchange factors (GEFs), and guanine nucleotide-dissociation inhibitors (GDIs) that drive Rho GTPase cycling between the inactive guanine diphosphate (GDP)-bound state and the active guanine triphosphate (GTP)-bound state to function properly (Jaffe and Hall, 2005; Nobes and Hall, 1995). The best characterized members of Rho GTPases are ras homolog gene family, member A (RhoA), cell division cycle 42 (Cdc42), and ras-related C3 botulinum toxin substrate 1 (Rac1) (Barnes and Polleux, 2009). In general, the activation of Cdc42 or Rac1 promotes neurite outgrowth, whereas active RhoA is considered to suppress neurite formation (Figure 1-4).

Specifically, RhoA negatively regulates neuritogenesis by recruiting and activating its specific kinase ROCK to destabilize actin-based cytoskeleton (Bito et al., 2000; Da Silva et al., 2003; Schwamborn and Püschel, 2004), while dominant inactive form of RhoA can enhance neurite growth (Schwamborn and Püschel, 2004). Importantly, the loss of Cdc42, either through RNAi downregulation (Schwamborn and Püschel, 2004) or genetic ablation (Garvalov et al., 2007), results in striking defects of axon specification, which may be caused by a specific increase of inactive/phosphorylated cofilin levels. Evidently, active/non-phosphorylated cofilin is enriched in the axonal growth cone, which is mediated by LIM kinase (LIMK) that is activated by p21-activated kinase 1 (PAK1) - a Cdc42 effector (Garvalov et al., 2007). Furthermore, downregulation of PAK1 leads to the disruption of neuronal polarization, while conversely hyperactivation of PAK1 promotes the formation of multiple axons (Jacobs et al., 2007). Notably, signalling mediated by RhoA, Cdc42 or Rac1 appears to converge at LIMK (Garvalov et al., 2007) to phosphorylate cofilin regulating axon establishment.

In addition, ras-related protein 1b (Rap1b), a member of the ras-family of small GTPases, acts in the upstream of Cdc42 to promote the specification of the future axon (Schwamborn and Püschel, 2004). It is suggested that PIP3 recruits Rap1b and Cdc42 into the neurite tips where they are activated by a Cdc42-GEF (Fivaz et al., 2008; Schwamborn and Püschel, 2004). Moreover, Cdc42 binds to PAR6 of the PAR polarity complex followed by PAR3 directly interacting with STEF/Tiam1 to activate Rac1, by which Cdc42 induces filopodia formation (Nishimura et al., 2005). Remarkably, active Rac1 can activate PI3K which consequently contributes to form a positive feedback loop consisting of PI3K, PIP3, Rap1b, Cdc42, PAR complex, Rac1 (Figure 1-5). This loop is implicated in driving symmetry breakage and promoting continuous axonal outgrowth (Arimura and Kaibuchi, 2007). Moreover, the localized

accumulation of Rap1b may restrict the axon-inducing effect of this positive feedback loop to a single neurite (Schwamborn and Püschel, 2004). Besides, inactivation of Cdc42/Rac1 (Pichaud et al., 2019; Zoughlami et al., 2013) or PIP3 degradation (Gerisch et al., 2012) may provide a key to exit this loop.

Consistently, more experimental evidence points to a negative feedback loop in line with the proposed positive feedback loop to control axon specification (Figure 1-5) (Andersen and Bi, 2000; Dotti and Banker, 1987). Observations indicate that an immature neurite contacting with a laminin-coated bead commences with fast outgrowth by an accumulation of PIP3 to its tip (Ménager et al., 2004). When a second neurite touches the laminin-coated bead, however, the first neurite stops elongating, suggesting a negative regulation induced by the second neurite (Ménager et al., 2004). Recent work implicates that local and long-range reciprocal regulation of cytosolic cyclic adenosine monophosphate (cAMP) and cyclic guanosine monophosphate (cGMP) coordinates the initiation of one axon and multiple dendrites (Shelly et al., 2010). Local cAMP increase in one neurite causes cAMP reduction in all other neurites where cGMP is elevated. Moreover, Ca^{2+} waves generated from the growing axon are delivered to the cell body where these long-range Ca^{2+} waves activate somatic RhoA through calcium/calmodulin-dependent protein kinase I (CaMK1) (Takano et al., 2017). Consequently, active RhoA diffuses to other neurites to prevent their outgrowth and differentiate them into dendrites.

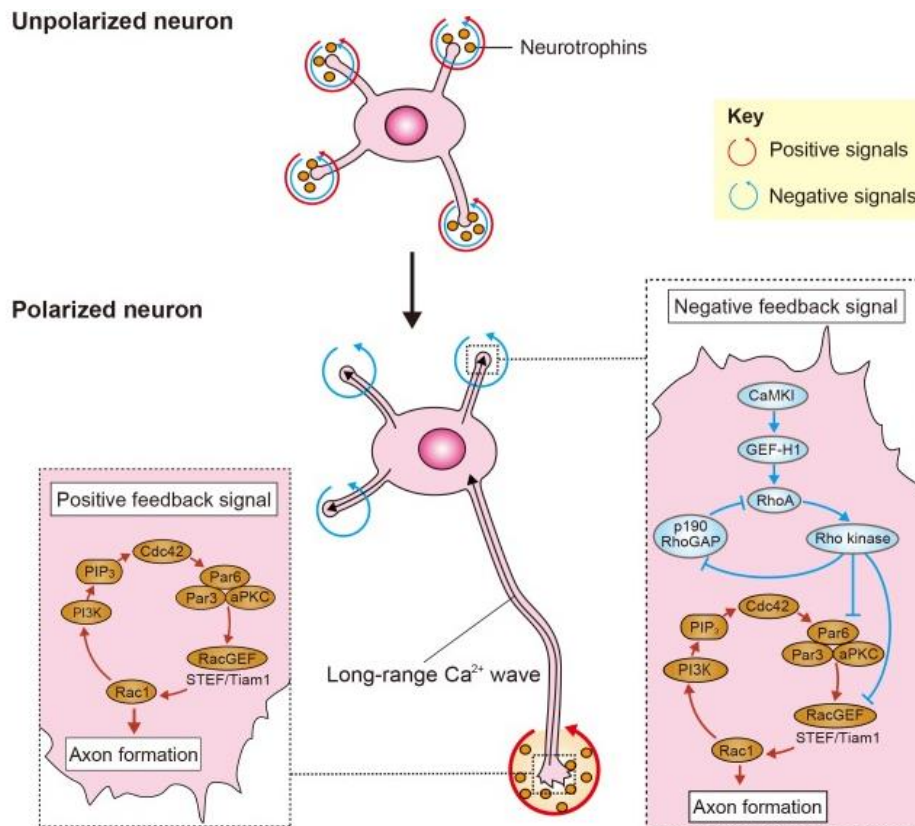


Figure 1-5: Positive and negative feedback signals for neuronal polarization. In unpolarized neurons, the positive, and negative feedback signals are balanced in all minor neurites (red and blue arrows). When the balance is upset by the local amplification of neurotrophins, the Rac1/PI3-kinase/PIP3/Cdc42/Par complex/RacGEFs pathway is continuously activated within one minor neurite and thereby induces axon specification and elongation (red arrows). Concurrently, the long-range Ca^{2+} waves are propagated from the nascent axon to the cell body. The Ca^{2+} waves activate the CaMKI/GEF-H1/RhoA/Rho-kinase pathway, which represses the positive feedback loop in all minor neurites to prevent the formation of multiple axons and determine dendritic specification (blue arrows). Figure from (Takano et al., 2019).

To conclude, positive feedback signals are continuously activated in one of the minor neurites resulting in axon specification and elongation. Meanwhile, negative feedback signals are propagated from the nascent axon terminal towards other immature neurites to inhibit their outgrowth, thereby leading to asymmetric growth.

1.3.1.4 Extracellular cues trigger polarization

Several studies show that an array of extracellular cues, which could trigger intracellular events, is orchestrating intracellular signalling underlying the initial

break of neuronal symmetry leading to axon-dendrite polarization (Arimura and Kaibuchi, 2007; Craig and Banker, 1994). As an illustration, secreted netrin1 guides axon outgrowth through its receptor colorectal cancer suppressor (DCC) to block RhoA signalling (Brankatschk and Dickson, 2006; Moore et al., 2008). Meanwhile, netrin1 also modulates actin retrograde flow in the axonal growth cone via PAK1-mediated Shootin1 phosphorylation (Toriyama et al., 2013). Wnt proteins direct the polarized emergence of a single axon (Hilliard and Bargmann, 2006; Prasad and Clark, 2006), in a way of the Wnt signalling pathway together with JNK induces the inhibition of GSK3 β (Ciani and Salinas, 2007; Oliva et al., 2006).

Moreover, semaphorin 3A (sema3A) promotes dendrite differentiation through suppression of axon development by elevating cGMP levels but reducing cAMP and PKA activity, which in turn downregulates LKB1 (a serine/threonine kinase)- SADKs (synapses of amphids defective kinases) signalling (Shelly et al., 2011). However, brain-derived neurotrophic factor (BDNF) binds to the receptor TrkA, which activates cAMP-dependent phosphorylation of PKA leading to LKB1 activation. Activated LKB1 then activates SADKs to facilitate axon specification in a manner of regulating microtubule dynamics (Barnes et al., 2008; Shelly et al., 2007).

Taken together, the commitment of polarity is implicitly mediated by complex and interconnected signalling networks stimulated by intrinsic and extrinsic regulators. These regulatory pathways can trigger a multitude of intracellular events that seems to converge on the modulation of actin and microtubule dynamics.

1.3.2 The role of cytoskeleton in neuronal polarization

Actin filaments and microtubules (MTs) are polar polymers in which subunits are arranged head-to-tail creating two different ends that can both either

polymerize or depolymerize (Nogales, 2000; Pollard and Cooper, 1986). These properties of inherent structural polarity and intrinsic dynamics make them well-suited to remodel rapidly in response to polarity signals (Hoogenraad and Bradke, 2009; Li and Gundersen, 2008).

1.3.2.1 The actin cytoskeleton

Filamentous actin (F-actin) is shaped by two helically intertwined strands consisting of polymerized globular actin (G-actin) subunits that bind and hydrolyse ATP (Pollard and Borisy, 2003). G-actin subunits preferentially incorporate into the barbed end but prefer to dissociate from the pointed end (Figure 1-6a). Recently, the work from our group revealed that somatic F-actin is released to the cell periphery to affect growth cone behaviours (Meka et al., 2019). These actin polymers are organized radially around the centrosome in aster-like structures releasing actin fibers/filaments. They intermingle with pericentriolar material 1 (PCM-1), whose downregulation impairs somatic F-actin dynamics and actin polymerization, thus boosting neurite outgrowth (Meka et al., 2019). Notably, in cultured hippocampal pyramidal neurons, a localized dynamic actin network is sufficient to specify axonal fate (Bradke and Dotti, 1997, 1999). By contrast, a relative rigid actin-cytoskeleton is found in the future dendrites bearing a static growth cone. Pharmacological depolymerization of the actin cytoskeleton induces nongrowing minor neurites into growing axons (Bradke and Dotti, 1999, 2000b; Schwamborn and Püschel, 2004). In this way, the local actin instability in the growth cone may reduce the impediment for the MT protrusion, which in turn leads to the rapid elongation of the putative future axon (Forscher and Smith, 1988; Tanaka et al., 1995). Thus, the regulation of the actin-based cytoskeleton appears to be a decisive factor underlying the establishment of neuronal polarity.

Actin dynamics, which influence F-actin stability, are modulated by multiple molecules involved in actin nucleation, branching, severing, bundling and ADP/ATP exchange (Figure 1-6b) (Pollard and Borisy, 2003). Importantly, many of them are the effectors of signalling pathways involved in axon formation. For instance, in cultured hippocampal neurons, the brain-specific profilin IIa, which is the effector of RhoA/ROCK signalling, enhances actin polymerization, which in turn promotes neurite sprouting (Da Silva et al., 2003). Neuronal Wiskott-Aldrich syndrome protein (N-WASp) regulates actin polymerization by activating the actin-related protein 2/3 (Arp2/3) complex in response to the signal from Cdc42 (Ishikawa and Kohama, 2007; Millard et al., 2004). Similarly, WASp-family verprolin-homologous protein (WAVE), which is concentrated at the leading edge of growth cones, modulates actin assembly through Arp2/3 (Takenawa and Miki, 2001) or profilin II (Pilo Boyl et al., 2007), thereby promoting axon extension (Figure 1-4).

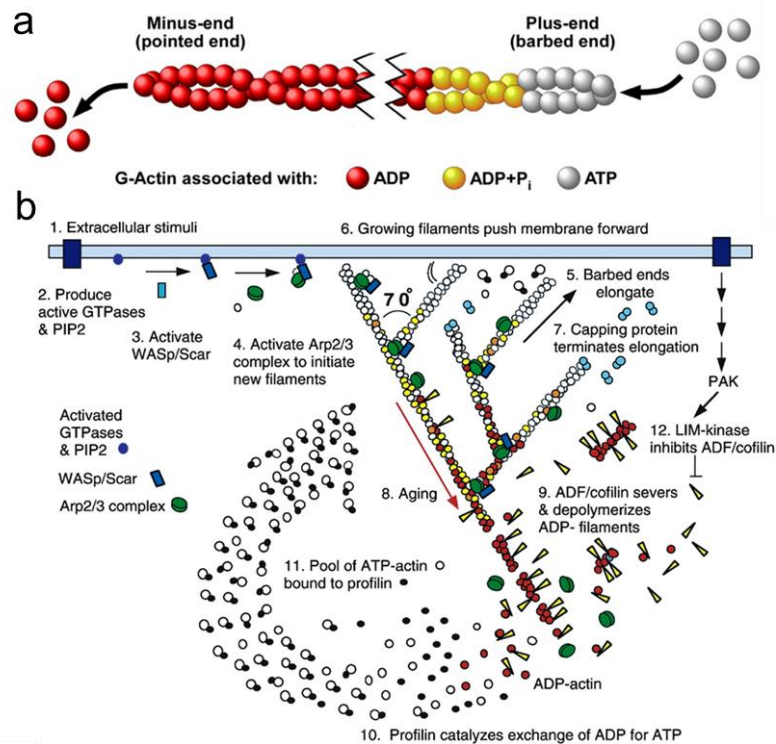


Figure 1-6: Actin-structure and dynamics. (a) Actin microfilaments consist of two helically intertwined strands of F-actin, which is itself composed of polymerized subunits of globular actin (G-actin).

G-actin subunits are arranged head-to-tail in the actin filament which creates two ends with distinct dynamic properties. G-actin is added to the 'barbed' end (polymerization), making it the faster-growing end, while depolymerized from the 'pointed' end, causing it growing slowly. Polymerizing G-actin is associated with ATP (white subunits) which is then hydrolyzed upon ageing in the filament (yellow subunits). Inorganic phosphate (Pi) is released slowly from G-actin (red subunits). (b) Simplified actin cycle. Extracellular signaling leads to the activation of WASP/Scar proteins which in turn induce actin nucleation and branching by the Arp2/3 complex to push membrane forward. Capping proteins terminate polymerization at the barbed end of the filament. ADF/cofilin –which may be inhibited by PAK and LIM kinase– promotes dissociation of the inorganic phosphate, severs ADP-actin filaments and promotes dissociation of ADP-actin from filament ends. Profilin catalyzes the ADP/ATP exchange of actin, thereby reconverting ADP-associated G-actin to the ATP-bound form. Moreover, profilin sequesters ATP-actin to rapidly release it just upon stimulation by WASP/Scar proteins. Figure from (Pollard and Borisy, 2003).

Moreover, cofilin activated by LIMK signalling associates with the pointed end of F-actin to promote actin depolymerization (Bernstein and Bamburg, 2010). Interestingly, assembled actin-bundles at the leading edge of growth cones are transported centripetally by myosin II towards the growth cone centre where actin-bundles are depolymerized, known as “retrograde flow” (Forscher and Smith, 1988; Lin et al., 1996). Then, genetic ablation of cofilin can block actin retrograde flow resulting in a failure of neuritogenesis (Flynn et al., 2012), suggesting that increased actin dynamics (augmented actin retrograde flow or actin disassembly) in the growth cone can facilitate neurite formation.

Despite the crucial role of actin in polarity formation, the regulation of actin dynamics does not seem to be the only determinant in axon specification. Some polarity regulators, like SADKs (Kishi et al., 2005) and GSK-3 β (Jiang et al., 2005; Yoshimura et al., 2005), appear to regulate MT stabilization to implement neuronal symmetry breakage.

1.3.2.2 The microtubule cytoskeleton

MTs are hollow cylinders composed of α/β -tubulin heterodimers that bind and hydrolyse GTP (Li and Gunderson, 2008). Tubulin heterodimers polymerize in a head-to-tail fashion to form polar protofilaments, which then are assembled into the wall of microtubule cylinder (Evans et al., 1985). Due to this specific

assembly of heterodimers, a MT bears two ends with different polymerization rates: the faster growing β -tubulin end (the plus-end) and the slow growing α -tubulin end (the minus-end) (Allen and Borisy, 1974). The minus-ends are anchored to a microtubule organizing centre (MTOC) (Figure 1-7a), which initiates MT assembly radially with plus-ends extending out (Lüders and Stearns, 2007). In axons, MT orientation is identified to be uniform with the plus-ends outward, while MTs in dendrites are reported to have a mixed polarity (Baas et al., 2016). Moreover, MTs undergo dynamic switching between prolonged phases of growth and shrinkage, a phenomenon called ‘dynamic instability’ (Mitchison and Kirschner, 1984). The transition from growth to shrinkage is referred to as ‘catastrophe’, whereas the opposite transition from shrinkage to growth is termed as ‘rescue’ (Figure 1-7c).

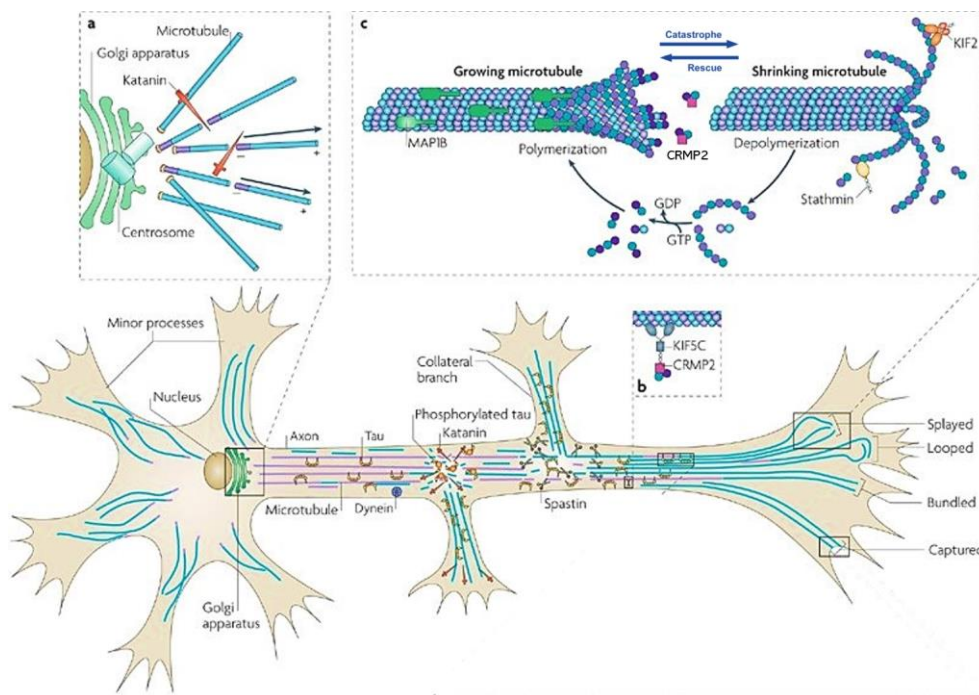


Figure 1-7: Organization and regulation of microtubules in hippocampal pyramidal neurons. Dynamic (blue) microtubules predominate in minor processes (short, unbranched neurites) and at the distal end of the axon and collateral branches, whereas stable (purple) microtubules are enriched in the proximal part of the axon. Short microtubule polymers release from the centrosome (a) and are transported along microtubules by motors such as dynein. Tubulin dimers or oligomers are delivered into the growth cone by a complex of kinesin family member 5C (KIF5C) and CRMP2 (also known as DPYSL2) (b). On entering the axonal growth cone microtubules splay, bend, loop, bundle or

get captured at the cell cortex. The binding, hydrolysis, and exchange of GDP/GTP on the β -tubulin monomer drive the switching between polymerization (assembly) and depolymerization (disassembly) of microtubules (c). Figure adapted from (Conde and Cáceres, 2009).

Several studies indicate that transecting the putative axon confers axonal fate to an alternative process, which may correlate with MT dynamics (Bradke and Dotti, 1997; Calderon de Anda et al., 2008; Dotti and Banker, 1987). Further investigation unveiled that the existence of a stable pool of MTs in the lesioned neurite is the determinant of either axon regeneration or axonal re-specification (Gomis-Rüth et al., 2008). Another study from the same year confirmed that stable MTs are enriched in a single neurite before axon formation and in the axon of morphologically polarized neurons (Figure 1-7) (Witte et al., 2008). Consistently, pharmacological promotion of MT stabilization using a photoactivatable form of microtubule-stabilizing compound Taxol directs axonal specification to a single unmaturing neurite (Witte et al., 2008), suggesting local MT stabilization is a decisive signal specifying neuronal polarization.

Interestingly, this polarized stabilization of MTs may also direct axonal trafficking to reinforce axon formation, coming from the observation that various motors of the kinesin and dynein superfamily, which are mostly plus-end and minus-end directed, respectively, bear a high binding affinity to stable MTs (Figure 1-7) (Goldstein and Yang, 2000; Westermann and Weber, 2003). As an illustration, the Kinesin-1 transports cargo preferentially along stable MTs into only a subset of neurites (Nakata and Hirokawa, 2003; Reed et al., 2006). Moreover, selective translocation of the Kinesin-1 motor domain into the nascent axon requires tubulin acetylation and detyrosination (stable forms of MTs) (Jacobson et al., 2006; Konishi and Setou, 2009; Reed et al., 2006). The axonal localization of Par3/6-aPKC complex responsible for polarity formation may be mediated by kinesin family member 3A (KIF3A) which accumulates in the axon (Nishimura et al., 2004; Shi et al., 2004). These data suggest a

stabilized MT array might provide a foundation for the compartment-specific transport to axons and dendrites.

MT stability is regulated by a variety of microtubule-associated proteins (MAPs) (Cassimeris and Spittle, 2001). Some MAPs can stabilize MTs through blocking catastrophes, promoting rescue events or stimulating tubulin-polymerization, even mediating protofilament cross-linking or microtubule-bundling. This is evident in the case of MAP2 which lowers the MT depolymerizing state to induce more stable MTs (Kowalski and Williams, 1993). On the contrary, some MAPs can promote catastrophe and prevent rescue as well as induce MT severing, or weaken lateral interactions between protofilaments (Cassimeris and Spittle, 2001) to destabilize MT. Moreover, various post-translational modifications (PTMs), which occur mainly at the carboxy-terminal tail of tubulin subunits, provide another potential mechanism to modify MT stability, including acetylation, detyrosination, polyamination, glutamylation and phosphorylation (Westermann and Weber, 2003). For example, the enzymatic removal of the C-terminal tyrosine of α -tubulin (detyrosination), and acetylation of α -tubulin become enriched in a polarized array of stable MTs which is important for generating cellular asymmetries (Wloga et al., 2017). In addition, the axon-inducing effect of Taxol features a dramatic increase in MT acetylation (Witte et al., 2008).

Remarkably, a substantial amount of polarity regulators is implied in promoting MT stabilization, which in turn promotes cellular asymmetries. Some regulators may stabilize MTs by regulating the affinity of these MAPs to MTs. To illustrate, GSK-3 β can inactivate MAPs, like MAP1b (Del Río et al., 2004) and Tau (Sperber et al., 1995), to weaken their binding to MTs leading to the decrease of MT stability, which in turn hinders the emergence of axons. Another example is SADKs that enhance MT stability via phosphorylating specific MAPs

(including Tau) (Kishi et al., 2005). On the other hand, some molecules may directly interact with MTs to modulate their dynamics. Stathmin acts on the plus-ends of MTs where it can be inactivated by Rac-DOCK7, to reduce MT catastrophe rate and promote axon formation (Pineiro and Gertler, 2006). CRMP2 binds to free tubulin-heterodimers to promote MT assembly in the growing axon and induces multiple axons upon overexpression (Figure 1-7b) (Fukata et al., 2002; Inagaki et al., 2001).

In summary, rearrangements of the actin and tubulin cytoskeleton are crucial to initiate the establishment of polarity, as they are the major final targets of a plethora of signalling pathways regulating axon formation. Before morphological polarization occurs, the future axon shows enhanced actin dynamics (Bradke and Dotti, 1999; Witte et al., 2008), which may confer a loose actin structure at the axonal growth cone permissive for MT invasion (Forscher and Smith, 1988), and accumulation of more stable MTs (Witte et al., 2008) to precede axon establishment.

1.4 Centrosome behaviour during neuronal polarization

Besides the commitment of actin/tubulin cytoskeleton, centrosome positioning is suggested to play an instructive role in the regulation of axon specification, based on observations from *in vitro* and *in vivo* studies (Andersen and Halloran, 2012; de Anda et al., 2010; de Anda et al., 2005; Sakakibara and Hatanaka, 2015; Zmuda and Rivas, 1998). The centrosome is composed of two centrioles surrounded by pericentriolar material (PCM) generating a radial organization of MTs (Sanchez and Feldman, 2017). An early study revealed that inhibition of MT nucleation at the centrosome impedes MT reassembly and compromises axonal growth (Ahmad et al., 1994), suggesting a potential mechanism mediated by the centrosome in axon formation.

In support of this idea, the work on Ti1 pioneer neurons of the embryonic grasshopper limb showed that a tubulin-containing cap (MTOC) and the Golgi apparatus are located at the pole from where axonogenesis is initiated (Lefcort and Bentley, 1989). Given that the centrosome colocalizes with the Golgi apparatus during neuronal development, it is plausible that the centrosome may regulate Golgi-derived vesicle trafficking (Sütterlin and Colanzi, 2010), by which the centrosome positions the Golgi to the base of the future axon and directs polarized microtubule-dependent secretory transport (Bornens, 2008; Hoogenraad and Bradke, 2009; Witte et al., 2008). *In vitro* experiments identified that the arising neurite upon the terminal mitosis closest to the centrosome/Golgi is selected to become the axon (Figure 1-8) (de Anda et al., 2005; Zmuda and Rivas, 1998). These data are complemented by the elegant work in the developing cortex that centrosomes of multipolar neurons translocate transiently to the site of axon formation before or at the time of initial axon sprouting (de Anda et al., 2010). Consequently, disruption of centrosomal activity or downregulation of the centriolar satellite protein PCM-1 precludes axon formation (de Anda et al., 2010). Therefore, the possibility arises that the position of the centrosome might be a robust predictor of the axon initiation site.

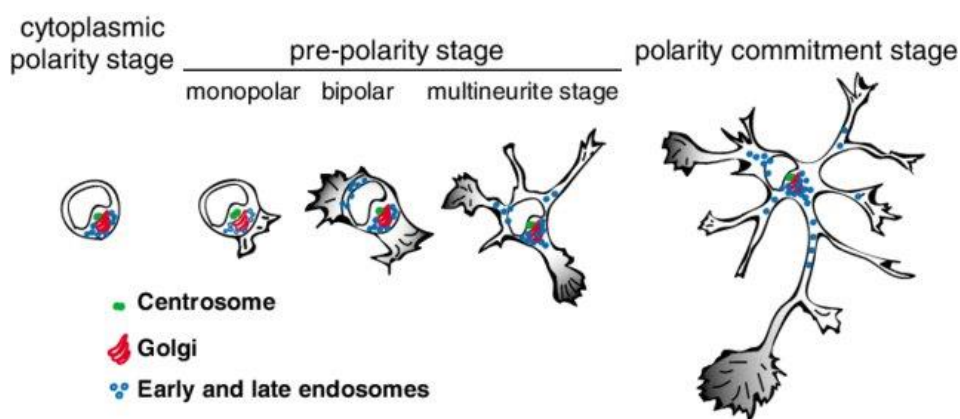


Figure 4-8: Neuronal polarization in relation to centrosome/Golgi. Illustration shows early stages of neuronal development of hippocampal neurons, in culture, from 0 h until 18-24 h. Within these first three stages the cell is developing from forming lamellipodia structures over the outgrowth of neurites until the axon specification. The centrosome/Golgi apparatus locate

to the site of axon extension. The illustration is from (Meka et al., 2019), adapted from (Calderon de Anda et al., 2008).

However, this positive correlation appears to be under debate on the grounds of several experimental findings (Distel et al., 2010; Zolessi et al., 2006). Studies in neurons of the tegmental hindbrain nuclei showed that axon outgrowth occurs independently of centrosome proximity (Distel et al., 2010). Also, *Drosophila* neurons devoid of centrioles still can establish their axons normally (Basto et al., 2006). Moreover, in retinal ganglion cells (RGCs) of the developing zebrafish embryo the centrosome orients to the pole where the future dendrite emerges (Zolessi et al., 2006). *In vivo* observations of locomoting bipolar neurons showed that the centrosome translocates to the base of the pia-directed leading process with the axon at the opposite side (Sakakibara et al., 2014). More work is needed to verify whether centrosome positioning directly gives the first spatial cue to break the cellular symmetry, or if it is simply an epiphenomenon of the polarization process (Etienne-Manneville and Hall, 2003; Stiess et al., 2010).

1.5 Objectives of this thesis

Developing neurons break their symmetry by defining the axon, which is specified by actin instability in the growth cone and microtubule stabilization along the shaft (Bradke and Dotti, 1999; Witte et al., 2008). Moreover, centrosome positioning is implicated in directing the axonal initiation site and disruption of centrosome-dependent microtubule organization compromises axonal growth (Ahmad et al., 1994). Furthermore, somatic F-actin concentrated near the centrosome is delivered to the growing neurites and inversely correlated with neurite growth (Meka et al., 2019). However, the exact mechanisms conferring axon-dendrite polarity remain rudimentary.

This thesis therefore aimed to further characterize the role of actin/microtubule in neuronal polarization during initial neuronal development. To this end I addressed the following major questions:

- 1) How do stable microtubules distribute in neurons along the process of polarization?
- 2) Does the centrosome play an instructive role for preferential microtubule stabilization in the growing axon?
- 3) Does somatic F-actin translocation act as an inhibitory factor to suppress neurite growth during neuronal polarization?
- 4) How is the somatic F-actin delivery regulated during axon specification?

My studies conclude that centrosome-dependent microtubule acetylation, spreading radially from the soma into the growing axon, induces the initiation of axon formation. Moreover, somatic F-actin preferentially translocates into the shorter neurites to inhibit neurite growth, while the neurite receiving less F-actin, but more stable microtubules is primed for rapid growth. Consequently, actin phosphorylation (destabilizes actin filaments) promoted by microtubule acetylation precludes somatic F-actin delivery, leading to asymmetric growth and axon formation.

2. Results

2.1 Centrosome-dependent microtubule stabilization sets the conditions for axon formation

Previous studies have shed light on the polarized distribution of stable microtubules in the developing axon, measured by the post-translational modifications of α -tubulin, including acetylated/tyrosinated α -tubulin (Westermann and Weber, 2003; Witte et al., 2008). Nevertheless, how these modified microtubules are spatially coordinated to initiate axon formation is unclear. To this end cultured rodent hippocampal neurons (Dotti et al., 1988) and cortical neurons were used as the model systems. Thereafter, cells were stained for different post-translational modifications of α -tubulin whose organization was evaluated.

2.1.1 Radial organization of acetylated microtubules in early developing neurons

According to previous data, the centrosome positioning might be a landmark to predict the site of axon outgrowth which requires more stable MTs (Andersen and Halloran, 2012; de Anda et al., 2010; Witte et al., 2008). To examine if the centrosome contributes to MT stabilization in the growing axon, the distribution of acetylated α -tubulin (AcetyTub)/polyglutamylated α -tubulin (PolyGluTub), and tyrosinated α -tubulin (TyrTub) (markers for stable and dynamic MTs, respectively), and α -tubulin were scrutinized in detail via super-resolution microscopy in cultured hippocampal neurons from stages 1-3.

Images captured with stimulated emission depletion (STED) microscopy revealed that stage 1 neurons had the AcetyTub concentrated around the centrosome (labeled by pericentrin), while PolyGluTub, TyrTub or α -tubulin extended across the cell body (Figure 2-1 and Figure 2-2, videos see in Meka et al., 2022). At stage 2, however, the AcetyTub spread throughout the cell body as PolyGluTub, TyrTub or α -tubulin, and started to penetrate the neurites

(Figure 2-1 and Figure 2-2). Morphologically polarized neurons (stage 3) exhibited a dramatic enrichment of AcetyTub in the longest neurite, presumably the future axon, compared to that in minor neurites (Figure 2-1A, C).

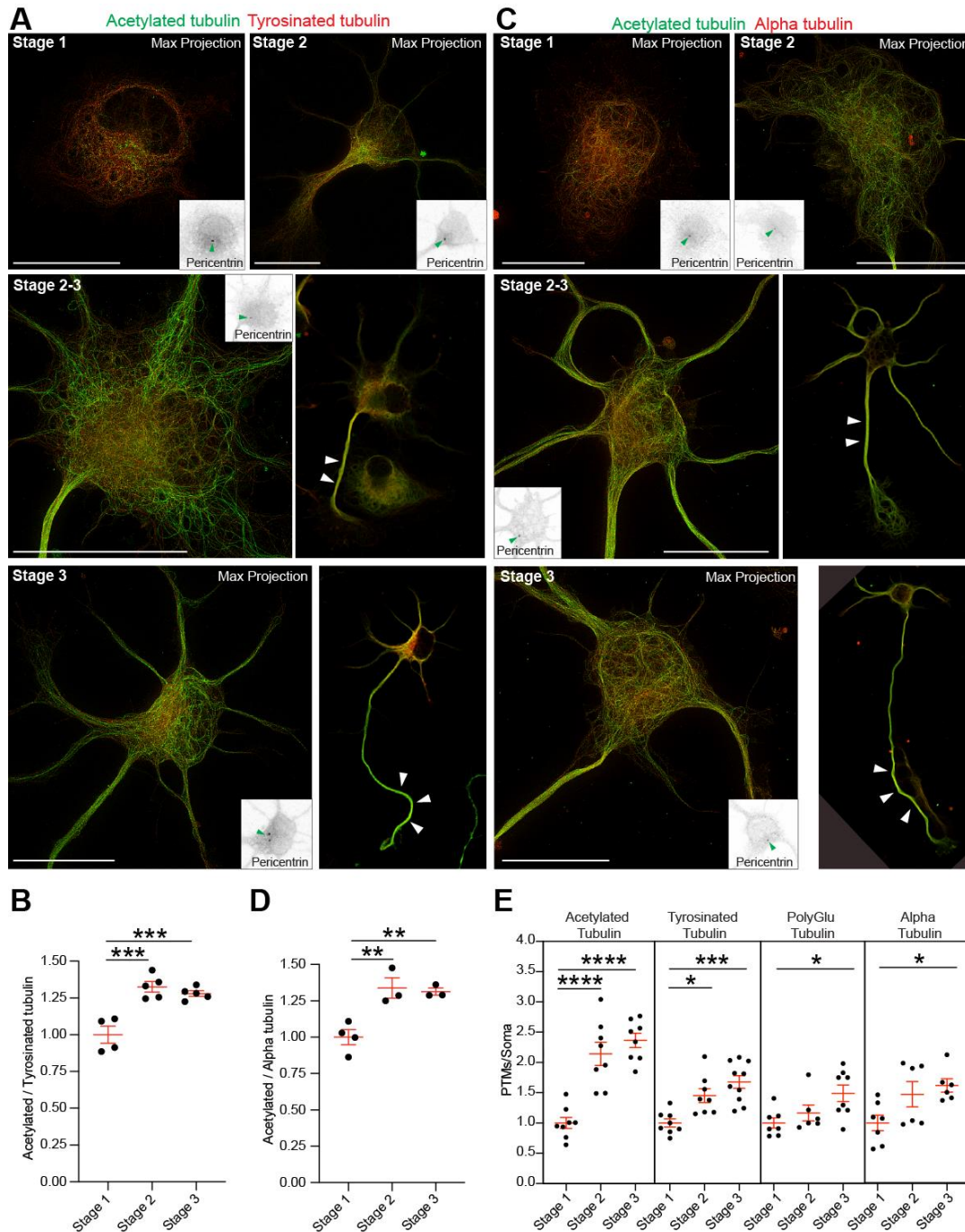


Figure 2-1: Acetylation of MTs spreads radially from the centrosomal area toward the growing neurites before morphological polarization and significantly into the growing axon after symmetry breakage. (A) STED images of acetylated and TyrTub immunostained hippocampal neurons at stages 1 and 2, transition from stage 2 to stage 3, and stage 3. **(B)** STED image quantifications showing ratio of acetylated to TyrTub signal area in the soma of stage 1, 2, and 3 neurons.

(C) STED images of acetylated and α -tubulin immunostained stage 1, 2, transition 2-3, and 3 hippocampal neurons. **(D)** STED image quantifications showing ratio of AcetyTub to α -tubulin signal area in the soma of stage 1, 2, and 3 neurons. **(E)** Area of tubulin PTMs-acetylated, tyrosinated, polyglutamylated tubulin, and α -tubulin normalized to soma area in stages 1, 2, and 3 neurons. In (A) and (C), white arrowheads denote AcetyTub enrichment; green arrowhead (insets) denotes centrosome (labeled by pericentrin). Scale bars: 10 μ m (A and C). Data in (B), (D), and (E) are represented as mean \pm SEM; replicates are distinguished by circles in the graphs. * $p < 0.05$, ** $p < 10^{-2}$, *** $p < 10^{-3}$, and **** $p < 10^{-4}$ by one-way ANOVA. (Quantification by Dr. Meka, ZMNH, Hamburg; imaging by Dr. Meka and Oliver Kobler, CNI, Magdeburg)

After differentiation from stage 1 to stage 3, the area enriched with AcetyTub was significantly enlarged and expanded from the centrosome to the cell periphery, based on the ratio of the PTM-positive area versus soma area (Figure 2-1A, C, E). Accordingly, the signal of other PTM-positive tubulins had a similar but weak trend, suggesting axonal polarization is preceded by stabilized MTs.

Notably, neurons exhibited a significant increase in the ratio of fluorescence intensities of AcetyTub versus TyrTub from stage 1 to stage 3 (Figure 2-1B), which is used to rate microtubule stability. Similar results were obtained by comparison of AcetyTub to α -tubulin (Figure 2-1D). It is noteworthy to mention that the increased ratio was due to a relative increase of AcetyTub over TyrTub or α -tubulin within the cell body. However, this was not the case for PolyGluTub to TyrTub/ α -tubulin, which showed no detectable changes (Figure 2-2B, D). These results suggest that a subset of stable MTs (acetylated MTs) spread out radially from the centrosomal area to the growing neurites, and eventually get enriched specifically in the longest neurite or future axon.

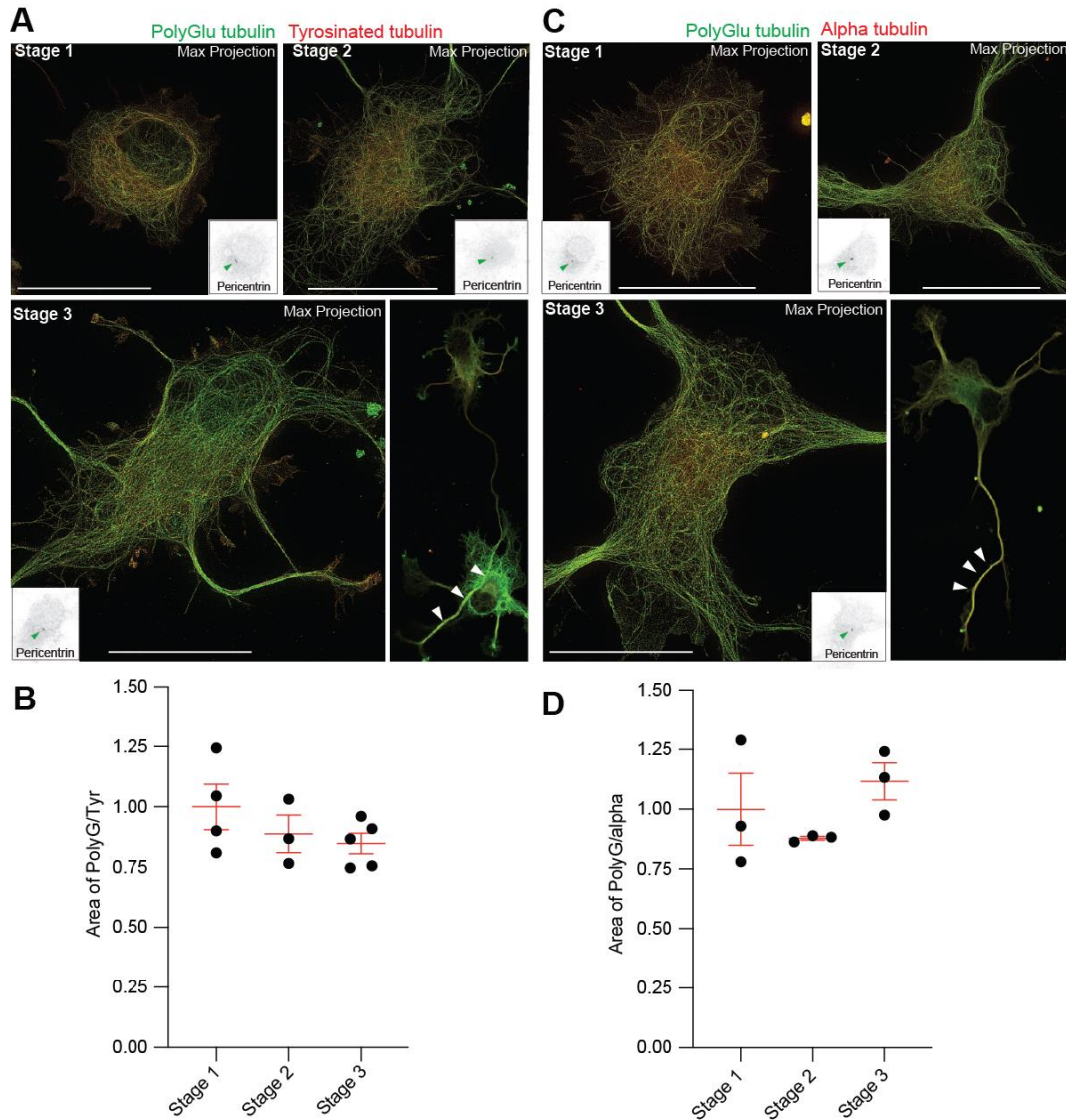


Figure 2-2: Polyglutamylated MT distribution related to tyrosinated MTs and α -tubulin around the centrosome in the soma of developing neurons. (A) STED images of polyglutamylated and tyrosinated tubulin immunostaining in stage 1, stage 2, and stage 3 hippocampal neurons. White arrowheads point to polyglutamylated tubulin enrichment in stage 2-3 cell and stage 3 growing axons. Insets: Centrosome labelled by anti-pericentrin antibody staining indicated by green arrowhead. Scale bar: 10 μ m. **(B)** Quantifications from STED images showing ratio of polyglutamylated to tyrosinated α -tubulin around the centrosome in the soma of developing neurons. STED tubulin signal area in the soma of stage 1 (n = 4), stage 2 (n = 3) and stage 3 (n = 5) neuronal soma. Mean \pm SEM values for stage 1 neurons = 1.000 ± 0.0947 and stage 2 neurons = 0.8886 ± 0.07745 , and stage 3 neurons = 0.8478 ± 0.0422 . P = 0.3117 by one-way ANOVA, post hoc Tukey's test. **(C)** STED images of polyglutamylated and α -tubulin immunostaining in stage 1, stage 2, transition stage 2-3 cell and stage 3 hippocampal neurons. White arrowheads indicated polyglutamylated tubulin enrichment in stage 2-3 cell and stage 3 growing axons. Insets: Centrosome labelled by anti-pericentrin antibody staining indicated by green arrowhead. Scale bar: 10 μ m. **(D)** Quantifications from STED images showing ratio of polyglutamylated to α -tubulin signal area in the soma of stage 1 (n = 3), stage 2 (n = 3) and stage 3 (n = 3) hippocampal neurons.

3) neuronal soma. Mean \pm SEM values for stage 1 neurons = 1.000 ± 0.1512 and stage 2 neurons = 0.8785 ± 0.0079 , and stage 3 neurons = 1.117 ± 0.0774 . $P = 0.3004$ by one-way ANOVA, post hoc Tukey's test. (Quantification by Dr. Meka, ZMNH, Hamburg; imaging by Dr. Meka and Oliver Kobler, CNI, Magdeburg)

2.1.2 An increase of somatic microtubule stability precedes axon formation

To test whether the MT remodeling in the soma influences axon extension, I applied a pharmacological treatment with cytochalasin D (CytoD) which is a well-known strategy to challenge neuronal polarity by disruption of actin polymerization and induction of multiple axons (Bradke and Dotti, 1999). Therefore, it is hypothesized that the formation of supernumerary axons induced by CytoD would be precluded due to the lack of stable MTs that support the extension of axons. To prove this, cultured hippocampal cells were treated with 2 mM CytoD right after plating (0 h) and ~30 h after plating for 2 days.

Importantly, at the time point of ~30 h after plating, most of the untreated cells were at stage 2 based on the morphological analysis (Figure 2-3B). Interestingly, cells treated with CytoD at 0 h did not produce multiple axon-like processes characterized by axonal identity marker Tau1 in comparison to the control DMSO-treated cells (Figure 2-3A, C). However, CytoD treatment at ~30 h after plating increased the proportion of neurons growing out multiple axons compared with the control group (Figure 2-3A, C). As shown in 2.1.1, stage1 neurons possessed less acetylated/stable MTs than stages 2/3 neurons (Figure 2-1), so it is possible that at 0 h the deficiency of acetylated/stable MTs prevents the induction of multiple axons. To explore this possibility, I treated cells parallelly with the MT-stabilizing drug Taxol (Witte et al., 2008) with a concentration of 5 nM for 2 days, which showed neurons producing more than one axon. At both time points (0 h and ~30 h after plating), Taxol treatment significantly increased the percentage of cells with several axons compared to control DMSO-treated cells (Figure 2-3A, C).

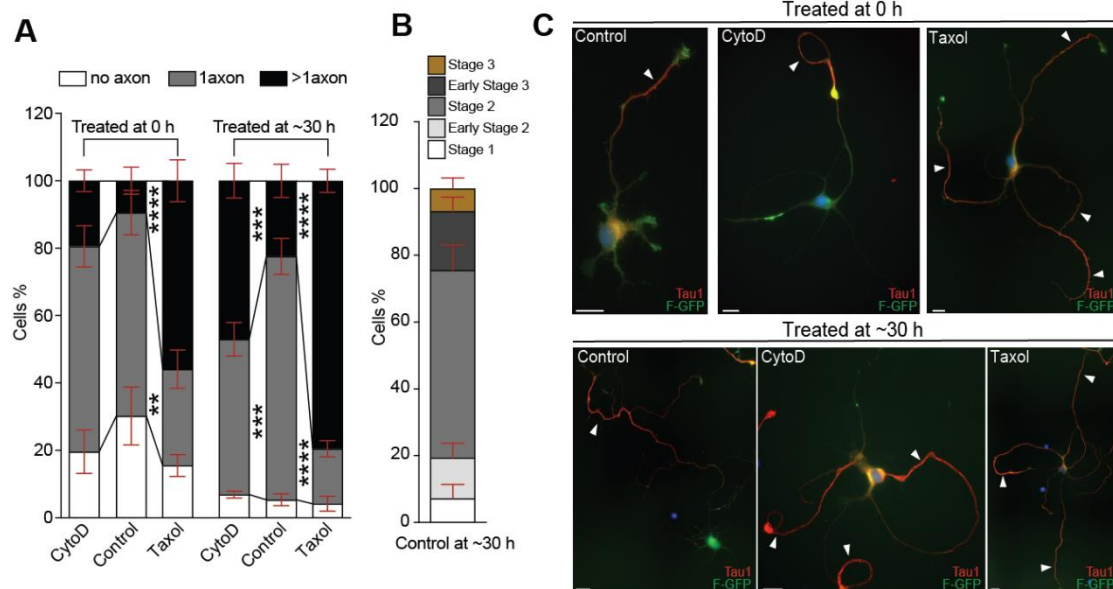


Figure 2-3: Pharmacological manipulation of the cytoskeleton unmasks actin disruption (by CytoD) induced multipolarity is time-dependent, and MT stabilization (by Taxol) induces multiple axon. (A) Quantifications show the percentage of neurons that were either treated immediately (0 h) or ~ 30 h of plating in vitro with DMSO or 2 μ M CytoD or 5 nM Taxol for 48 h differentiated to have no axon or 1 axon or more than 1 axon. Mean \pm SEM values for percentage of cells treated at 0 h with DMSO: no axons = 30.22 ± 8.554 , 1 axon = 60.32 ± 6.606 , more than 1 axon = 9.463 ± 3.979 ; CytoD: no axons = 19.65 ± 6.441 , 1 axon = 60.94 ± 6.129 , more than 1 axon = 19.42 ± 3.226 ; Taxol: no axons = 15.56 ± 3.195 , 1 axon = 28.54 ± 5.698 , more than 1 axon = 55.91 ± 6.196 ; treated at ~ 30h with DMSO: no axons = 5.333 ± 1.781 , 1 axon = 72.23 ± 5.354 , more than 1 axon = 22.44 ± 4.914 ; CytoD: no axons = 6.898 ± 1.021 , 1 axon = 46.09 ± 4.951 , more than 1 axon = 47.02 ± 5.115 ; Taxol: no axons = 4.180 ± 2.181 , 1 axon = 16.34 ± 2.419 , more than 1 axon = 79.48 ± 3.403 . $\alpha = 0.05$ by two-way ANOVA, post hoc Tukey's test, **** $P < 0.0001$, *** $P < 0.001$, ** $P < 0.01$. Data were obtained from 4 different hippocampal cultures. **(B)** Quantifications showing the percentage of neurons (untreated) after ~ 30 h of plating in vitro in different stages of development, stage 1 to stage 3. **(C)** Images of Farnesylated-GFP (F-GFP) transfected neurons that were either treated immediately (0 h) or ~ 30 h of plating in vitro with DMSO or 2 μ M CytoD or 5 nM Taxol for 48 h. The cells were then PFA fixed for Tau1 (shown in red) immunostainings to confirm axonal identity of the neurites (indicated by white arrowheads). Scale bar: 10 μ m. (Quantification by Dr. Meka, ZMNH, Hamburg)

Consistently, when the treated cells were kept growing *in vitro* for 7 days to further corroborate the axonal identity with Ankyrin-G immunostaining (see details in Meka et al., 2022), neurons treated at 0 h with CytoD did not augment the proportion of Ankyrin-G-positive processes, while neurons treated with Taxol at 0 h produced several Ankyrin-G-positive processes compared with control DMSO-treated neurons. Moreover, the long-term time-lapse analysis

(see details in Meka et al., 2022), which enabled monitoring the developmental process of stage 1 and 2 hippocampal cells treated with CytoD/Taxol, further verified that the stage 2 neurons, rather than stage 1 neurons, produced multiple axons when treated with CytoD. These results confirmed that the shortage of stable MTs at stage 1 is the limiting factor to produce multiple axons in the absence of an organized actin network.

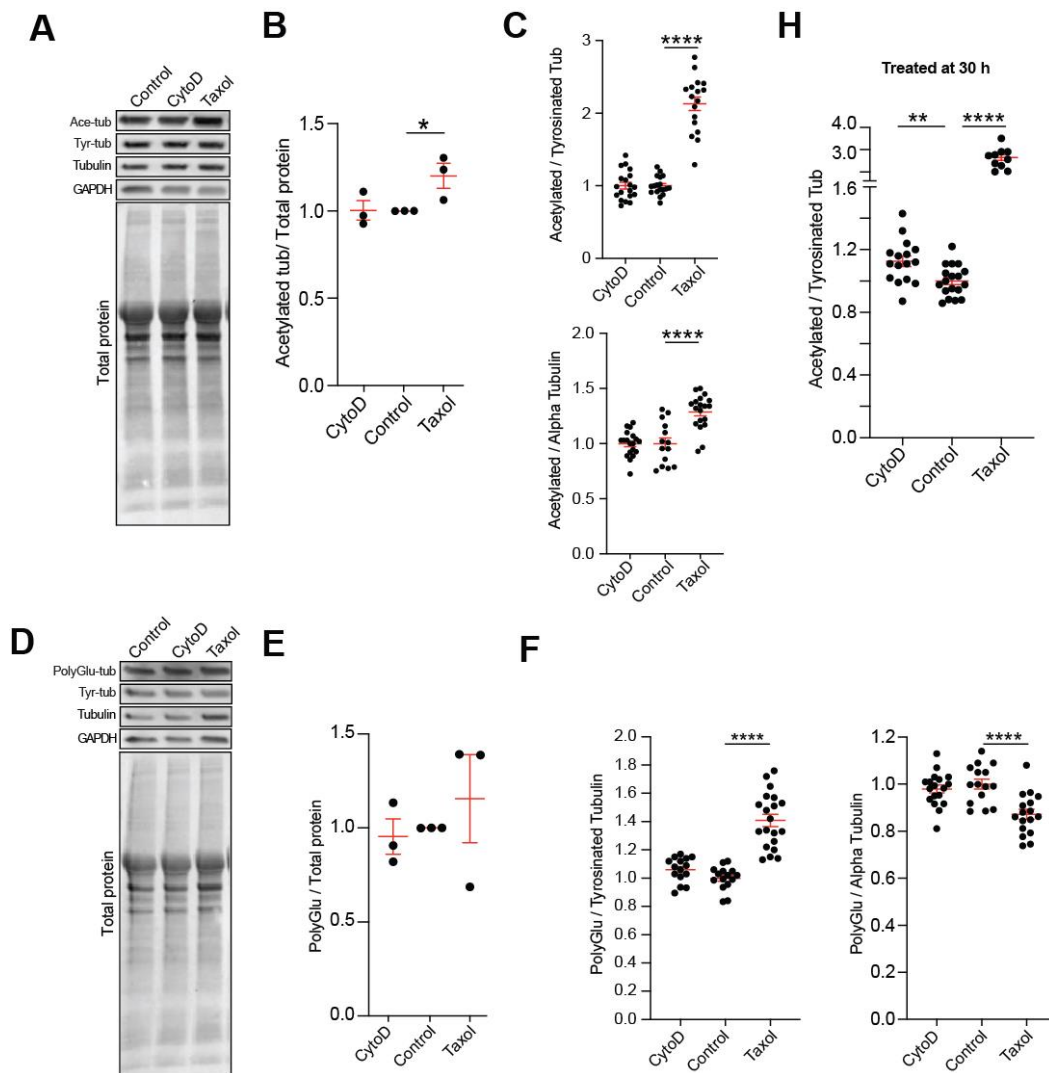


Figure 2-4: Contrary to MT stabilization (by Taxol), CytoD-induced multipolarity is dependent on the developmental stage of the neurons. (A) Western blot images of tubulin PTMs (acetylated, tyrosinated), total tubulin, GAPDH and Revert loading (for labeling total protein) from rat cortical neuron lysates treated with 2 μ M CytoD and 5 nM Taxol immediately (0 h) after plating and cultured for 18 h. **(B)** Normalized acetylated to total tubulin levels from rat cortical neuron lysates from untreated, treated with 2 mM CytoD and 5 nM Taxol immediately (0 h) after plating, and cultured for 18 h. Scale bars, 10 mm (A). **(C)** Ratio of acetylated to TyrTub (up) and acetylated to α -tubulin (down) signal

intensities in the soma of untreated, 2 mM CytoD-treated, and 5 nM Taxol-treated neurons immediately (0 h) after plating and PFA fixed 18 h later. **(D)** Western blot images of tubulin PTMs (polyglutamylated, tyrosinated), total tubulin, GAPDH and Revert loading (for labeling total protein) from rat cortical neuron lysates treated with 2 μ M CytoD and 5 nM Taxol immediately (0 h) after plating and cultured for 18 h. Data in B and C are represented as mean \pm SEM; replicates are distinguished by circles in the graphs. * $p < 0.05$ and **** $p < 10^{-4}$ by unpaired t test. **(E)** Quantifications comparing normalized polyglutamylated to total tubulin levels from rat cortical neuron lysates from untreated, treated with 2 μ M CytoD and 5 nM Taxol immediately (0 h) after plating, and cultured for 18 h cell lysates were obtained from 3 different experiments. **(F)** Quantifications comparing the intensity ratio of polyglutamylated to tyrosinated tubulin (left) and polyglutamylated to α -tubulin (right) in the soma of untreated, 2 μ M CytoD- and 5 nM Taxol-treated neurons 0 h after plating, and PFA-fixed 18h later. Polyglutamylated to tyrosinated tubulin: Mean \pm SEM values of Control cells = 0.9998 ± 0.0214 , CytoD treated cells = 1.061 ± 0.02252 , Taxol treated cells = 1.408 ± 0.0435 . $P < 0.0001$ by one-way ANOVA, post hoc Tukey's test, **** $P < 0.0001$. $n = 15$ in Control, 15 in CytoD and 20 in Taxol group. Polyglutamylated tubulin to α -tubulin: Mean \pm SEM values of Control cells = 1.000 ± 0.02103 , CytoD treated cells = 0.9794 ± 0.01698 , Taxol treated cells = 0.8721 ± 0.02129 . $P < 0.0001$ by one-way ANOVA, post hoc Tukey's test, **** $P < 0.0001$. $n = 15$ in Control, 18 in CytoD and 17 in Taxol group. **(H)** Quantifications comparing signal intensity ratios of acetylated and tyrosinated tubulin in the soma of untreated, 2 μ M CytoD and 5 nM Taxol treated neurons ~ 28 h after plating, and PFA-fixed 18 h later. Mean \pm SEM values of Control cells = 1.000 ± 0.02338 , CytoD treated cells = 1.126 ± 0.03439 , Taxol treated cells = 2.646 ± 0.1255 . $P < 0.0001$ by one-way ANOVA, post hoc Tukey's test, **** $P < 0.0001$ for Control vs. Taxol groups. ** $P = 0.0041$ by unpaired Student's t-test for Control vs. CytoD groups. $n = 18$ in Control, 16 in CytoD and 12 in Taxol groups. (Western Blot by Dr.Henis, ZMNH, Hamburg; quantification by Dr. Meka, ZMNH, Hamburg)

To further investigate the association of acetylated/stable MTs with axon formation, I performed STED and confocal microscopy analysis of AcetyTub/TyrTub-labeled neurons to examine MT remodeling more directly, coupled with western blot (WB) analysis to test for changes in protein content in cells treated with CytoD and Taxol for 2 days, respectively.

Results from the fluorescence intensity ratios of AcetyTub to TyrTub/ α -tubulin in the soma indicated that cells treated with CytoD at 0 h, contained much fewer somatic acetylated MTs in comparison to those treated with Taxol, while they showed no difference to control DMSO-treated cells (Figure 2-4C). Similar results were obtained for total AcetyTub by WB analysis (Figure 2-4A, B). Regarding PolyGluTub, cells treated with CytoD/Taxol at 0 h showed no detectable increment of this MT modification with WB analysis, compared to

DMSO-treated cells (Figure 2-4D, E). Nevertheless, the levels of PolyGluTub normalized to TyrTub, were increased in the soma upon Taxol treatment (Figure 2-4F). Interestingly, the intensity ratio of PolyGluTub to α -tubulin in the soma decreased significantly after Taxol treatment (Figure 2-4F), which contrasted with the ratio of acetylated tubulin to α -tubulin. Therefore, it gives a hint that MT stabilization, especially acetylation promotes axon outgrowth in early developing neurons. Importantly, when CytoD/Taxol was applied to cells at ~30 h after plating, both indicated a significant increment in AcetyTub intensity compared to the control DMSO-treatment (Figure 2-5B, C).

Overall, these results suggest that somatic acetylated MT enrichment is required for axon formation. Additionally, the results show that multipolarity induced by CytoD is stage-dependent, since stage 2 cells with more stable MTs, but not stage 1 cells, subsequently form multiple axons.

2.1.3 The centriolar protein Cep120 modulates MTs stability determining axon formation

As shown in 2.1.1, acetylated/stable MTs are concentrated around the centrosome followed by a radial diffusion and eventually enriched in the future axon as cultured neurons differentiate from stage 1 to stage 3. Moreover, axonal growth is compromised by inhibition of MT nucleation at the centrosome (Ahmad et al., 1994). Hence, if or how does the centrosome mechanistically regulate acetylation/stabilization of MTs in the developing axon? To this end, Cep120 was perturbed to evaluate the necessity of the centrosome in MT remodeling, as Cep120 is a centriolar protein shown to affect MT stability, and loss of Cep120 impairs centriole maturation, cilia formation and MT acetylation at the cilia (Betleja et al., 2018; de Anda et al., 2010; Joseph et al., 2018; Xie et al., 2007).

Immunostaining data indicated that Cep120 was present across stages 1-3 in cultured developing neurons (see details in Meka et al., 2022). Cep120 short hairpin RNA (shRNA) was used to specifically silence the expression of Cep120 in cortical neurons (de Anda et al., 2010; Xie et al., 2007), to investigate the effects on MT stabilization and axon formation. To this end, Cep120 shRNA or control shRNA together with tDimer expressing plasmids were electroporated into embryonic cortices at embryonic day 15 (E15). Two days later at E17, cortical neurons were dissociated from these transfected cortices. In parallel, Cep120-GFP together with tDimer expressing plasmids were introduced to upregulate Cep120 expression. Dissociated cortical neurons were then cultured for additional 48-72 h and prepared for immunostaining to assess MT modifications and neuronal morphology.

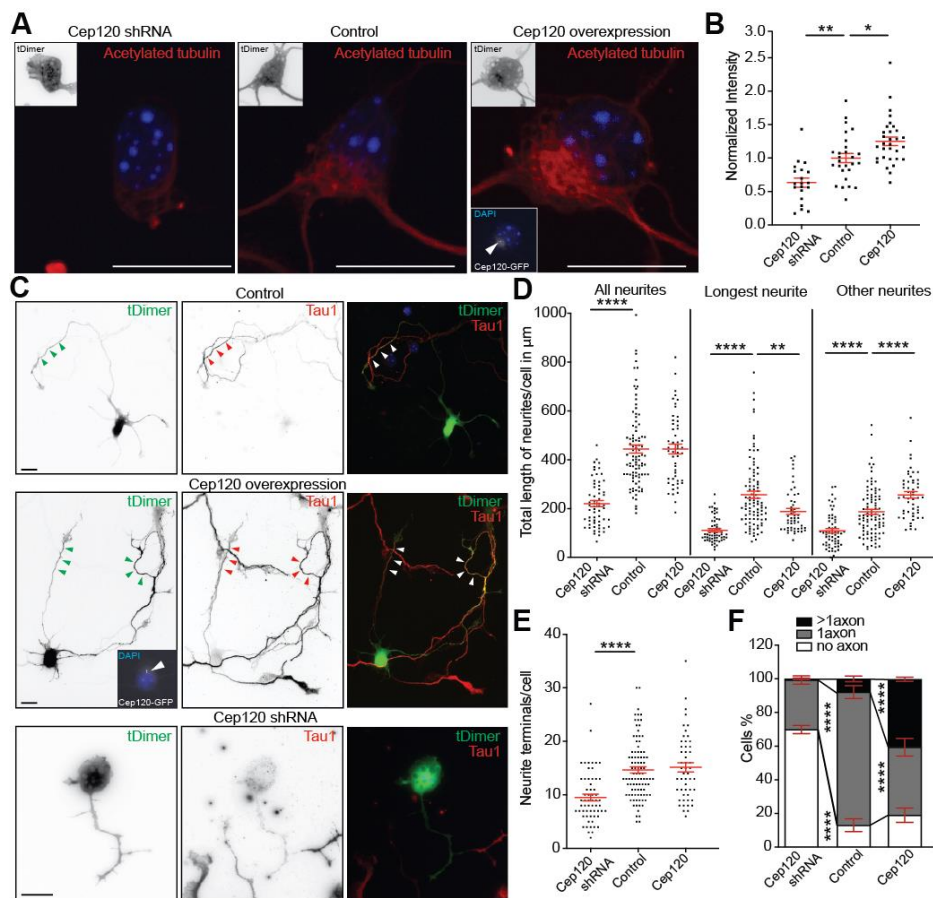


Figure 2-5: Cep120 downregulation and upregulation, through MT acetylation, bidirectionally regulate axon formation. (A) Confocal maximum projection images of mouse

cortical neurons co-transfected at E15 via IUE with tDimer and Cep120 shRNA, or control or Cep120-GFP (arrowhead in the inset) cultured at E17 for 48 h immunostained with AcetyTub antibody. **(B)** Normalized AcetyTub intensities in the soma of neurons expressing Cep120 shRNA, control, and Cep120-GFP as shown in A. **(C)** Epifluorescence images of mouse cortical neurons co-transfected via IUE at E15 with tDimer and Cep120 shRNA or control or Cep120-GFP (indicated by arrowhead in the inset) cultured at E17 for 48 or 72 h immunostained with Tau1 antibody to confirm the axonal identity of the neurites, indicated by white arrowheads. Quantification of neurite length (in mm) **(D)** and neurite terminals **(E)** in neurons expressing Cep120 shRNA, control, and Cep120-GFP as shown in C. **(F)** Percentage of Cep120 shRNA, control, and Cep120-GFP neurons, as shown in C, differentiated to have no axon, 1 axon, and >1 axon. Data shown in B, D, E, and F were obtained from cortical cultures of 3 or more IUE embryos from at least 2 different mothers. (Quantification partially by Dr. Meka and Carina Meta Friedrich, ZMNH, Hamburg)

The immunostaining and fluorescence intensity quantification of PTM-tubulin in the transfected neurons demonstrated that Cep120 downregulation reduced the levels of AcetyTub (Figure 2-5A, B), PolyGluTub, TyrTub, and total tubulin (Figure 2-6A) in the soma compared to control tDimer-transfected neurons. Conversely, Cep120 overexpression significantly augmented the levels of AcetyTub (Figure 2-5A, B), but not that of PolyGluTub, TyrTub, and total tubulin (Figure 2-6A) in the soma compared to controls, indicating that overexpression of Cep120 specifically enhanced the formation of acetylated MTs. These data imply that Cep120 is an instructive factor regulating MT stabilization. To further test this, neurons expressing Cep120 shRNA or Cep120-GFP were treated with a short pulse of nocodazole, which destabilizes/depolymerizes MTs. Consequently, Cep120 overexpression protected MTs against the depolymerization effect of nocodazole and correspondingly increased the content of AcetyTub in the soma area (Figure 2-6B, C). Importantly, Cep120 overexpression induced neurons to extend several axons and, overall, transfected neurons developed a more complex structure characterized by longer neurites compared to control neurons (Figure 2-5C-F). In contrast, the downregulation of Cep120 expression precluded axon formation and decreased the complexity of neurons, which featured fewer neurites and reduced neurite length (Figures 2-5C-F). Likewise, *in vivo* data indicated that

the morphological complexity of migrating neurons was modulated by the levels of Cep120 in a similar manner (see details in Meka et al., 2022). To sum up, the presence of Cep120 influences MT stability during the polarized emergence of axons.

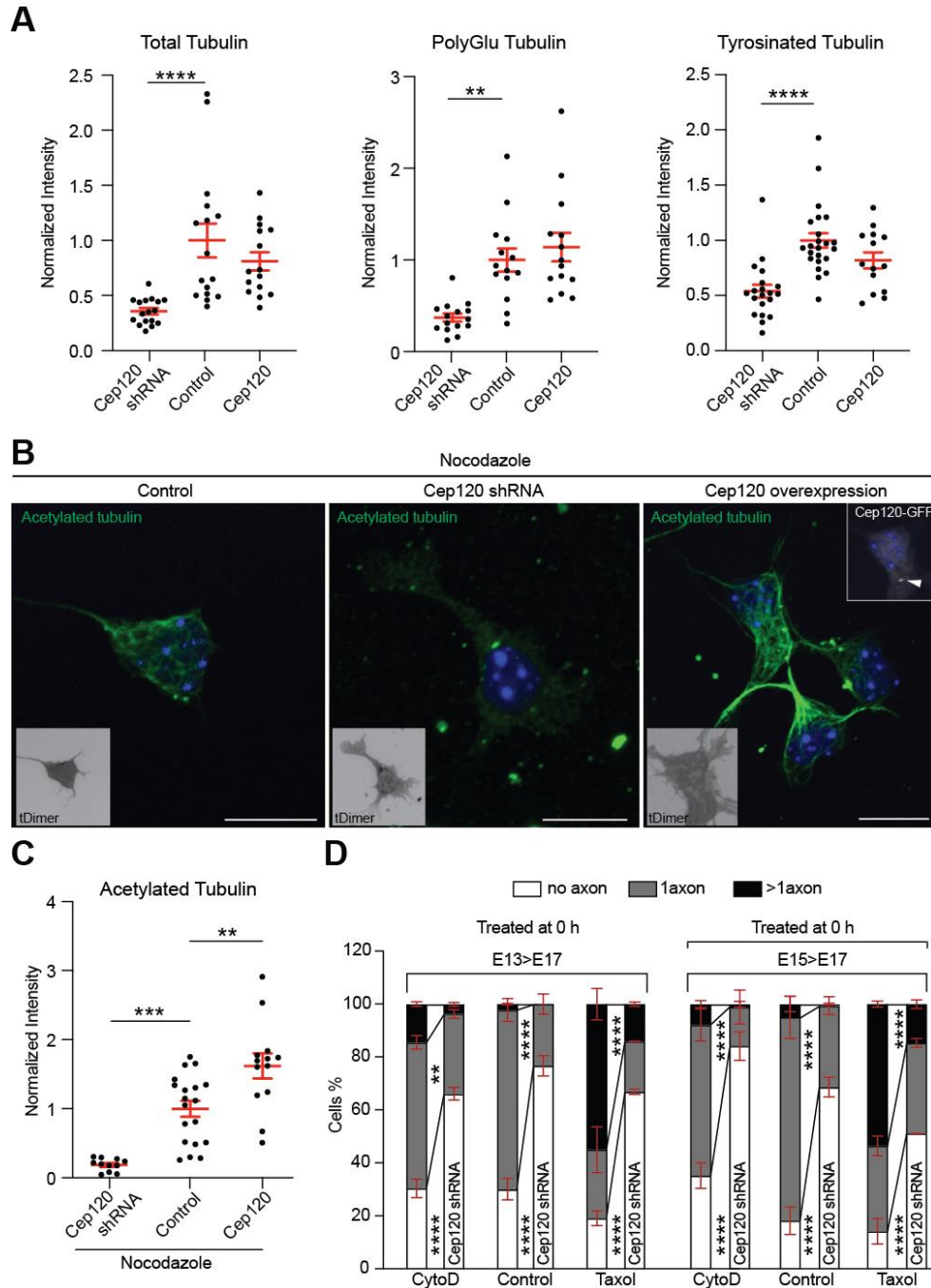


Figure 2-6: Effects of Cep 120 knockdown and overexpression on tubulin PTMs and axon formation. (A) Quantifications (left to right) comparing normalized total tubulin, polyglutamylated and tyrosinated tubulin intensities in the soma of neurons expressing control, Cep120 shRNA, and

Cep120-GFP. Total tubulin: $P = 0.0001$ by one-way ANOVA, post hoc Tukey's test, **** $P < 0.0001$, ** $P = 0.0071$. $n = 16$ control, 17 Cep120sh and 15 Cep120-GFP cells; PolyGlu tubulin: $P < 0.0001$ by one-way ANOVA, post hoc Tukey's test, **** $P < 0.0001$, ** $P = 0.0012$. $n = 14$ control, 15 Cep120sh and 14 Cep120-GFP cells; Tyrosinated tubulin: $P < 0.0001$ by one-way ANOVA, post hoc Tukey's test, **** $P < 0.0001$, * $P = 0.0193$. $n = 23$ control, 20 Cep120sh and 14 Cep120-GFP cells. **(B)** Confocal maximum projection images of mouse cortical neurons co-transfected at E15 via IUE with tDimer and Cep120 shRNA, or control or Cep120-GFP (indicated by arrowhead in the inset), cultured at E17 for 48 h and treated with 6 μM Nocodazole for 30 min before fixing the cells with 4% PFA for 2 min, followed by 3 min ice-cold methanol, and immunostained with acetylated tubulin antibody. Scale bar: 10 μm . **(C)** Quantifications comparing normalized acetylated tubulin intensities in the soma of Nocodazole-treated neurons expressing, control ($n = 19$), Cep120 shRNA ($n = 11$), and Cep120-GFP ($n = 13$) as shown in B. $P < 0.0001$ by one-way ANOVA, post hoc Tukey's test, **** $P < 0.0001$, *** $P = 0.0002$, ** $P = 0.0030$. Data shown in A-C were obtained from cortical cultures of IUE mouse embryos from 2 different mothers. **(D)** Quantifications showing the percentage of cortical neurons from E13 versus E15 IUE brains co-transfected with Cep120sh and Venus, cultured at E17 and treated immediately (0 h) after plating with 2 μM CytoD or 5 nM Taxol for 2 days. Neurons differentiated to have no axon or 1 axon or more than 1 axon. Axonal identity in PFA-fixed cells was confirmed by Tau1 immunostainings. $\alpha = 0.05$ by two-way ANOVA, post hoc Tukey's test, **** $P < 0.0001$, *** $P < 0.001$, * $P < 0.05$. Data were obtained from cortical cultures of IUE mouse embryos from 2 different mothers. (Quantification partially by Dr. Meka and Carina Meta Friedrich, ZMNH, Hamburg)

To further explore the hypothesis that Cep120 is required and sufficient for axon formation, neurons with Cep120 knockdown by shRNA interference, were treated with Taxol, which promotes MT stabilization. It turned out that the Taxol treatment was unable/not enough to overcome the axon extension defect caused by Cep120 downregulation since these cells failed to form multiple axons, unlike the Taxol-treated control cells (Figure 2-7D). Similar results were obtained with CytoD application to Cep120 shRNA transfected cells, which could not produce supernumerary axons no matter when they lost the expression of Cep120, either at an early stage before polarization (E13), or at a later already polarized stage (E15) (Figure 2-7D). Altogether, these results show that Cep120 organizes acetylated MTs and thereby regulates axon formation.

2.2 Somatic F-actin translocation acts as an inhibitor for neurite growth

The above results indicated that during the early developing stages, the centrosome regulates MT stabilization/acetylation to set a proper context initiating axon formation. Interestingly, besides the role of the centrosome in organizing microtubules, it can also serve as an actin organization center *in vitro* (Farina et al., 2016). Notably, the recent work from us revealed that in neurons, somatic actin is organized around the centrosome, forming actin-asters to release actin filaments/F-actin into the growing neurites (Meka et al., 2019). However, the underlying mechanisms of this somatic F-actin translocation and the potential role of the somatic F-actin in regulation of asymmetrical outgrowth remained unsolved.

2.2.1 Somatic F-actin translocates into neurites to restrict cellular growth

In the process of neuronal polarization, the axon is preferentially specified with the fastest growth rate followed by dendrite development, indicating these two distinct domains are not growing simultaneously. It is suggested that some internal inhibitory signaling from the growing axon propagates to all other minor neurites (future dendrites) precluding their growth during axon elongation (Andersen and Bi, 2000). It is thereby plausible to assume that somatic F-actin might be such a negative signal to negatively regulate neurite growth. To investigate this, I performed photoactivation in cultured hippocampal cells (stages 2-4) transfected with photoactivatable GFP-Utrophin (PaGFP-UtrCH), which specifically binds to F-actin (Burkel et al., 2007). PaGFP-UtrCH photoactivation is irreversible in response to 405 nm light with an emission peak at 517 nm. Here, I followed the same protocols of photoactivation in the soma previously reported by us (Meka et al., 2019). To trace the movement of somatic F-actin, several somatic F-actin puncta (photoactivated circle around 5 μm diameter) were illuminated at once which could yield enough traceable activated signals when spreading further.

The previous work indicated that in DIV1 neurons (stage 1), somatic F-actin was organized near the centrosome. During further development, they were released rapidly into the periphery, which was visualized by photoactivation of somatic PaGFP-UtrCH (Meka et al., 2019). At stage 2 and 3, photoactivated PaGFP-UtrCH signal dispersed from the activated area into the whole cell body and finally segregated preferentially into the tips of minor/shorter processes, rather than the longest neurites, which could be the growing axon (Figure 2-7A).

Consistently, the quantification showed that the photoactivated PaGFP-UtrCH signal decreased in the photoactivated area of the soma over time (Figure 2-7B). Meanwhile, photoactivated PaGFP-UtrCH signal gradually reached shorter neurites and increased continuously over time indicating somatic F-actin translocation/movement (Figure 2-7B). Once one neurite morphologically preferentially elongated (from stage 2 to stage 3), less photoactivated PaGFP-UtrCH signal was detected in this neurite, which was further confirmed by the analysis of the correlation between neurite length and the intensity of PaGFP-UtrCH signal (Figure 2-7B). At stage 4, however, when dendrite outgrowth was ongoing, the somatic photoactivated PaGFP-UtrCH signal remained in the cell body without detection of photoactivated PaGFP-UtrCH signal in neurites (Figure 2-7C, D). It suggests that this somatic F-actin delivery is restricted into early developing neurons. Overall, these results indicate that the somatic F-actin is translocated preferentially into shorter neurites and its abundance could negatively correlate with neurite growth.

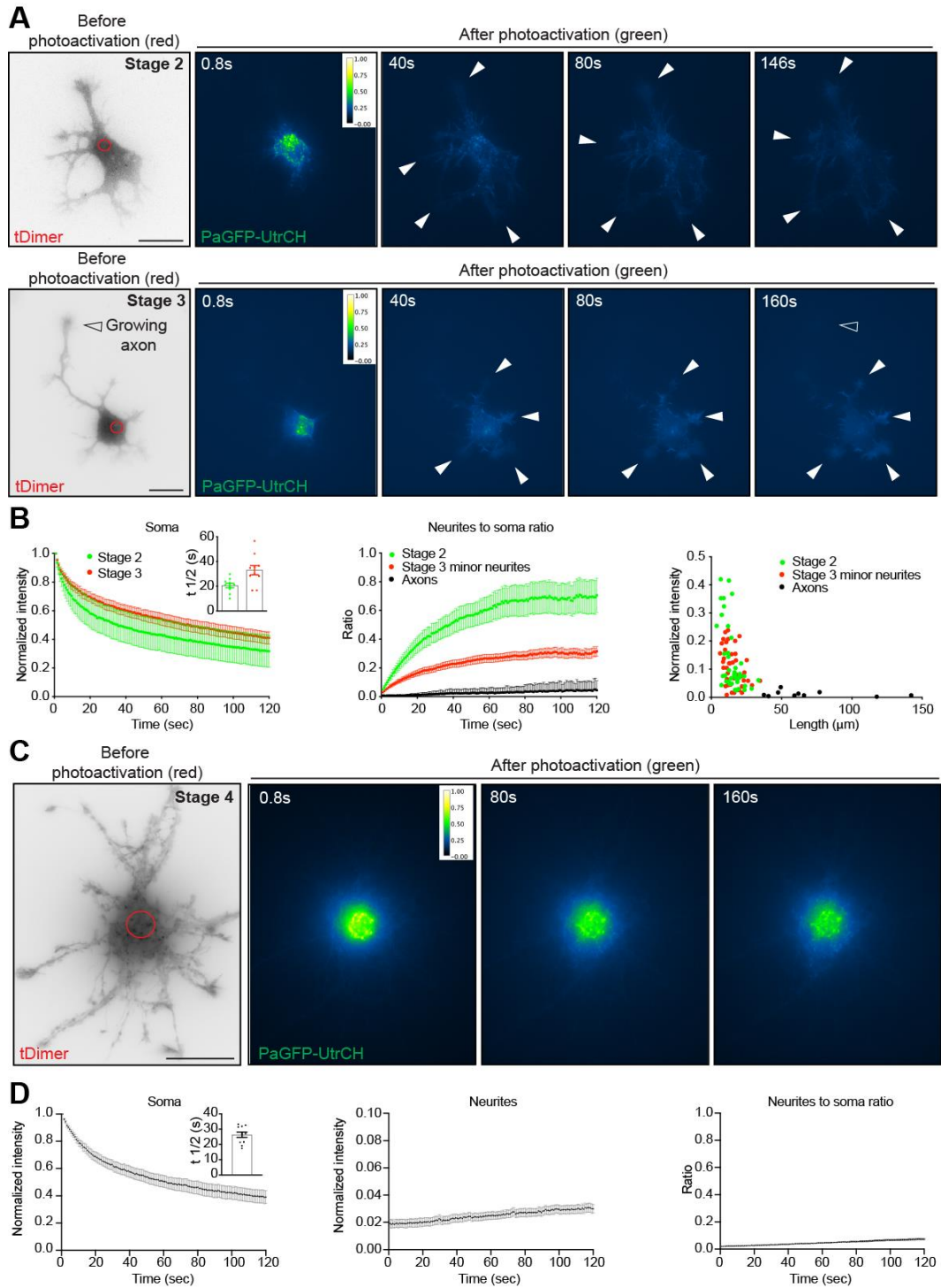


Figure 2-7: Radial somatic F-actin is specifically delivered to shorter neurites in developing stage 2 and stage 3 neurons, but not to longer neurites or more matured stage 4 DIV8 neurons. (A) PaGFP-UtrCH and tDimer co-transfected stage 2 (upper row) and stage 3 (lower row) rat hippocampal neuron photoactivated in the soma with 405 nm laser (red circle with a diameter of 5.239 μ m). **(B)** Left panel: normalized intensity values in the photoactivated area of PaGFP-UtrCH expressing stage 2 and stage 3 cells. Inset graph: mean \pm SEM half-time ($t_{1/2}$) values in seconds: stage 2 = 20.60 \pm 1.819; stage 3 = 33.02 \pm 3.862. Middle panel: photoactivated signal in neurite tips over time relative to the average initial signal from the illuminated area for PaGFP-UtrCH expressing stage 2,

stage 3 cells. Right panel: quantification showing normalized intensity of photoactivated somatic PaGFP-UtrCH/F-actin enriched in the neurite tips in dependence on the length of the corresponding neurites. $n = 10$ per stage, cells were obtained from at least 3 different cultures. **(C)** PaGFP-UtrCH and tDimer co-transfected DIV8 (stage 4) rat hippocampal neuron photoactivated in the soma with 405 nm laser (red circle with a diameter of $5.239 \mu\text{m}$). **(D)** Left panel: normalized intensity values in the photoactivated area of PaGFP-UtrCH expressing DIV8 (stage 4) cells. Inset graph: mean \pm SEM half-time ($t_{1/2}$) values in seconds = 26.28 ± 1.711 . Middle panel: photoactivated signal in neurite shafts at 20 microns away from the soma over time relative to the average initial signal from the illuminated area for PaGFP-UtrCH expressing stage 4 cells. Right panel: neurite shaft to soma photoactivated signal intensity ratio of PaGFP-UtrCH. $n = 11$ cells from at least 3 different cultures. (Quantification and imaging by Dr. Meka, ZMNH, Hamburg)

To investigate whether somatic F-actin translocation into neurites suppresses neurite growth, I applied somatic PaGFP-UtrCH photoactivation in stage 2-3 neurons to track the translocation of photoactivated PaGFP-UtrCH signal into neurites and monitor neurites growth afterwards. Accordingly, the length of neurites before and after photoactivation was measured to examine how neurites behave in relation to the content of F-actin that they received. In stage 2 neurons, 1 h after photoactivation the neurite receiving less photoactivated PaGFP-UtrCH signal displayed apparent growth according to the measurement of the length (Figure 2-8A-C). Conversely, neurites receiving more photoactivated PaGFP-UtrCH signal retracted (Figure 2-8A-C). Moreover, the scenario was the same in the stage 3 neurons, where photoactivated PaGFP-UtrCH signal mostly translocated into shorter neurites, while the growing axon kept elongating with little detectable photoactivated PaGFP-UtrCH signal (Figure 2-8D-F). These results strongly suggest that somatic F-actin could serve as an inhibitory signal for neurite growth.

To further investigate this idea, I adopted a strategy to pharmacologically disrupt somatic F-actin organization by using CytoD, which induces somatic F-actin aggregation around the centrosome and blocks its transport into the cell periphery (Meka et al., 2019). Time-lapse analysis was performed to monitor neurite growth on stage 2 neurons expressing Lifeact-GFP during and after

CytoD treatment. Lifeact-GFP is an extensively used probe to visualize F-actin structure and dynamics in live-imaging study (Meka et al., 2019; Riedl et al., 2008; Xu and Du, 2021), which could offer a clear view of how changed F-actin behavior will influence neurite growth.

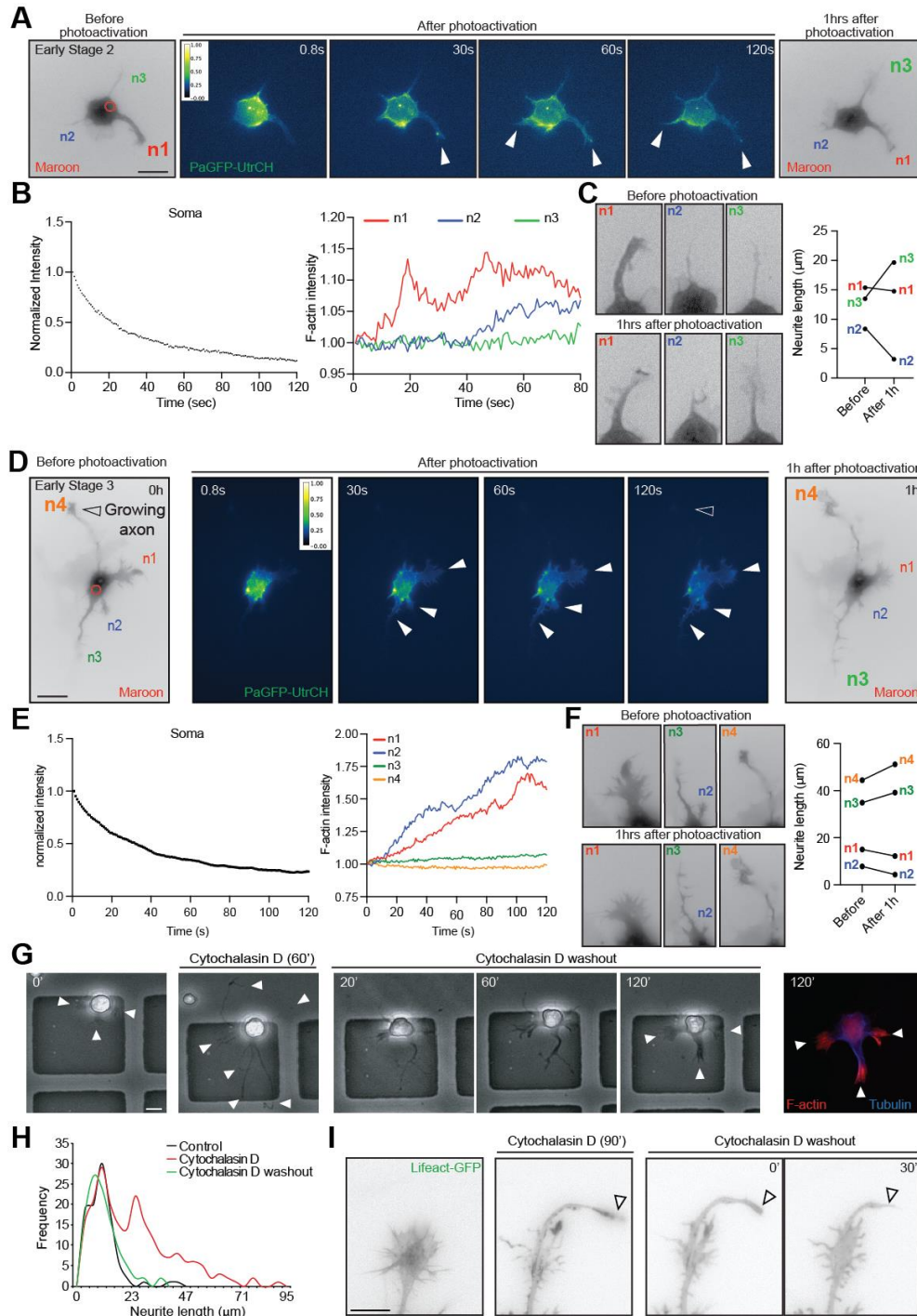


Figure 2-8: Somatic F-actin delivery negatively regulates neurite growth, and accordingly disruption of F-actin promotes neurite growth. (A) PaGFP-UtrCH and mMaroon1

co-transfected stage 2 rat hippocampal neuron photoactivated in the soma with 405 nm laser (red circle with a diameter of 5.239 μm), mMaroon1 imaged again 1 h after photoactivation to track neurite morphology changes. **(B)** Left panel: normalized intensity values in the photoactivated area of PaGFP-UtrCH expressing stage 2 cell. Right panel: photoactivated signal in neurite tips from 3 neurites, n1, n2, and n3 over time relative to the average initial signal from the neurite tips. **(C)** The changes in neurite length before and 1 h after photoactivation are shown in the cropped images of the neurites of the cell shown in A and the paired analysis graph. **(D)** PaGFP-UtrCH and mMaroon1 co-transfected early stage 3 rat hippocampal neuron were photoactivated in the soma with 405 nm laser (red circle with a diameter of 5.239 μm), mMaroon1 was imaged 1 h after photoactivation to track neurite morphology changes. **(E)** Left panel: normalized intensity values in the photoactivated area of PaGFP-UtrCH expressed in early stage 3 cell. Right panel: photoactivated signal in neurite tips from 4 neurites, n1, n2, n3 and n4 over time relative to the initial signal. **(F)** The changes in respective neurite length before and 1 h after photoactivation are shown in the cropped images of the neurites of the cell shown in D and the paired analysis graph. **(G)** Stage 2 cells treated for 60 min with 2 μM Cytochalasin D undergo neurite elongation, which was normalized after 120 min of washout. Post hoc immunostaining with F-actin (phalloidin-568) and tubulin (blue). **(H)** Quantification showing neurite outgrowth with Cytochalasin D treatment compared to control and after Cytochalasin D washout. **(I)** Images showing a neurite growth cone of a Lifeact-GFP transfected DIV 1 hippocampal neuron in the course of 90 min Cytochalasin D treatment and followed by washout. Kymographs with respective timestamps depict the loss of retrograde F-actin flow upon Cytochalasin D treatment and recovery followed by washout. (Quantification and imaging by Dr. Calderon de Anda and Dr. Meka, ZMNH, Hamburg)

As expected, the addition of CytoD induced neurite growth as previously shown (Bradke and Dotti, 1999) (Figure 2-8G, H). The morphology of growth cones underwent drastic changes caused by the removal of F-actin and impaired actin network shown by Lifeact-GFP (Figure 2-8I). Once CytoD was washout, however, F-actin reorganized in the neurite tips and induced neurite retraction, pushing neurons back into a less differentiated state (Figure 2-8G, I). Altogether, these results support the idea that somatic F-actin translocation into neurites act as an inhibitory signal for neurite growth.

2.2.2 Myosin II motors mediate somatic F-actin translocation into neurites

The above data indicated that during initial neuronal development, somatic F-actin is delivered radially into distal growth cones. However, what is the mechanism underlying this somatic F-actin delivery? Previous studies revealed that myosin II, which is an actin-directed motor, mediates actin assembly and

transport during contractile ring formation required for cytokinesis (Murthy and Wadsworth, 2005). Moreover, myosin II drives actin-bundle translocation during retrograde flow, thus coordinating F-actin treadmilling to sustain the motility of neuronal growth cones (Ishikawa and Kohama, 2007; Kollins et al., 2009; Medeiros et al., 2006; Wilson et al., 2010). Thus, it is conceivable to hypothesize that myosin II could be a suitable candidate to mediate somatic F-actin translocation into neurites.

To investigate the role of myosin II in somatic F-actin transport, PaGFP-myosin IIA plasmids were introduced into the cultured hippocampal cells which are used to examine whether somatic PaGFP-myosin IIA moves in a similar manner as somatic F-actin did after photoactivation. The results from 2.2.1 unveiled the characteristics of somatic F-actin translocation: at stage 2, somatic F-actin is delivered radially into minor process tips, and then at stage 3 during which one specific process elongates preferentially, somatic F-actin translocation is polarized into shorter neurites, not into this longer one. Therefore, I examined stage 2-stage 3 neurons to monitor myosin II movement. The time-lapse images showed that the photoactivated PaGFP-myosin IIA translocated from the soma into neurites in a similar fashion as photoactivated PaGFP-UtrCH with a preference for shorter neurites (Figure 2-9). The quantifications visualized both photoactivated signals decreased in the illuminated area of the soma over time concomitant with a fast increase of activated signals in the tips of shorter neurites (Figure 2-9B, C), while both activated UtrCH and myosin IIA signals were weakly detected in the longest neurites (Figure 2-9C).

I next applied a pharmacological strategy using blebbistatin - a specific inhibitor of myosin II - to further test the correlation of myosin II with somatic F-actin delivery (Kovács et al., 2004; Limouze et al., 2004). In the stage 1 neuron, the

activated somatic PaGFP-UtrCH signal was restricted to the soma area due to blebbistatin application, preventing their dispersion into the cell periphery or the small extensions (buds) of the cell body (Figure 2-9D, E). Further quantification analysis indicated that the buds of blebbistatin-treated neurons received no detectable PaGFP-UtrCH signal when photoactivated in the soma, unlike that of control neurons (Figure 2-9E). These results suggest the blebbistatin-induced myosin II inhibition affects somatic F-actin delivery.

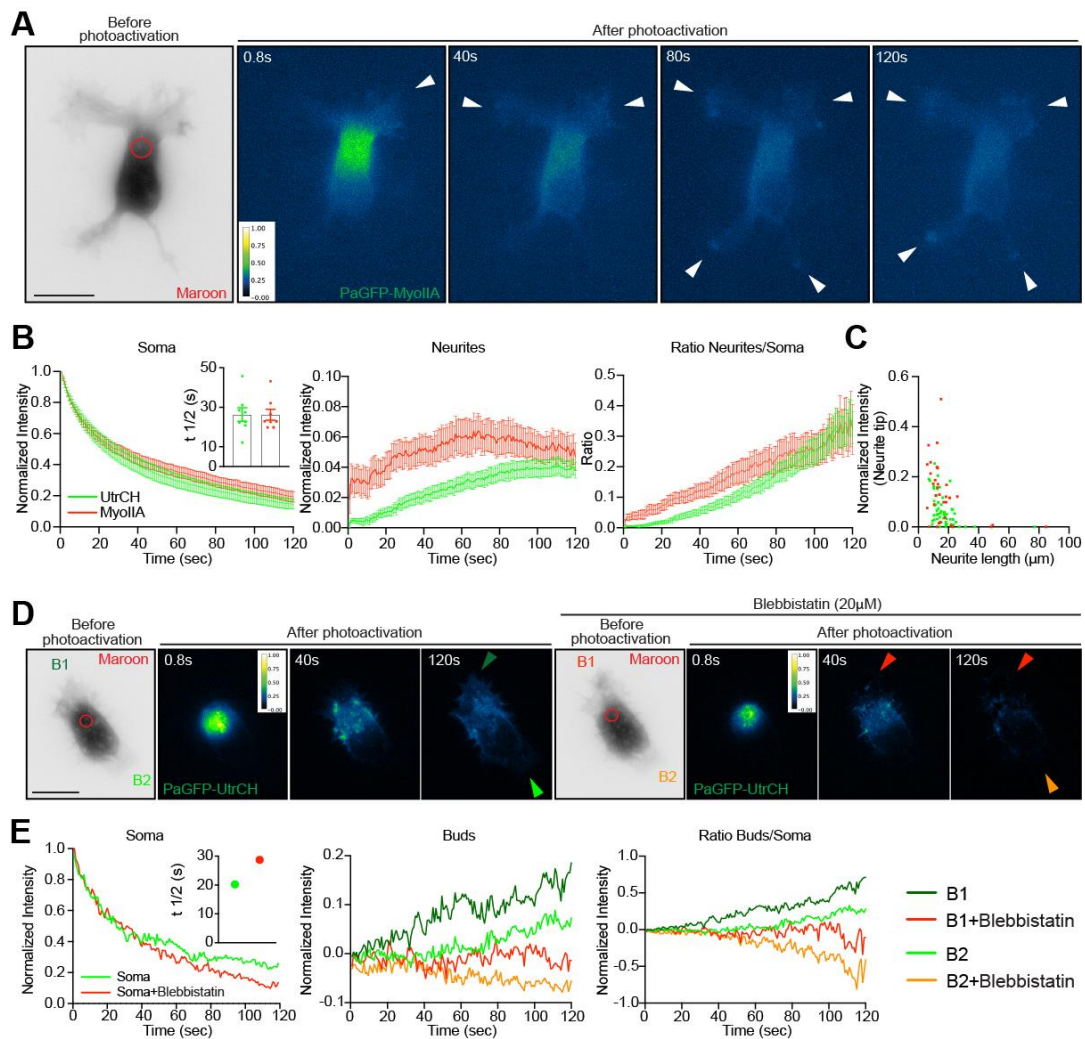


Figure 2-9: Radial delivery of somatic F-actin is myosin II-dependent. (A) PaGFP-Myosin IIA and mMaroon1 co-transfected stage 2 rat hippocampal neuron photoactivated in the soma with 405 nm laser (red circle with a diameter of 5.239 μm). (B) Left panel: normalized intensity values in the photoactivated area of PaGFP-UtrCH and PaGFP-Myosin IIA expressing stage 2 cells. Inset graph: mean \pm SEM half-time ($t_{1/2}$) values in seconds PaGFP-UtrCH = 26.32 ± 3.447 and PaGFP-Myosin IIA = 26.19 ± 2.801 . Middle panel: photoactivated signal in neurite tips relative to the average initial signal from the illuminated area for PaGFP-UtrCH/Myosin IIA expressing stage 2 cells. Right panel: ratio of

photoactivated PaGFP-UtrCH/Myosin IIA in neurite shaft to that in soma **(C)** Quantification showing normalized intensities of photoactivated somatic F-actin and Myosin IIA enriched in the neurite tips in dependence on the length of the corresponding neurites. For data shown in B and C, $n = 8$ cells per group from at least 3 different cultures. **(D)** PaGFP-UtrCH and mMaroon1 co-transfected stage 1 rat hippocampal neuron photoactivated in the soma with 405 nm laser (red circle with a diameter of 5.239 μm) before and 30 min after 20 μM Blebbistatin treatment. B1 and B2 indicated on the stage 1 cell are the buddings quantified in D. **(E)** Left panel: normalized intensity values in the photoactivated area before and after 20 μM Blebbistatin treatment. Inset graph: half-time ($t_{1/2}$) values in seconds Before = 20.22 and Blebbistatin treatment = 28.74. Middle panel: photoactivated signal in buds relative to the average initial signal from the illuminated area before and after 20 μM Blebbistatin treatment. Right panel: buds to soma photoactivated signal intensity ratio before and after 20 μM Blebbistatin treatment. (Quantification and imaging by Dr. Meka, ZMNH, Hamburg)

Accordingly, in stage 3 neurons, inhibition of myosin II reduced the translocation of photoactivated somatic PaGFP-UtrCH into neurites (Figure 2-10). Much less PaGFP-UtrCH signal was detected in the growth cones of either axons or minor neurites of blebbistatin-treated cells in comparison to that of control cells (Figure 2-10C, D). On average from all stage 3 neurons treated with blebbistatin, the speed of activated signal decay in the photoconverted area was significantly slowed down as indicated by the signal half-life time ($t_{1/2} = 36.11 \pm 2.548\text{s}$) compared to control cells ($t_{1/2} = 26.73 \pm 3.534\text{s}$). In the same time-frame, somatic PaGFP-UtrCH signal was thus more restricted to the soma area after blebbistatin treatment (Figure 2-10C). In other words, inhibition of myosin II activity hindered/hampered the translocation of somatic F-actin. Moreover, blebbistatin-treated neurons developed several long neurites, which is a multiple-axon-like phenotype, indicating that less somatic F-actin translocation facilitated neurite elongation. In contrast, the control neurons achieved the typical polarized growth with a long growing axon and several shorter neurites (Figure 2-11). Importantly, although blebbistatin-treatment affected somatic F-actin translocation into neurites, the reduced photoactivated somatic PaGFP-UtrCH signal that moved into neurites still followed an inverse correlation with the neurite length, as documented by the correlation analysis between neurite length and activated signal intensity (Figure 2-10D). These

results suggest that myosin II mediates somatic F-actin translocation into neurites but the preference for somatic F-actin flow into minor neurites is not inherent to the myosin II motor.

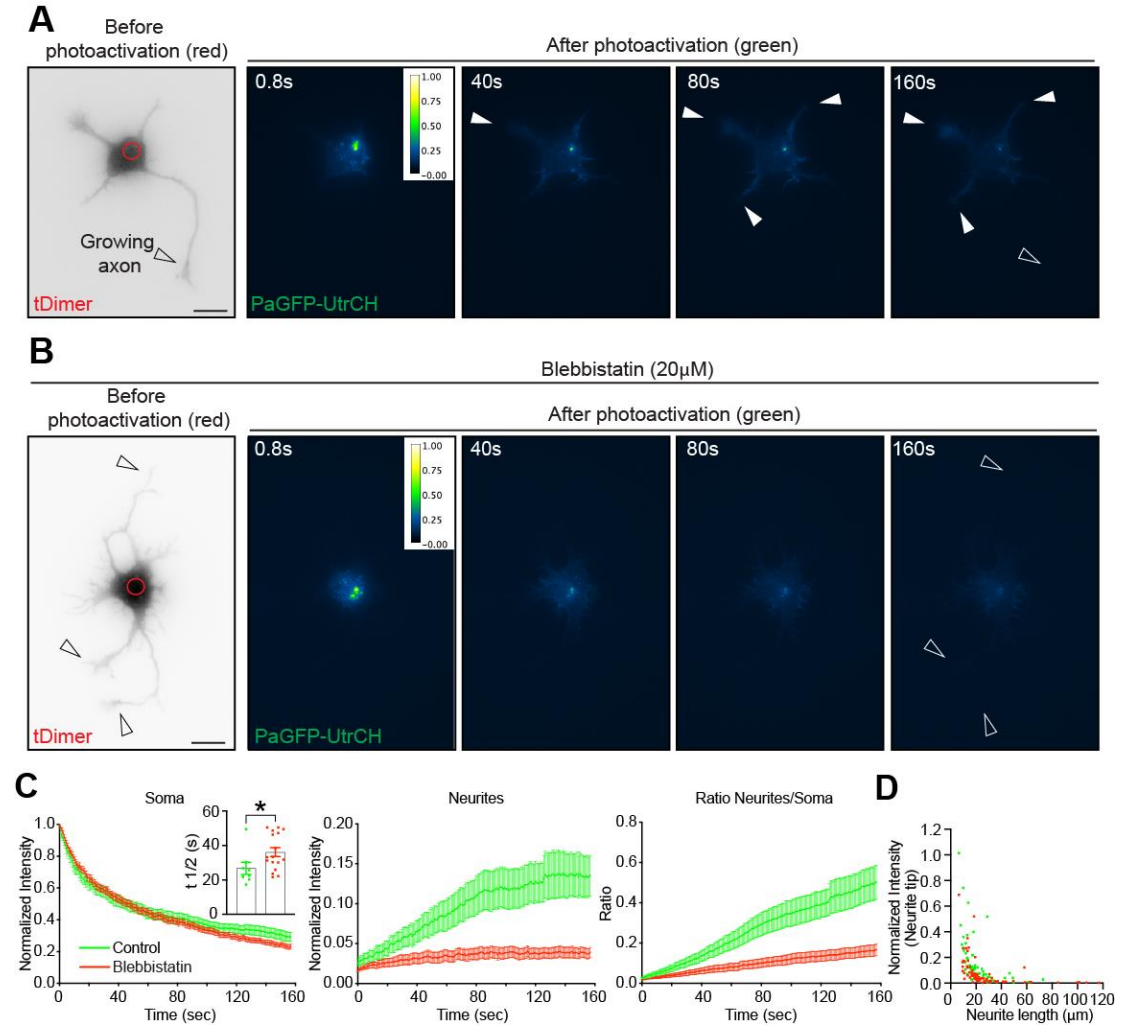


Figure 2-10: Myosin II inhibition (via 20 μ M Blebbistatin) affects somatic F-actin delivery.

(A-B) PaGFP-UtrCH and tDimer co-transfected DIV1-rat hippocampal control (A) and 20 μ M Blebbistatin-treated (B) neurons were photoactivated in the soma with 405 nm laser (red circle with a diameter of 5.239 μ m). **(C)** Left panel: normalized intensity values in the photoactivated area of untreated controls and 20 μ M Blebbistatin-treated DIV1 (stage 3) PaGFP-UtrCH expressing cells. Inset graph: mean \pm SEM half-time ($t_{1/2}$) values in seconds Controls = 26.73 ± 3.534 and Blebbistatin cells = 36.11 ± 2.548 . Middle panel: photoactivated signal in neurite tips relative to the average initial signal from the illuminated area for controls and 20 μ M Blebbistatin-treated DIV 1 (stage 3) PaGFP-UtrCH expressing cells. Right panel: Signal intensity ratio of the neurite shaft to soma in photoactivated controls and 20 μ M Blebbistatin-treated DIV1 (stage 3) PaGFP-UtrCH expressing cells. **(D)** Quantification showing photoactivated somatic F-actin in Control and Blebbistatin-treated cells. Normalized F-actin intensity enriched in the neurite tips was plotted against the length of the neurites from which they were obtained. Data shown in C and D, $n = 17$

Control and 18 Blebbistatin-treated cells from at least 2 different cultures. (Quantification by Robin Scharrenberg, imaging by Dr. Meka, ZMNH, Hamburg)

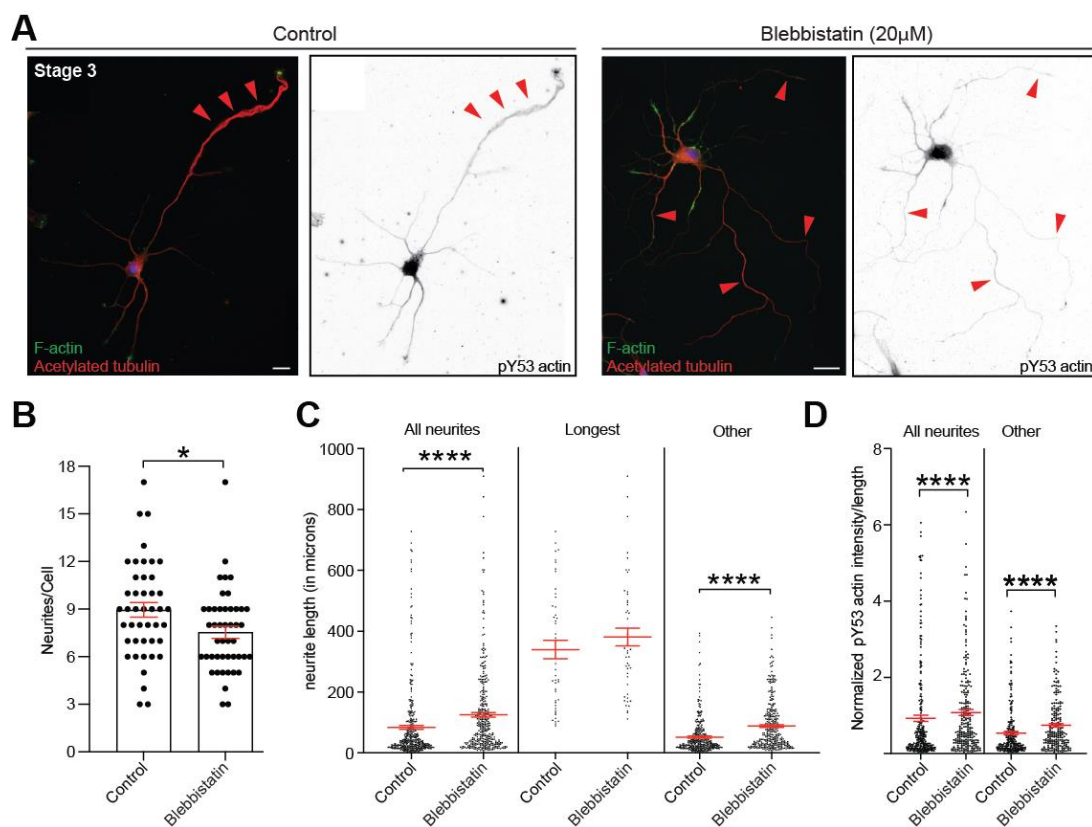


Figure 2-11: Myosin II inhibition (via 20 μM blebbistatin) results in neurite elongation. (A)

Control and 20 μM Blebbistatin-treated neurons, treated at DIV1 and fixed at DIV3, immunostained with pY53 actin and AcetyTub and F-actin (labelled by phalloidin-488). **(B)** Quantifications show neurites per cell in Control and 20 μM Blebbistatin-treated neurons, treated at DIV1 and fixed at DIV3. Mean \pm SEM neurite number, Control neurons = 8.955 ± 0.4586 , Blebbistatin-treated neurons = 7.543 ± 0.3778 ; * $P = 0.0128$ by Mann-Whitney non-parametric test. **(C)** Quantifications showing neurite length analysis in Control and 20 μM Blebbistatin-treated neurons, treated at DIV1 and fixed at DIV3. Mean \pm SEM length values, for all neurites from Control neurons = 83.91 ± 6.275 , Blebbistatin-treated neurons = 125.1 ± 7.654 ; for longest neurites from Control neurons = 339.6 ± 30.14 , Blebbistatin-treated neurons = 380.7 ± 28.87 ; for shorter neurites from Control neurons = 51.98 ± 3.104 , Blebbistatin-treated neurons = 88.06 ± 4.518 ; n.s. = not significant, **** $P < 0.0001$ by Mann-Whitney non-parametric test. **(D)** Quantification of pY53 actin intensity values normalized to length of neurites (per cell) from Control and 20 μM Blebbistatin-treated neurons at stage 3. Mean \pm SEM values, for all neurites from Control neurons = 0.9249 ± 0.08225 , Blebbistatin-treated neurons = 1.079 ± 0.07809 ; for shorter neurites from Control neurons = 0.5349 ± 0.04283 , Blebbistatin-treated neurons = 0.7408 ± 0.04664 ; **** $P < 0.0001$ by Mann-Whitney non-parametric test. Data were obtained from 259 Control neurites and 242 Blebbistatin-treated neurites. Data shown in B, C and D, $n = 44$ cells (Control group), 46 cells (Blebbistatin group).

2.3 Actin phosphorylation at tyrosine-53 in neurites promotes neurite elongation

Somatic F-actin translocation is mediated by myosin II, but the preference of somatic F-actin translocation is not changed when blocking myosin II activity. Moreover, in stage 4 neurons during which dendrites initiate their development, the photoactivation live-imaging showed somatic F-actin is restricted to the soma. These data imply that myosin II motors act as a cargo transport vehicle for somatic F-actin without the ability to decide the way forward. And this motor-mediated delivery could be dynamically regulated when axons and dendrites start to elongate. Therefore, it brings up the next question: what specifies this preference?

2.3.1 Actin phosphorylation at tyrosine-53 in neurite shafts counteracts somatic F-actin translocation

To elucidate the mechanism which drives the preferential translocation of somatic F-actin into minor neurites but not the growing axon, I decided to test the characteristics of the actin-cytoskeleton during axon determination. Myosin II, which bears an actin binding site and an ATPase motor domain, binds to actin-bundles and moves towards the actin-filament barbed (+) end to regulate intracellular trafficking and thereby influences neuronal polarity (Ross et al., 2008; Ikebe 2008; Ana Rita Costa and 2020). Moreover, the phosphorylation of actin at tyrosine-53 (Y53) is a highly conserved post-translational modification in various species, which inhibits actin polymerization and induces rapid reorganization of actin filaments (Bertling et al., 2016; Liu et al., 2006). Therefore, it is conceivable to envision that myosin II moves along actin filaments to transport somatic F-actin into neurites, while unstable actin filaments in the neurite shaft might preclude the myosin II-dependent translocation of somatic F-actin to further modulate the polarized establishment of axons and dendrites.

As an entry point, I first evaluated the subcellular localization of actin phosphorylation at tyrosine-53 (pY53) during axon formation by immunostaining stage 2-4 hippocampal pyramidal neurons. Phalloidin was used to better visualize the outline of cells. The fluorescence intensity analysis showed that pY53 actin was enriched in the longest neurite of neurons at stage 2 and then concentrated in the growing axon of stage 3 neurons (Figure 2-12A-D). Results from the correlation analysis of neurite length to intensity revealed that pY53 was positively correlated with the neurite length (Figure 2-12B, D).

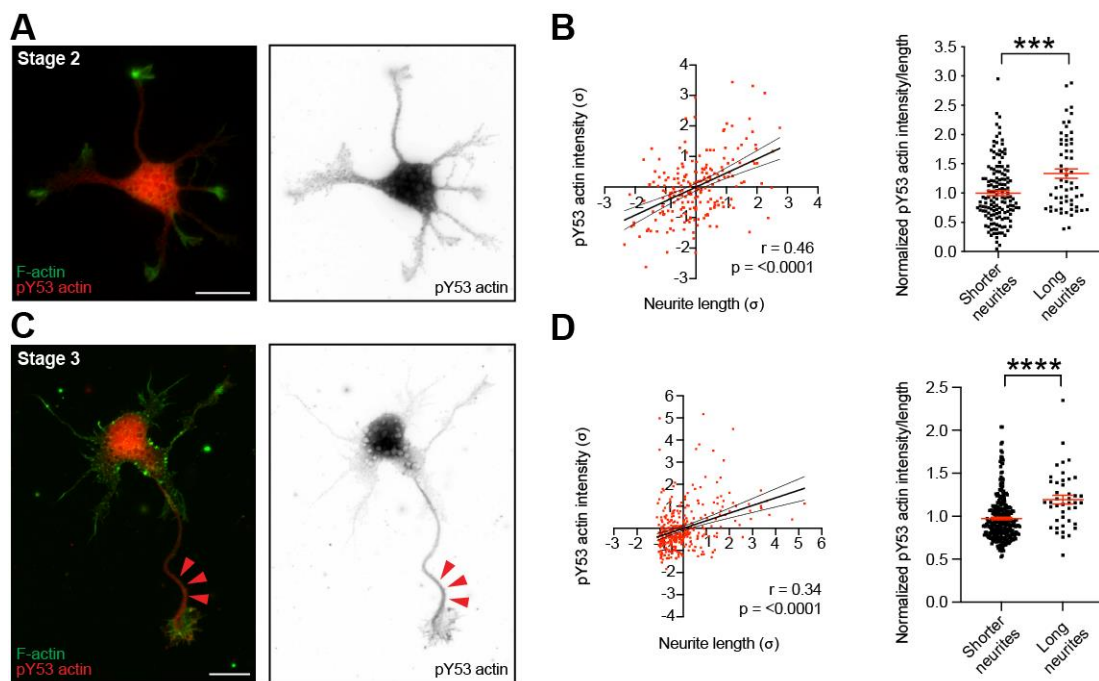


Figure 2-12: pY53 actin is enriched in the shaft of the longest neurite in developing neurons. (A) Stage 2 neuron immunostained with pY53 actin and F-actin (labelled by phalloidin-488). (B) Left panel: linear regression analysis of neurite length and pY53-actin intensity (normalized to length) in stage 2 cells; values were normalized according to a standard score, and axes are represented in units of SD (σ). Linear regression line equation: $Y = 0.4612 \cdot X - 9.973e-006$. Pearson correlation coefficient (r value) and p value of significance as indicated. Thin lines denote 95% confidence intervals. Right panel: quantification of pY53 actin intensity values normalized to length from shorter neurites and longer neurites (per cell) at stage 2. Mean \pm SEM values for normalized pY53 intensities in shorter neurites = 1.000 ± 0.04169 and long neurites = 1.333 ± 0.08102 . *** $P = 0.0006$ by Mann-Whitney non-parametric test. Data were obtained from 210 neurites of 51 neurons from 3 different cultures. (C) Stage 3 neuron immunostained with pY53 actin and F-actin (labelled by phalloidin-488). (D) Left panel: linear regression analysis of neurite length and pY53 actin intensity (normalized to length) in stage 3 cells; values were normalized according to a standard score, and axes are represented in units of SD (σ). Linear regression

line equation: $Y = 0.3452 \cdot X - 2.568e-007$. Pearson correlation coefficient (r value) and p value of significance are as indicated. Thin lines denote 95% confidence intervals. Right panel: quantification of pY53 actin intensity values normalized to length from shorter neurites and longer neurites (per each cell) at stage 3. Mean \pm SEM values for normalized pY53 intensities in shorter neurites = 0.9725 ± 0.01504 and longer neurites = 1.192 ± 0.05046 . **** P <0.0001 by Mann-Whitney non-parametric test. Data were obtained from 344 neurites of 43 neurons from 3 different cultures. (Quantification and imaging partially by Carina Meta Friedrich, ZMNH, Hamburg)

Additionally, in stage 4 neurons (Figure 2-13A, B), pY53 actin was clustered in both axonal and dendritic compartments labeled by Tau1 and MAP2, respectively, with dendrites displaying a higher level of pY53 actin than axons. Next, to characterize the distribution of pY53 actin in relation to somatic F-actin translocation, photoactivation was conducted in cultured neurons expressing PaGFP-UtrCH. Subsequently, these cells were fixed for immunostaining which showed that the neurites carrying more pY53 actin received less photoactivated somatic PaGFP-UtrCH and were longer (Figure 2-13C-F). These data indicate that somatic F-actin delivery is precluded from the growing neurites with the enrichment of pY53 actin.

Interestingly, blebbistatin treatment, which impaired somatic F-actin delivery (see 2.2.2), induced neurite elongation consistent with previous studies (Lilienberg et al., 2021; Yu et al., 2012). Especially the non-axonal neurites elongated significantly compared to control neurons. Importantly, these induced long neurites showed an increase in the level of pY53 actin (Figure 2-11). All together, these data suggest that neurite growth positively correlates with pY53.

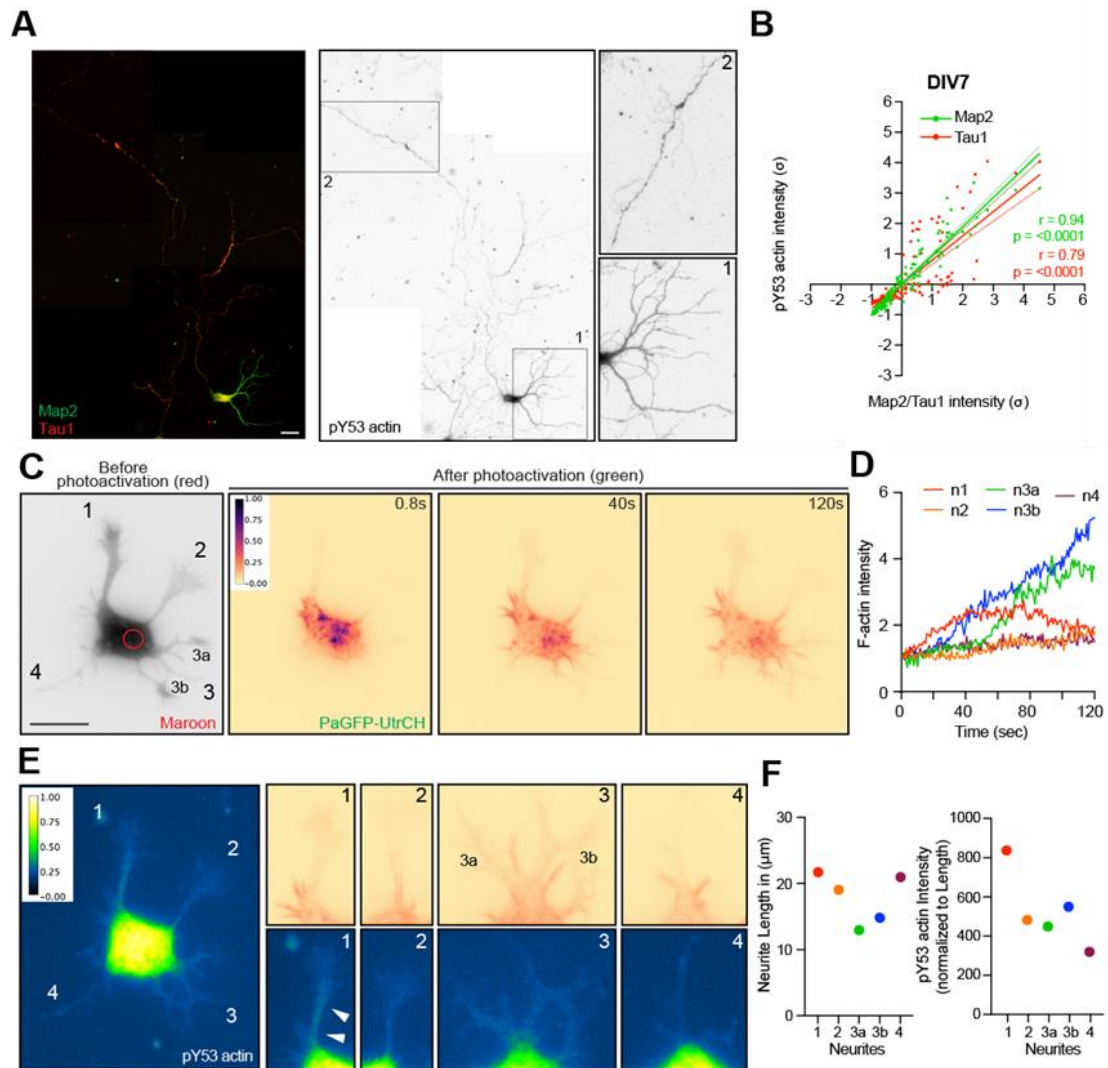


Figure 2-13: pY53 actin is eventually enriched in the dendrites of matured neurons (DIV7). (A) DIV7 (stage 4) neuron immunostained with pY53 actin, axonal marker Tau1 and dendritic marker MAP2. (B) Linear regression analysis of pY53 actin vs Tau1 and pY53 actin vs MAP2 intensities from DIV 7 (stage 4) neurons; values were normalized according to a standard score, and axes were represented in units of SD (σ). Linear regression line equation for pY53 actin vs Tau1 intensities: $Y = 0.7952 \cdot X - 1.124e-007$, pY53 actin vs MAP2 intensities: $Y = 0.9498 \cdot X - 1.833e-007$. Pearson correlation coefficient (r value) and p value of significance are as indicated. Thin lines denote 95% confidence intervals. Data were obtained from $n = 21$ neurons (153 neurites) from 3 different cultures. (C) PaGFP-UtrCH and mMaroon1 co-transfected stage 2 rat hippocampal neuron photoactivated in the soma with 405 nm laser (red circle with a diameter of 5.239 μm). (D) Photoactivated signal enriched in the neurite tips from 4 neurites n1, n2, and n3a, n3b and n4 over time relative to the initial signal (shown in C). (E) Stage 2 neuron from E, immunostained with pY53 actin. Cropped images from all 4 neurites showing enrichment of photoactivated signal (upper panels) and pY53 immunostaining (lower panels). (F) Graphs depicting the length of individual neurites before photoactivation from mMaroon1 channel shown in E (left) and pY53 actin intensity (normalized to Length) values of individual neurites after photoactivation followed by pY53 actin immunostaining. (Quantification and imaging partially by Dr. Meka, ZMNH, Hamburg)

2.3.2 Phosphorylation-induced actin instability in the neurite shaft promotes axon formation

To directly assess the relevance of pY53 in neurite outgrowth/neuronal polarization, actin mutants that can mimic actin-Y53 phosphorylation (Y53E) and cannot be phosphorylated at tyrosine-53 (Y53A) were introduced into neurons to modulate pY53 actin levels (Bertling et al., 2016). Therefore, wt actin-mCherry, Y53E actin-GFP, and Y53A actin-mCherry plasmids separately were introduced into cortical cells via IUE strategy, then transfected cells were plated on pre-coated coverslips. Two days after plated, neurons (DIV3) were fixed for immunostaining to label growing axons with the axonal marker Tau1. The analysis showed that the preclusion of actin phosphorylation (Y53A) reduced the number of neurons extending an axon compared to the expression of wt actin (Figure 2-14A, C). By contrast, the expression of actin-Y53 mimicking phosphorylation (Y53E) induced the formation of longer axons compared to that of wt actin, but no negative effect on axon formation (Figure 2-14A, B). In conclusion, these results support the notion that pY53 promotes neurite growth during axon establishment.

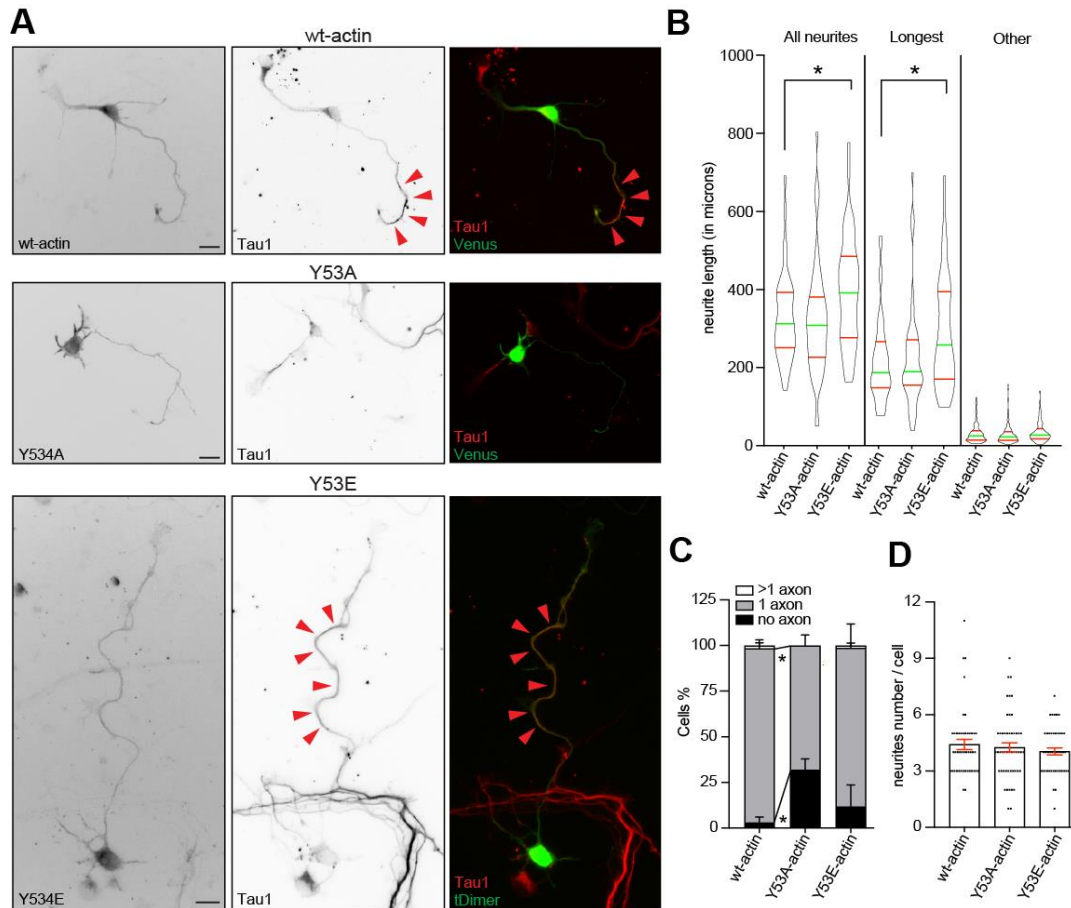


Figure 2-14: Phospho-mimicking actin-Y53 mutation (Y53E) promotes neurite growth but phospho-dead actin-Y53 mutation (Y53A) impairs axon formation. (A) Images of mouse cortical neurons co-transfected via IUE at E15 with Venus/tDimer and wt-actin or Y53A or Y53E cultured at E17 for 72 h immunostained with Tau1 antibody to confirm the axonal identity of the neurites, indicated by red arrowheads. **(B)** Quantification of neurite length (in μm) expressing wt-actin, Y53A or Y53E, as shown in A. Mean \pm SEM values for the length of all neurites in wt-actin cells ($n = 45$) = 326.9 ± 16.69 , Y53A cells ($n = 50$) = 324.2 ± 20.65 , Y53E cells ($n = 44$) = 396.3 ± 21.09 . Mean \pm SEM values for the length of the longest neurite in wt-actin cells = 217.8 ± 16.09 , Y53A cells = 228.0 ± 19.35 , Y53E cells = 290.0 ± 21.69 . Mean \pm SEM values for length of other neurites in wt-actin cells = 31.90 ± 2.018 , Y53A cells = 28.99 ± 1.879 , Y53E cells = 35.19 ± 2.299 . $P < 0.0001$ by one-way ANOVA, post hoc Tukey's test, * $P < 0.05$. **(C)** Percentage of neurons expressing wt-actin, Y53A or Y53E, as shown in A, differentiated to have no axon, 1 axon, and >1 axon. Mean \pm SEM values for percentage of wt-actin ($n = 56$) cells with no axon = 3.00 ± 3.00 , 1 axon = 95.50 ± 4.50 , more than 1 axon = 1.50 ± 1.50 ; percentage of Y53A-actin ($n = 56$) cells with no axon = 32.10 ± 5.80 , 1 axon = 67.90 ± 5.80 ; percentage of Y53E-actin ($n = 55$) cells with no axon = 11.80 ± 11.8 , 1 axon = 86.80 ± 13.20 , more than 1 axon = 1.30 ± 1.30 . $P = 0.05$ by two-way ANOVA, post hoc Tukey's test, * $P < 0.05$. **(D)** Quantification of neurite terminals expressing wt-actin, Y53A or Y53E as shown in (A). Mean \pm SEM values for neurite terminal per cell in wt-actin cells ($n = 45$) = 4.422 ± 0.2743 , Y53A cells ($n = 50$) = 4.260 ± 0.2488 , Y53E cells ($n = 44$) = 4.045 ± 0.1922 . $P < 0.0001$ by one-way ANOVA test, post hoc Tukey's test, n.s.: not significant. Figures B, C and D, data were obtained from cortical cultures of 3 or more IUE embryos from at least 2 different mothers. (Quantification partially by Carina Meta Friedrich, ZMNH, Hamburg)

To further elucidate the molecular characteristics of the neurites enriched with pY53 actin, hippocampal neurons were transfected with Kif5c-tdTomato, which expresses truncated Kinesin-1 that accumulates transiently in neurites of stage 2 neurons and only in the emerging axon of stage 3 neurons (Jacobson et al., 2006). Selective translocation of truncated Kinesin-1 is thereby known as the earliest marker of axonal identity and moves along stable MTs (Hammond et al., 2010; Jacobson et al., 2006). Afterwards, these neurons were fixed 1-2 days later after plated and prepared for immunostaining to visualize the correlation of actin phosphorylation and Kif5c accumulation. The analysis clearly showed that the neurite with an enrichment of pY53 signal was the one bearing the Kif5c-tdTomato signal in stage 2 and 3 neurons (Figure 2-15A-D). Moreover, neurites positive for Kif5c-tdTomato also carried a higher level of acetylated α -tubulin (Figure 2-15A-D) in agreement with previous studies (Reed et al., 2006). To further monitor somatic F-actin translocation during axon selection, neurons were co-transfected with PaGFP-UtrCH and Kif5c-tdTomato, and then used for somatic photoactivation. The translocation of photoactivated somatic PaGFP-UtrCH occurred preferentially into neurites lacking Kif5c-tdTomato signal (Figure 2-15E-G). Altogether, these data indicate that truncated Kinesin-1 (Kif5c) localizes in the growth cone of the neurite with increased pY53 actin and acetylated α -tubulin signals, hinting that pY53 actin collaborates with microtubule acetylation to reinforce axon formation.

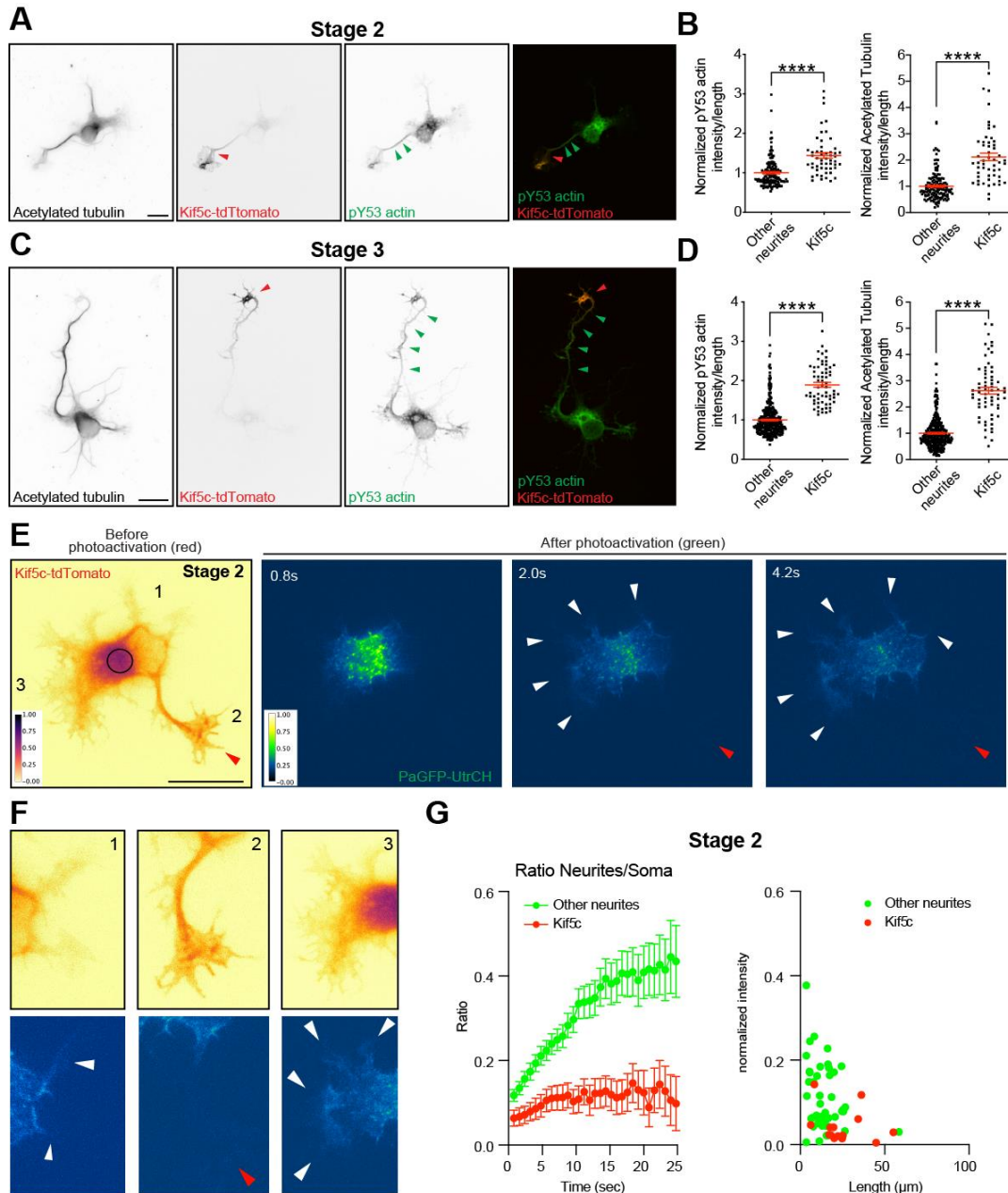


Figure 2-15: pY53 actin and acetylated tubulin are enriched in the shaft of neurites bearing Kif5c. (A) Images for Kif5c-tdTomato transfected stage 2 neurons immunostained with pY53 actin and AcetyTub. (B) Left panel: quantification of pY53 actin intensity values normalized to length from neurites and Kif5c-positive neurites (per cell) at stage 2. Mean \pm SEM values for normalized pY53 intensities in shorter neurites = 1.000 ± 0.02989 and long neurites = 1.437 ± 0.07009 . **** $P < 0.0001$ by Mann-Whitney non-parametric test. Right panel: quantification of AcetyTub intensity values normalized to length from neurites and Kif5c-positive neurites (per cell) at stage 2. Mean \pm SEM values for normalized AcetyTub intensity in shorter neurites = 1.000 ± 0.04479 and long neurites = 2.119 ± 0.1409 . **** $P < 0.0001$ by Mann-Whitney non-parametric test. Data were obtained from 198 neurites of 46 neurons from 3 different cultures. (C) Images for Kif5c-tdTomato transfected stage 3 neurons immunostained with pY53 actin and AcetyTub. (D) Left panel: quantification of pY53 actin intensity values normalized to length from neurites and Kif5c-positive neurites (per cell) at stage 3. Mean \pm SEM values for normalized pY53

intensities in shorter neurites = 1.000 ± 0.02135 and long neurites = 1.893 ± 0.06266 . **** $P < 0.0001$ by Mann-Whitney non-parametric test. Right panel: quantification of AcetyTub intensity values normalized to length from neurites and Kif5c-positive neurites (per cell) at stage 2. Mean \pm SEM values for normalized AcetyTub intensity in shorter neurites = 1.000 ± 0.03061 and long neurites = 2.624 ± 0.1325 . **** $P < 0.0001$ by Mann-Whitney non-parametric test. Data were obtained from 415 neurites of 59 neurons from 3 different cultures. **(E)** PaGFP-UtrCH and Kif5c-tdTomato co-transfected stage 2 rat hippocampal neuron photoactivated in the soma with 405 nm laser (red circle with a diameter of 5.215 μm). **(F)** Cropped images of the neurites of the cell shown in E. **(G)** Left panel: intensity ratio of photoactivated signal over time in neurite shafts 12 microns away from the illuminated area, relative to the average initial signal from the illuminated area of PaGFP-UtrCH expressing stage 2 cells. Right panel: quantification showing photoactivated somatic F-actin mean-normalized intensity enriched in the neurite tips against the length of their corresponding neurites. $n = 15$ cells per group from 4 different cultures.

2.3.3 Microtubule acetylation favours actin phosphorylation at tyrosine-53 in neurites to facilitate neuronal polarization

To investigate the determinants of pY53 actin enrichment in the neurite shaft, I decided to further check whether acetylated α -tubulin and pY53 actin coexist in the same neurite fated for axonal growth, since acetylated α -tubulin clusters in the growing axon. Cultured hippocampal neurons were co-stained with anti-pY53 actin and anti-acetylated α -tubulin antibodies to characterize the distribution of pY53 actin and acetylated MTs. The analysis indicated that there was a positive correlation between these two post-translational modifications in the neurite shafts of stage 2 and 3 neurons, specifically in the growing axon of stage 3 neurons (Figure 2-16A-D). Briefly, a neurite displaying more acetylated α -tubulin also contained more phosphorylated actin. Meanwhile, the measurement of the intensity of PolyGluTub gave similar results (Figure 2-17A, B). Moreover, the high-resolution images provided a much clearer view that acetylated α -tubulin and phosphorylated actin align/entwine each other (Figure 2-16E).

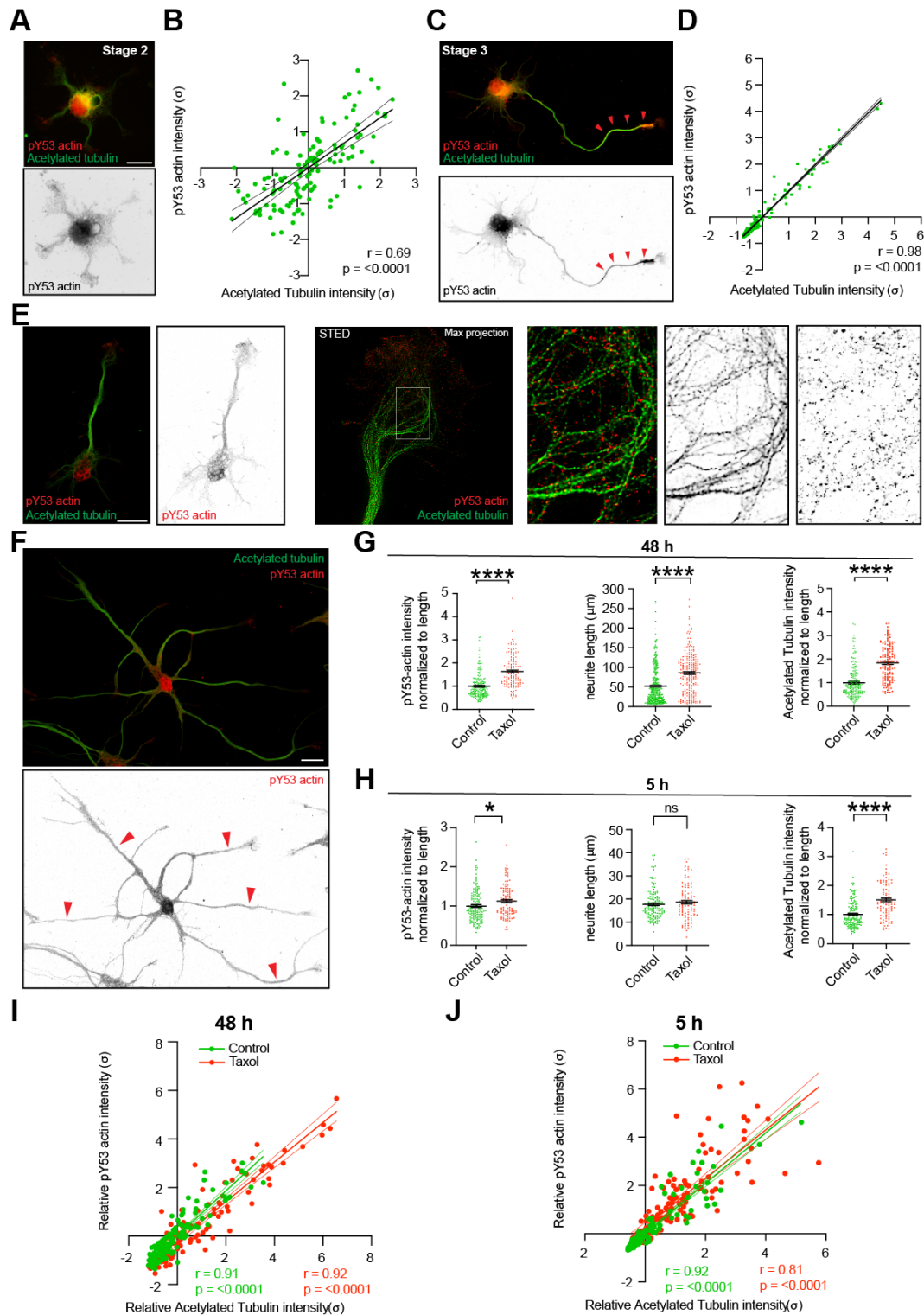


Figure 2-16: pY53 actin distribution and acetylated tubulin profile correlate strongly in the neurite shafts of developing neurons. (A) Stage 2 and (C) Stage 3 neurons immunostained with anti-pY53 actin and anti-AcetyTub antibodies. (B) Linear regression analysis of AcetyTub and pY53 actin intensities in stage 2 cells; line equation: $Y = 0.6963 * X + 7.634e-008$. Data were obtained from 128 neurites of 49 neurons from 2 different cultures. (D) Linear regression analysis of AcetyTub and pY53 actin intensities in stage 3 cells; line equation $Y = 0.9852 * X - 2.720e-007$. Data were obtained from 175 neurites of 30 neurons from 3 different cultures. (E) STED images of the growth cone of a stage 3 neuron

immunostained with anti-pY53 actin and anti-AcetyTub antibodies, inset from the white rectangle shows AcetyTub and pY53 actin signals overlap. **(F)** Rat hippocampal neuron treated with 5 nM Taxol (24 h after plating) for 48 h, immunostained with anti-pY53 actin and anti-AcetyTub antibodies. **(G)** Quantifications from Control and Taxol-treated (incubate with 5 nM Taxol 24 h after plating for 48 h) neurons. Left and Right panel: Data were obtained from 175 neurites from 30 Control cells and 134 neurites from 30 Taxol-treated (48 h) cells from 3 different cultures. Middle panel: Data were obtained from 344 neurites from 43 Control cells and 229 neurites from 43 Taxol-treated (48 h) cells from 3 different cultures. Left panel: quantification of relative pY53 actin intensity values normalized to the length of the neurite shafts. Mean \pm SEM values from control neurons = 1.000 ± 0.04077 and Taxol-treated (48 h) neurons = 1.633 ± 0.05916 . Middle panel: quantification of neurite length. Mean \pm SEM values from Control neurons = 52.05 ± 2.488 and Taxol-treated (48 h) neurons = 85.76 ± 3.452 . Right panel: quantification of relative AcetyTub intensity values normalized to the length of the neurite shafts. Mean \pm SEM values from Control neurons = 1.000 ± 0.05084 and Taxol-treated (48 h) neurons = 1.839 ± 0.06441 . **** P < 0.0001 by Mann-Whitney non-parametric test. **(H)** Quantifications from Control and Taxol-treated (incubate with 5 nM Taxol immediately after plating for 5 h) neurons. Data were obtained from 143 neurites from 64 Control cells and 99 neurites from 52 Taxol-treated (5 h) cells from 2 different cultures. Left panel: quantification of pY53 actin intensity values normalized to the length of the neurite shafts. Mean \pm SEM values from Control neurons = 1.000 ± 0.03340 and Taxol-treated (5 h) neurons = 1.136 ± 0.04187 . ** P = 0.0100. Middle panel: quantification of neurite length. Mean \pm SEM values from Control neurons = 17.67 ± 0.5277 and Taxol-treated (5 h) neurons = 18.60 ± 0.7689 . P = 0.3866, n.s: not significant. Right panel: quantification of AcetyTub intensity normalized to the length of the neurite shafts. Mean \pm SEM values from Control neurons = 1.000 ± 0.03860 and Taxol-treated (5 h) neurons = 1.505 ± 0.06407 . **** P < 0.0001 by Mann-Whitney non-parametric test. **(I)** Linear regression analysis of AcetyTub and pY53 actin intensities in Control and Taxol (48 h) groups; Linear regression line equations for pY53 actin intensities from the Control group: $Y = 1.046 * X + 1.704e-007$; from Taxol (48 h) group: $Y = 1.008 * X + 0.2777$. Data were obtained from 175 neurites of 30 Control neurons and 134 neurites of 30 Taxol-treated neurons from 3 different cultures. **(J)** Linear regression analysis of AcetyTub and pY53 actin intensities in Control and Taxol (5 h) groups; line equations for pY53 actin intensities from Control group: $Y = 0.9235 * X + 0.01825$, from Taxol (5 h) group: $Y = 0.8150 * X - 0.2079$. Data were obtained from 143 neurites from 64 Control cells and 99 neurites from 52 Taxol-treated (5 h) cells from 2 different cultures. Data in B, D, I, J: values were normalized according to a standard score, and axes were represented in units of SD (σ). Pearson correlation coefficient (r value) and p value of significance were as indicated. Thin lines denote 95% confidence intervals. (Quantification and imaging partially by Dr. Meka, ZMNH, Hamburg)

To further understand the crosstalk between actin phosphorylation and tubulin acetylation during axon formation, I applied Taxol to induce neurite elongation with promotion of tubulin acetylation (Meka et al., 2022; Witte et al., 2008). The quantification indicated that Taxol treatment did increase the level of AcetyTub compared to the control group. Importantly, it was coupled with a similar increase of pY53 actin levels in the neurites (Figure 2-16F-G). However, under

the same conditions the PolyGluTub levels increased upon Taxol treatment, but its distribution showed a weaker correlation with pY53 actin (Figure 2-17C, D) compared to the AcetyTub (Figure 2-16G, I).

Notably, on the other hand, a short period of treatment with Taxol (5 h), which did not affect the neurite length, still increased tubulin acetylation in the neurites together with an elevation of actin phosphorylation (Figure 2-16H, J). These results suggest that actin phosphorylation is not completely length-dependent but more directly influenced by tubulin acetylation.

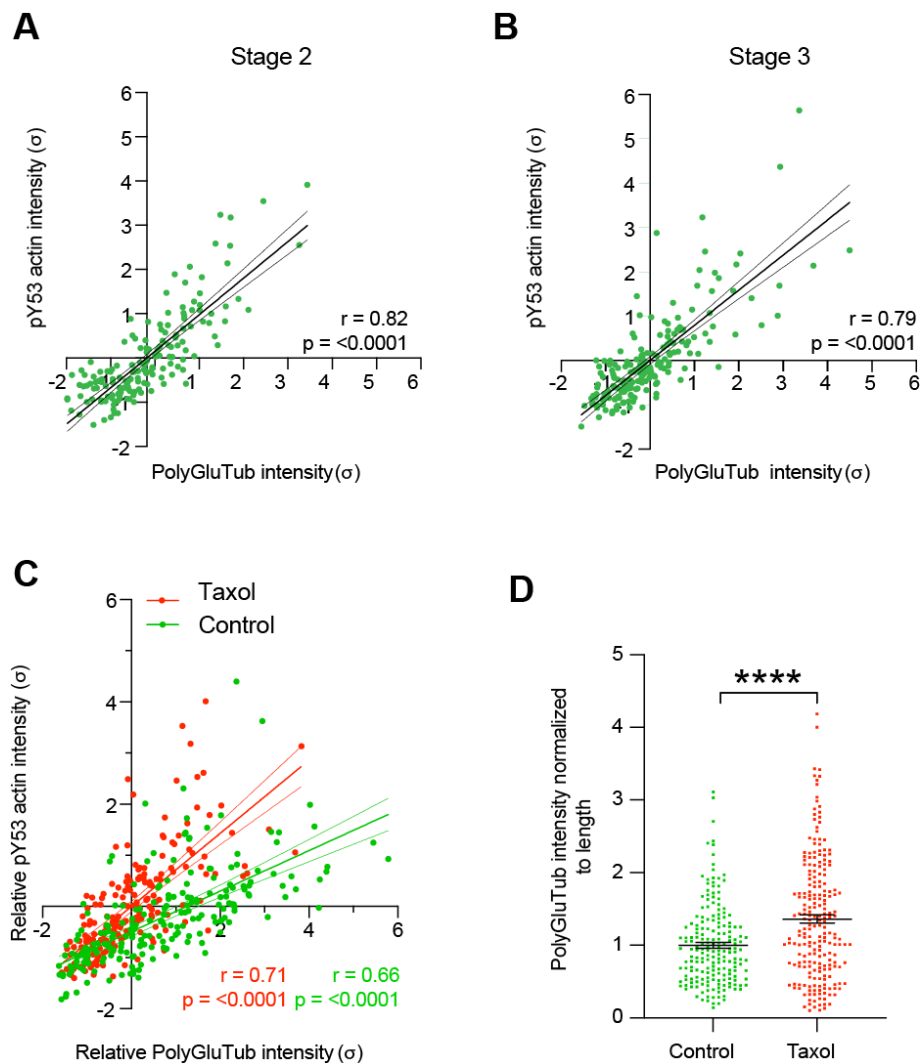


Figure 2-17: PolyGluTub and pY53 actin distribution correlation in neurite shafts of stage2, stage3 and Taxol-treated neurons. (A) Linear regression analysis of PolyGluTub and pY53 actin intensities in stage 2 cells; Linear regression line equation: $Y = 0.8620 \cdot X + 4.790e-008$. Data were obtained from 167 neurites of 38 neurons from 2 different cultures. (B) Linear regression analysis of

PolyGluTub and pY53 actin intensities in stage 3 cells; Linear regression line equation $Y = 0.7925 * X + 1.284e-007$. Data were obtained from 194 neurites of 22 neurons obtained from 3 different cultures. **(C)** Linear regression analysis of PolyGluTub and pY53 actin intensities in Control and Taxol (48 h) groups; Linear regression line equations for pY53 actin intensities from Control group: $Y = 0.7151 * X - 5.742e-007$; from Taxol group: $Y = 0.3959 * X - 0.4918$. Data were obtained from 194 neurites of 22 Control neurons and 220 neurites of 27 Taxol-treated (48 h) neurons from 3 different cultures. **(D)** Quantifications from Control and Taxol-treated (48 h) neurons. Data were obtained from 194 neurites from 22 control cells and 220 neurites from 27 Taxol-treated (48 h) cells from 3 different cultures: quantification of relative PolyGluTub intensity values normalized to length from the neurite shafts. Mean \pm SEM values from Control neurons = 1.000 ± 0.03952 and Taxol-treated (48 h) neurons = 1.361 ± 0.05624 . **** P < 0.0001 by Mann-Whitney non-parametric test. Data in A, B, C: values were normalized according to a standard score, and axes are represented in units of SD (σ). Pearson correlation coefficient (r value) and p value of significance are as indicated. Thin lines denote 95% confidence intervals. (Quantification partially by Dr. Meka, ZMNH, Hamburg)

To further test this hypothesis, cultured neurons were treated with nocodazole, which induces MT depolymerization. It turned out that nocodazole treatment did decrease the levels of AcetyTub, and accordingly also reduced the levels of pY53 actin (Figure 2-18). Interestingly, the correlation remained significant. Altogether, these results show that pY53 actin precludes somatic F-actin translocation into neurites and that this actin modification is influenced by tubulin acetylation, ultimately leading to timely neurite growth, first the axon and then the dendrites.

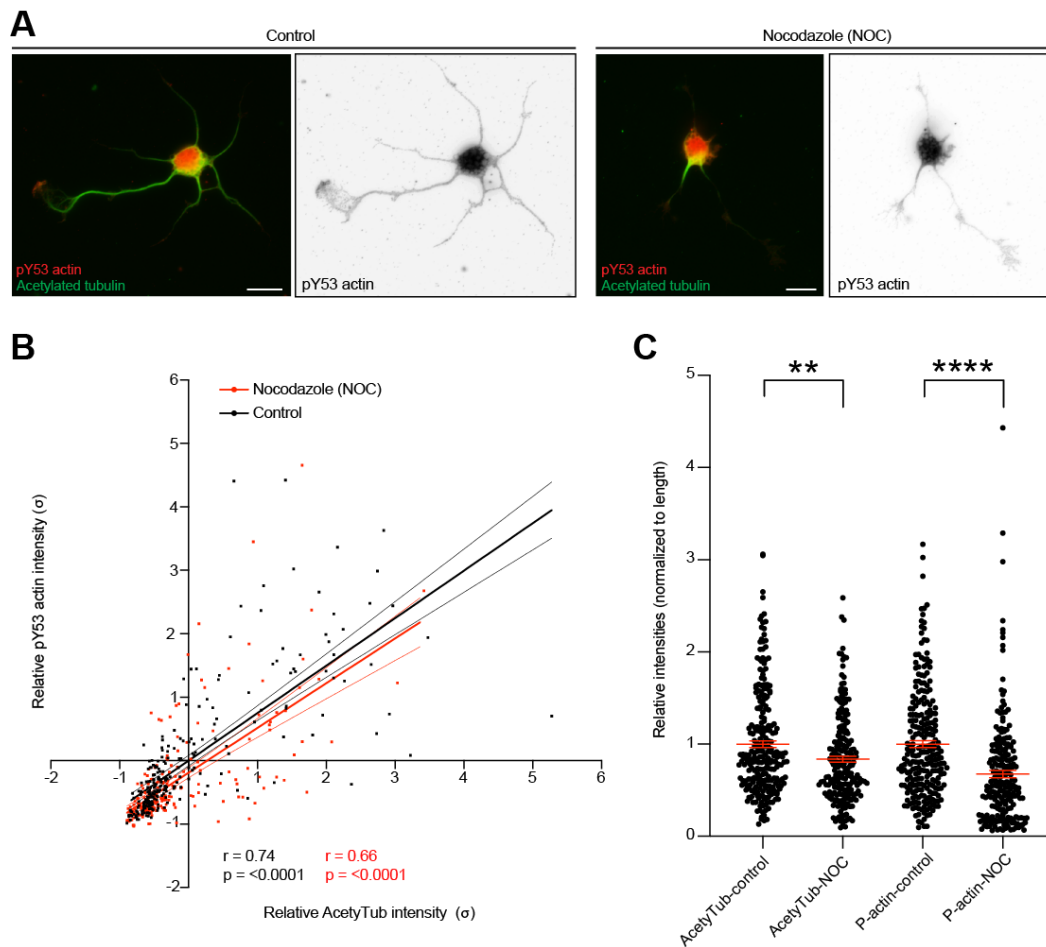


Figure 2-18: Nocodazole-induced MT destabilization decreases pY53 actin levels in DIV1 neurons. **(A)** Control and 6 μM Nocodazole-treated (for 30 min at DIV1) neurons, immunostained with anti-pY53 actin and anti-AcetyTub antibodies. **(B)** Linear regression analysis of relative AcetyTub and pY53 actin intensities in Control and Nocodazole-treated neurons; values were normalized according to a standard score, and axes were represented in units of SD (σ). Linear regression line equation for the Control group: $Y = 0.7486 \cdot X - 8.957e-008$, Nocodazole group: $Y = 0.7051 \cdot X - 0.1897$. Pearson correlation coefficient (r value) and p value of significance were as indicated. Thin lines denote 95% confidence intervals. **(C)** Quantification of AcetyTub and pY53 actin intensity values normalized to length of neurites (per cell). Mean \pm SEM values for normalized AcetyTub intensity in the Control group = 1.000 ± 0.03592 and Nocodazole group = 0.8360 ± 0.03182 . ** $P = 0.0025$ by Mann-Whitney non-parametric test. Mean \pm SEM values for normalized pY53 actin intensity in Control group = 1.000 ± 0.03695 and Nocodazole group = 0.6758 ± 0.03851 . **** $P < 0.0001$ by Mann-Whitney non-parametric test. For figures B and C, data were obtained from 61 Control cells (252 neurites), and 56 Nocodazole-treated cells (219 neurites) from 3 different cultures. (Quantification by Dr. Meka, ZMNH, Hamburg)

Collectively, this study provides new insight into the regulation of how the cytoskeleton determines neuronal polarization: in early developing neurons, the centrosome modulates microtubule modification/stabilization to direct the formation of axon. Specifically, Cep120-dependent microtubule acetylation initially organized near the centrosome spreads out radially into cell periphery as the unpolarized state is broken, eventually concentrates in one specific neurite which is conferred axonal identity, while the distributions of polyglutamylation and tyrosination or α -tubulin do not follow the same pattern during axon formation. Besides being an MTOC, the centrosome also acts as a center for actin organization. For the first time, I identified that somatic F-actin is delivered into neurites via myosin II to function as a negative factor inhibiting neurite growth. The specific neurite receiving less somatic F-actin is growing as an axon. During dendrite elongation, radial somatic F-actin translocation into neurites is drastically diminished from all neurites suggesting that cellular growth is restricted by the somatic F-actin flow. Mechanistically, the enrichment of actin phosphorylation at tyrosine-53 in the neurite shafts, which promotes actin instability, counteracts this somatic F-actin translocation to promote neurite elongation. Moreover, the truncated Kinesin-1, which is the earliest hallmark of axon formation, localizes preferentially in the neurite with an increase of actin phosphorylation. The axon-inducing effect of microtubule acetylation favors actin phosphorylation at tyrosine-53 to promote axon growth. Finally, microtubule acetylation in synergy with actin phosphorylation facilitates polarity establishment.

3. Discussion

The formation of axons and dendrites is critical for proper neuronal functions. This hierarchical polarized growth is initiated by axon specification followed by dendrite development (de Anda et al., 2010; Dotti et al., 1988; Noctor et al., 2004). One important question in neurobiology is how a neuron accomplishes this polarized growth sequentially. The prevailing view is that neuronal polarization is initiated by intrinsic activation of signalling pathways underlying the first symmetry breakage that precedes axon formation (Arimura and Kaibuchi, 2007; Barnes et al., 2008; da Silva and Dotti, 2002). Further studies identified that tubulin and the actin cytoskeleton appear to be the major endpoint of these intrinsic polarity regulators leading to axon-dendrite polarization (Andersen and Bi, 2000; Bradke and Dotti, 1999; Li and Gundersen, 2008; Neukirchen and Bradke, 2011; Witte et al., 2008; Zhao et al., 2017). Thus, the neurite with highly dynamic F-actin in the growth cone and more stable microtubules develops as an axon, whereas the remaining become dendrites. Importantly, somatic F-actin organized around the centrosome is radially delivered into growth cones as a source of actin to regulate growth cone behavior (Meka et al., 2019). With this study, I aimed to investigate the molecular mechanisms by which microtubule stabilization preferentially occurs in axons and whether somatic F-actin plays a role during neuronal polarization.

This study unveiled that a centrosomal protein, Cep120, directs the organization of acetylated microtubules, hence supporting axon extension. Moreover, I detected that somatic F-actin translocation into neurites functions as a growth inhibitor. Therefore, the neurite that grows as an axon receives less somatic F-actin. Mechanistically, actin phosphorylation at tyrosine-53 (pY53) in the neurite shafts precludes this somatic F-actin translocation, thus promoting neurite growth. Notably, pY53 is promoted by microtubule acetylation. In summary, this study sheds light on how stable microtubule organization

together with somatic F-actin translocation into neurites can govern neuronal polarization. Notably, it provides a new model to explain the sequential growth of neurites during neuronal polarization with the axon forming first followed by the dendrite elongation.

3.1 The centrosome organizes MT stabilization for axon specification

3.1.1 Axon-related radially arranged acetylated MTs invade neurites

Microtubule post-translational modifications (PTMs) are interpreted as a “tubulin code” to grant MT differential properties which are important for MTs performing specific functions (Wloga et al., 2017). Especially, PTMs-induced stable MTs play an instructive role in regulating the initiation of neuronal polarization. To start the polarized growth, one out of several morphologically equal neurites is singled out to develop into the axon. Local MT stabilization, determined by measuring AcetyTub, deTyrTub or PolyGluTub precedes this process, termed axon formation (Baas et al., 2016; Witte et al., 2008). Selective accumulation of the Kinesin-1 motor domain into the nascent axon is facilitated by tubulin acetylation and detyrosination (Jacobson et al., 2006; Konishi and Setou, 2009; Reed et al., 2006). Moreover, the translocation of Kinesin-1 into Taxol-induced multiple axon-like processes correlates with the enrichment of tubulin acetylation, detyrosination, and glutamylation (Hammond et al., 2010). Overall, the polarization of axon appears to require a higher percentage of stable MTs compared with their dendritic counterparts (Baas et al., 2016). Nonetheless, the exact mechanisms of how MT stabilization is acquired in the establishment of axons remain unclear.

In this section, I demonstrated that before neurite extension, the acetylated MTs preferentially surrounded the centrosome in the cell body (Figure 2-1). Once neurites sprout, the acetylated MTs spread over the soma to penetrate nascent neurites and eventually enriched in the growing axon, consistent with the results

from Witte *et al.* that the early polarization of stabilized MT in one neurite precedes axon formation (Witte et al., 2008). Interestingly, it seems that only AcetyTub, but not PolyGluTub, follows an initial radial organization, whereas PolyGluTub spreads out more in the cell body, instead of concentrating around the centrosome at stage 1. Additionally, coupling with radially spreading out, the levels of AcetyTub in the soma area increased accordingly in a graded manner, especially in the transition from stage 1 to stage 2 during which axonal fate is determined. These observations suggest the involvement of specific tubulin PTMs in the establishment of early axonal identity. Importantly, somatic acetylated MTs in radial organization initially might set the conditions to break the neuronal symmetry to support axon formation.

3.1.2 Regulation of somatic MT stabilization promotes the formation of axons

Changes in the morphology of neurons, like the formation of supernumerary axons, are often used as a readout for altered polarity (Arimura and Kaibuchi, 2007). Thus, it is conceivable that an analysis of neurons with multiple axon-like processes would offer the possibility to further explore the correlation between somatic stable MT and axon formation. To this end, I pharmacologically altered MT dynamics using the MT stabilizer Taxol with a low concentration (Witte et al., 2008), together with CytoD which disrupts F-actin assembly to induce multiple axons (Bradke and Dotti, 2000b). Taxol-treated neurons formed multiple axons with MT acetylation significantly increased in the soma as well as enriched in the axons. Interestingly, my study uncovered that CytoD did not induce multiple axons in the less developed stage 1 cells, containing relatively fewer stable/acetylated MTs in the soma, while later-stage neurons did produce more than one axon after CytoD treatment (Figure 2-3). Thus, the behavior of somatic acetylated MTs is the essential key to induce

axon formation. Importantly, it is confirmed for the first time that CytoD-induced multipolarity is stage-dependent, which requires enough stable MTs.

In addition, other PTMs of α -tubulin, including polyglutamylation, tyrosination, and even α -tubulin also followed a similar increase in the soma. It could be explained that coordination of MT stabilization might be required to control developmental transitions by building MT networks and modulating polarized transport in axon determination. As proof, tubulin polyglutamylation is proposed to mediate interactions of MAPs and MTs. Moderately polyglutamylated tubulins (~3 glutamyl units) are the optimal binding sites for Tau, MAP1b, MAP2, and Kinesin-1 (Bonnet et al., 2001; Boucher et al., 1994; Larcher et al., 1996), whereas MAP1a preferentially binds to tubulins with a higher degree of glutamylation (~6 glutamyl units) (Bonnet et al., 2001). Interestingly, glutamylation of α -tubulin undergoes a progressive increase in its degree of glutamylation from 2 to 6 glutamyl units during neuronal development (Audebert et al., 1994). On the contrary, loss of polyglutamylation causes abnormal trafficking mediated via MT-dependent motor proteins (Ikegami et al., 2007; Reed et al., 2006). Moreover, defects in tubulin-tyrosine-ligase contribute to the increase of MT stability which in turn accelerates neurite outgrowth with a premature axonal differentiation (Erck et al., 2005). Interestingly, these deficient neurons tend to form supernumerary axons, similar to the phenotype induced by pharmacological MT stabilization. This hints that tyrosinated tubulin is required for the proper control of neurite steering and extension, as confirmed by the detection of tyrosinated tubulin predominantly in growth cones (Witte et al., 2008). Of note, it will be interesting to unveil the role of enzymes mediating PTMs in more detail during neuronal polarization for future studies.

3.1.3 The centrosome directs microtubule stability to initiate axon outgrowth

The centrosome, the best-studied MTOC organizing MT nucleation (Sanchez and Feldman, 2017), was recently identified to localize close to the area where neurons form the first neurite, which later develops into the axon during early neuronal differentiation (de Anda et al., 2005; Zmuda and Rivas, 1998). Cep120, as a centriolar protein at the centrosome, bears a microtubule-binding domain which is essential for directly binding microtubules *in vitro* (Lin et al., 2013). Intriguingly, Cep120 is involved in the nucleation and organization of microtubules at the centrosome with respect to its ability to regulate the distribution of PCM proteins (Bettleja et al., 2018; de Anda et al., 2010; Joseph et al., 2018; Xie et al., 2007). In addition, loss of Cep120 leads to defective ciliary assembly and elimination of ciliogenesis signaling (Bettleja et al., 2018). It is plausible to hypothesize that centrosome/Cep120 could be a critical element in directing the organization of acetylated MTs supporting the establishment of axons.

As shown in this study, the radial organization of acetylated MTs initially concentrated around the centrosome. Interference of Cep120 expression had bidirectional effects on the levels of AcetyTub in the soma across stages 1-3 (Figure 2-6). Importantly, overexpression of Cep120 induced the occurrence of supernumerary axons. Conversely, Cep120 downregulation impeded axon formation and decreased the complexity of neurons bearing fewer neurites, and reduced neurite length. This finding is consistent with the results from Anda *et al.* that the specific downregulation of Cep120 in the developing cortex precluded axon formation and impaired neuronal migration (de Anda et al., 2010). Further investigation *in vivo* showed that lack of Cep120 altered the morphology of migrating neurons in the CP by precluding the formation of a leading process (Meka et al., 2022). Therefore, it strongly indicates that the

centrosome/Cep120 correlates with this preferential polarization of MT acetylation determining axon formation.

Another intriguing point worthy to highlight is that differentiated neurons reassign MTOC function from centrosomal sites to non-centrosomal sites to generate non-radial MT organization for specific functions (Sanchez and Feldman, 2017; Wilkes and Moore, 2020). Initially, the centrosome, inherited from the mother-progenitor neurons, nucleates MTs to support neurite outgrowth (Rao et al., 2016; Stiess et al., 2010; Yamada and Hayashi, 2019). After axon initiation, the centrosome-dependent MT organization shifts to acentrosomal organization, as confirmed by the observation that centrosome ablation during axon elongation has no effect on axon extension or regeneration (Stiess et al., 2010). However, before morphological axonogenesis *in vivo*, centrosome ablation inhibits axon formation while decreasing the content of somatic growing MTs (Andersen and Halloran, 2012; Meka et al., 2019). Considering these studies, the vital role of the centrosome in neuronal polarization might promote the initial axon specification/outgrowth, as also confirmed by my results that the centrosome directs acetylated MTs radially into one specific neurite in the initial neuronal development, which leads to an early bias of MT stability between different neurites, setting the proper conditions for axon specification.

As neurons are polarized with one axon and multiple dendrites, axonal MTs are predominantly oriented plus-ends-out (Yau et al., 2016). By contrast, dendritic MTs have mixed polarity in vertebrate neurons or minus-ends-out orientation in *C. elegans* and *Drosophila*, which implies the existence of non-centrosomal MTOCs (ncMTOCs) (Goodwin et al., 2012; Stone et al., 2008; Yau et al., 2016). Of note, Golgi outposts appear to be a ncMTOC directly nucleating MTs to shape dendrite morphology (Ori-McKenney et al., 2012). Moreover, in cultured

rodent hippocampal neurons, RanGTP is verified to be an acentrosomal site to take over MT nucleation (Ems-McClung et al., 2020; Wilkes and Moore, 2020). Furthermore, Augmin and gamma-tubulin ring complex (γ TuRC) strongly mediate non-centrosomal MT nucleation as well as ensure the uniform plus end-out orientation in axons of matured neurons (Sánchez-Huertas et al., 2016; Stiess et al., 2010). This suggests that the centrosome is vital to promote the initiation of axon formation, while once the axonal fate is determined to start growing (axon elongation), other functional-like components gradually take over the predominant role in MT-nucleation to accomplish the polarized structure. However, why the centrosome gradually loses MOTC activity, and how MT remodeling shifts from a “centrosomal” to an “acentrosomal” manner remains poorly understood.

3.1.4 Somatic microtubule dynamics versus PTMs

MTs are highly dynamic polymers, growing by addition of heterodimers to the plus-end. Similarly, MTs shrink rapidly by loss of α/β -tubulin subunits known as “catastrophe”. Under certain conditions, shrinking MTs could switch back to growth again which is considered dynamic instability (Brouhard and Rice, 2018; Mitchison and Kirschner, 1984; Zwetsloot et al., 2018). A growing body of studies point out that regulations of MT assembly are essential for axonal growth. For instance, the promotion of MT assembly and decrease of shrinkage rate lead to MT mass partially stable but still dynamic in neurons. Consequently, this MT mass is involved in modulating axonal differentiation (Fukata et al., 2002). In this regard, it is worth substantiating that how MT dynamics behave in these early somatic MTs.

Further observation on monitoring MT growth in the soma of the early-developing-neurons via live imaging with EB3 which is a microtubule-plus-end-binding protein (Komarova et al., 2009; Meka et al., 2022; Stepanova et al.,

2003), indicated that during neuronal polarization, somatic MTs went through distinct changes with increased growth speed and length, suggesting MTs are highly dynamic near the centrosome (Meka et al., 2022), in line with the results from TyrTub staining (Figure 2-1). Specifically, at stage 2, somatic MTs displayed drastic changes before axon extension, compared to that at stage 1 and stage 3 (Meka et al., 2022). Therefore, such changes might bring up the proper context to break cellular symmetry, leading to axon extension. However, in contrast to high MT dynamics near the centrosome, acetylated MTs were detected preferentially surrounding the centrosome in fixed neurons, indicating more stable MTs in this region. Notably, a recent study revealed that inhibition of tubulin-deacetylation pharmacologically has no significant effects on MT dynamics (e.g., growth rate and shortening rate) (Matov et al., 2010). Nevertheless, the acetylated MTs were more resistant to nocodazole-induced depolymerization (Matov et al., 2010). Altogether, stable MTs might not forcefully imply fewer dynamic MTs. Instead, the increased stability and polymerization may allow MTs to protrude with their dynamic ends more distally, thereby promoting axon formation.

Interestingly, the alterations of MT dynamics in the soma area during neuronal polarization might be influenced by Cep120, confirmed by the results from proteomics analysis that lack of Cep120 downregulated the levels of proteins associated with MT dynamics, such as MAP2, Tau, EB1, DCX, CRMP2, MAP1b, and Tubb2b, etc. (Meka et al., 2022). Moreover, transforming acid coiled-coil protein 3 (TACC3) comets moved anterogradely with selective accumulation in the longest neurites and positively correlated with somatic AcetyTub in polarizing neurons (Meka et al., 2022). Furthermore, overexpression of Cep120 rescued the TACC3 disability-induced defection of somatic acetylated MTs (Meka et al., 2022). Therefore, it is conceivable that

Cep120 in coordination with TACC3 regulates MT stabilization directing axon formation.

3.2 Actin-Y53 phosphorylation regulates somatic F-actin translocation to promote neuronal polarization

3.2.1 Myosin II-mediated somatic F-actin translocation suppresses neurite growth

Somatic F-actin is demonstrated to be a fast and continuous source of actin polymers translocated into the cell periphery (Meka et al., 2019). My study verified that this novel somatic F-actin functions as a negative factor for neurite growth when they are delivered into the neurite tips (Figure 2-8). During axon extension, the shorter neurites received more somatic F-actin by which their growth was hampered. Importantly, this somatic F-actin flow was arrested in the soma at later stages during which neurons initiated the dendritic growth. Therefore, it gives a hint that this somatic F-actin could be a regulator to mediate axon-dendrite sequential growth, cooperating with the positive loop which is continuously activated to guide axon outgrowth (see 1.3.1.3). Further investigation indicated that myosin II mediated somatic F-actin delivery, as also confirmed by which inhibition of myosin II pharmacologically disrupted somatic F-actin transport into growth cones that induced the elongation of shorter neurites but not the one growing as the axon (Figure 2-10).

Of note, it is reported that there are two major isoforms of myosin II in neurons, myosin IIA and IIB sharing overlapping functions (Costa and Sousa, 2020; Togo and Steinhardt, 2004). The existence of myosin IIA and IIB is throughout the soma and neurites, and enriched at growth cones of early-stage neurons. In my study, PaGFP-myosin IIA as well as PaGFP-myosin IIB was constructed to perform photoactivation. However, myosin IIB movement/accumulation cannot be significantly detected with our current technology. It is noteworthy to

emphasize that myosin II isoforms differ in ATPase activity and duty ratio (Costa and Sousa, 2020). Specifically, myosin IIA bears a higher rate of ATP hydrolysis and pushes actin filaments translocation more rapidly (Kim et al., 2005), while myosin IIB carries a higher duty ratio indicating that it can spend more time remaining strongly bound to actin, which in turn facilitates to crosslink actin filaments (Wang et al., 2003). Moreover, they present different subcellular distributions in the growth cone, which a highly dynamic structure composed of a central domain, a transition zone and a peripheral domain (Lowery and Van Vactor, 2009) (Figure 3-1). Myosin IIA is highly enriched in the axon shaft and the central domain. In contrast, myosin IIB exists extensively in the transition zone and peripheral domain (Costa and Sousa, 2020). In light of these lines, the distinct subcellular location and kinetic property of myosin IIB might explain the results of PaGFP-myosin IIB in the photoactivation experiments. Above all, my data showed that myosin IIA might be the predominant motor mediating somatic F-action delivery from the soma area to the neurite tips.

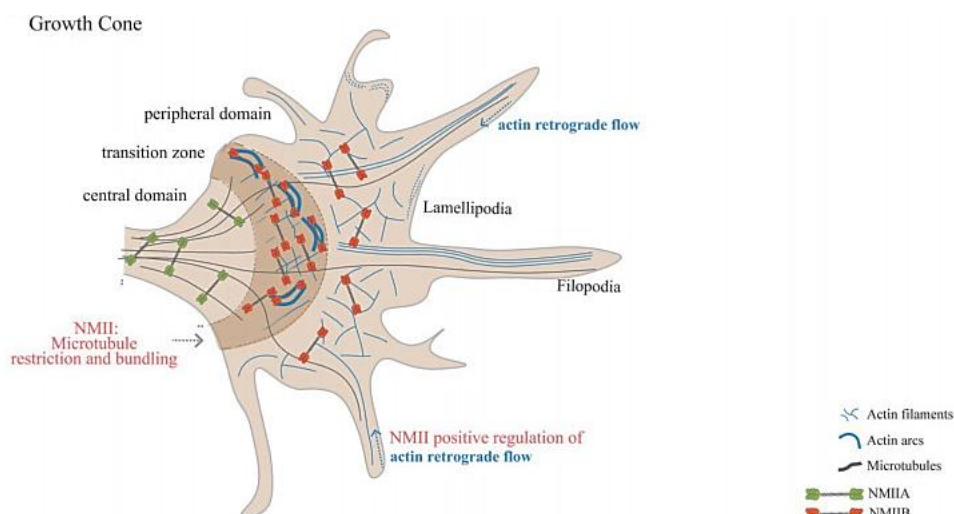


Figure 3-1: Myosin II in axonal growth cone. Schematic representation of the growth cone. The growth cone includes a central domain, mainly consisting of bundled microtubules (grey lines), a transition zone, enriched in actin arcs (blue hemicircular lines) and a peripheral domain, enriched in actin (blue lines) in the form of lamellipodia and filopodia. Actin bundles assemble near the growth cone leading edge, translocate rearward by retrograde flow towards the transition zone (blue dashed arrows in the peripheral domain) and recycle through bundle severing. Nonmuscle myosin IIA (NMIIA, green) is mainly located

within the central domain and NMIIIB (red) in the transition zone and peripheral domain, figure from (Costa and Sousa, 2020).

My results do not clarify the molecular mechanism by which somatic F-actin inhibits neurite extension. Several studies have observed that the local assembly of F-actin at growth cones affects neurite growth (Baas, 1999; Bradke and Dotti, 1999; Forscher and Smith, 1988). Therefore, it is reasonable to assume that somatic F-actin might have effects on this local assembly at growth cones to regulate neurite extension. In the peripheral domain of the growth cone, actin bundles assemble near the leading edge, meanwhile, these actin-bundles are translocated rearward by retrograde flow and recycle through bundle severing within the transition zone to sustain growth cone dynamics and guide axon growth (Costa and Sousa, 2020; Medeiros et al., 2006; Zhang et al., 2003). In this regard, somatic F-actin might disturb this balance of assembly-disassembly and/or resist severing to form a relatively stable actin network which may restrain MT from protrusion into the peripheral domain (Dupraz et al., 2019; Schaefer et al., 2002) resulting in neurite growth inhibition.

To my knowledge, this is the first time to show that neuronal differentiation can be mediated by somatic F-actin delivery into growth cones. It was suggested an intrinsic feedback system with inhibitory internal signals propagated from the nascent axon would be transmitted to dendrites and preclude the extension of dendrites during axon formation (Andersen and Bi, 2000), my results now suggest that the somatic F-actin translocation into neurites could function as a novel internal inhibitory signal restricting neurite extension, which in turn acts a signal from the soma to ensure the axon-dendrite sequential outgrowth.

3.2.2 Actin-Y53 phosphorylation modulates somatic F-actin delivery

Myosin II consists of two regulatory light chains (RLCs) and two essential light chains (ELCs), tightly bound to two heavy chains (Vicente-Manzanares et al., 2009). The heavy chain folds into the myosin II globular head containing the

conserved motor domain where the actin-binding and the ATP-binding sites reside (Vicente-Manzanares et al., 2009). A recent study revealed that blebbistatin preferentially binds to the myosin II-ADP-Pi complex and thereby slows down the phosphate release, and further identified the aqueous cavity located between the actin-binding cleft and the nucleotide-binding site of the myosin head is the blebbistatin-binding site, indicating that this conformer blocks myosin II in “an actin-detached state” – forming a myosin II-ADP-Pi-blebbistatin complex with low actin affinity (Kovács et al., 2004), which consequently might impede myosin II-mediated transport along actin-cytoskeleton. Therefore, it explains the result that inhibition of myosin II with blebbistatin resulted in a reduced translocation of somatic F-actin into neurites. Whereas the reduced somatic F-actin flow still went into neurites following a negative correlation with the neurite length, suggesting that it is not inherent to the myosin II motor that the preferential delivery of somatic F-actin into minor neurites, but not into the growing axon. Then, what mediates the preferential delivery of somatic F-actin into shorter neurites?

Actin post-translational modifications are considered a powerful mechanism to modify the actin-cytoskeleton in a temporally and spatially controlled manner (Bertling et al., 2016; Terman and Kashina, 2013), including oxidation, arginylation, phosphorylation, and SUMOylation (Bertling et al., 2016; Terman and Kashina, 2013). In particular, the phosphorylation of actin-Y53 is highly conserved serving as a regulator of reorganization and stabilization of the actin-cytoskeleton in mammalian neurons (Bertling et al., 2016). Actin-Y53 phosphorylation stabilizes the D-loop of actin which in turn decreases the affinity between actin molecules and shortens actin filaments (Baek et al., 2008; Liu et al., 2006), resulting in an exceptionally dynamic actin network (Bertling et al., 2016). Hence, it is plausible to envision that unstable actin-cytoskeleton

in neurites might hinder the translocation of myosin II-dependent somatic F-actin into growth cones.

Further investigation verified that the level of actin-Y53 phosphorylation in the neurite shafts is a vital determinant for somatic F-actin delivery. In the developing course from stage 2 to stage 3, the neurite enriched with pY53 actin received nothing or quite less somatic F-actin. Meanwhile, this neurite was the longest one with axonal characteristics (growing rapidly, highly dynamic growth cone). Notably, blebbistatin-induced long neurites contained a higher level of pY53 actin. Moreover, once dendrites started to extend, pY53 actin level increased significantly in these neurites (dendrites) resulting in the arrest of somatic F-actin in the soma. Thus, these results suggest that neurite growth is supported by actin-Y53 phosphorylation in the shafts/neurites, which in turn precludes somatic F-actin translocation into the growth cones.

3.2.3 Actin-Y53 phosphorylation favours axon/neurite elongation

To further understand the importance of pY53 in neurite growth/neuronal polarization, I adopted actin mutants to manipulate the levels of pY53 actin in cortical neurons, which unveiled that the introduction of constitutively phosphorylated actin (Y53E) promoted the formation of longer axons. On the contrary, the existence of phospho-dead actin (Y53A) had negative effects on neurons extending axons (Figure 2-14). Additionally, the neurite with increased pY53 actin signal was the one bearing Kif5c signal (Figure 2-15). Interestingly, the neurites positive with Kif5c also contained a higher level of acetylated tubulin (Figure 2-15) consistent with the work from Reed et al. (Reed et al., 2006). Further photoactivation investigations revealed that photoactivated somatic PaGFP-UtrCH moved preferentially into neurites lack of Kif5c signal (Figure 2-15) which confirmed that somatic F-actin is selectively delivered into non-axonal neurites during axon formation.

Given that actin phosphorylation at Y53 is highly conserved, the next question is: which kinase phosphorylates actin-Y53? One study showed that overexpression of tyrosine receptor kinase B (TrkB) increases tyrosine phosphorylation of β -actin in mouse cortex (Semenov et al., 2006). Tumor necrosis factor (TNF- α) induces rapid tyrosine phosphorylation of paxillin and focal adhesion kinase (FAK) which regulate actin re-distribution (Koukouritaki et al., 1999). Moreover, FAK can interact with a variety of signal transduction molecules including Src (protein tyrosine kinase) and related kinases, PI3K, p130^{Cas} and paxillin to modulate cell motility, focal adhesion and cytoskeleton remodeling (Cary et al., 1998; Goldmann, 2012; Gu et al., 1999). Notably, the FAK/Src complex induces tyrosine phosphorylation of p130^{Cas} (Crk-associated substrate) involved in actin organization (Abbi and Guan, 2002; Camacho Leal Mdel et al., 2015; Goldmann, 2012). Plausibly, TrkB, FAK or Src family kinases could be the potential candidates to mediate actin-Y53 phosphorylation. Currently, I have updated a kinase-catalyzed-crosslinking-and-streptavidin-purification (K-CLASP) strategy to find out the specific kinase (Bahl et al., 2021; Dedigama-Arachchige and Pflum, 2016). In this assay, rat cortical cell lysate was incubated with a biotinylated actin-wt-peptide containing the sequence surrounding Tyr-53, and ATP-arylazide (ATP-ArN3) under ultraviolet (UV) radiation to identify the potential tyrosine kinases as well as interacting proteins of potential functional relevance by mass spectrometry (MS). The verification of this will have to wait for further investigation.

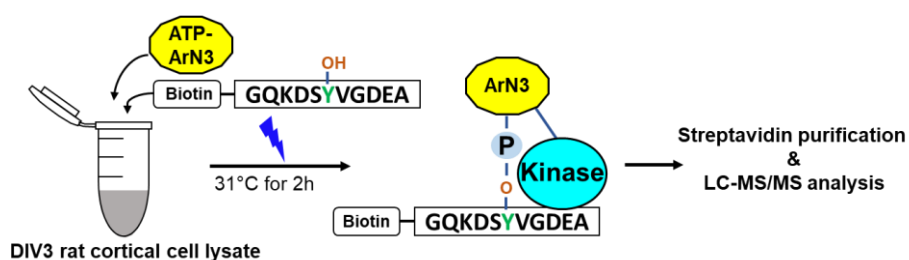


Figure 3-2: Illustration of K-CLASP technique to identify the interactome of actin-Tyr53-containing peptide. K-CLASP utilizes γ -modified ATP analog ATP-ArN3 to covalently couple kinase-

substrate pairs via photo-crosslinking. Biotin-tagged (streptavidin) actin-Y53-wt-peptide or Y53A-actin-peptide is incubated with the cell lysate in the presence of ATP-ArN3 and UV irradiation. The crosslinked peptide-kinase complex is then streptavidin purified and analyzed by tandem mass spectrometry (MS/MS) to identify the captured kinase. Adapted from (Bahl et al., 2021).

3.3 Interplay of microtubule acetylation and actin-Y53 phosphorylation promotes neuronal polarization

Interestingly, actin-Y53 phosphorylation and MT acetylation are co-enriched in the growing axon of stage 3 neurons (Figure 2-16B). However, pY53 actin distribution showed a weaker correlation with PolyGluTub compared to AcetyTub (Figure 2-17B). Moreover, Taxol-induced enhancement of MT acetylation increased pY53 actin levels in all neurites (Figure 2-16G, H). Accordingly, nocodazole treatment, which induces MT depolymerization, reduced the levels of pY53 actin (Figure 2-18C). Interestingly, overexpression of pY53 actin (Y53E) only induced neurons with longer axons without producing multiple axons (Figure 2-14C) which could be a result of that initial axon formation is MT stability-dependent (see details in 2.1) (Meka et al., 2022), and also hints that the important role of pY53 actin is to promote neurite elongation. Thus, these results suggest that actin-Y53 phosphorylation is more directly influenced by tubulin acetylation. MT stability might be a trigger mediating this specific actin phosphorylation in the growing neurite. More experiments are required to explore this possibility.

Several lines of evidence unveiled that a crosstalk between F-actin and MTs is crucial for the establishment of polarity, coupled with re-arrangements of F-actin and MTs (Pimm and Henty-Ridilla, 2021). To illustrate, MAPs, like MAP2c, can interact with MT as well as F-actin directly to alter their dynamics which in turn promotes neurite formation (Cunningham et al., 1997; Dehmelt et al., 2003; Ozer and Halpain, 2000). CLIP170, a plus-end tracking protein (+TIPs) required for dendritic morphology, recruits actin to the MT plus-end via EB1 to accelerate F-actin polymerization (Henty-Ridilla et al., 2016). Moreover, MTs might

penetrate the highly dynamic axonal growth cone along actin bundles mediated by orientation-sensitive motor proteins to drive axon growth (Huda et al., 2012; Szikora et al., 2017). Furthermore, MT polymerization at the leading edge of growth cones contributes to Rac activation. Subsequently, activated Rac promotes actin polymerization and membrane protrusion (Seetharaman and Etienne-Manneville, 2019). Notably, the work from Zhao *et al.* indicated that MT stabilization during initial axon extension leads to the enhancement of F-actin dynamics via EB3-Drebrin E-mediated interaction (Zhao et al., 2017). These results suggest that the tubulin-actin crosstalk occurs bidirectionally assisted by coordination of coupling molecules, cellular signals, physical properties and even the temporal context (Pimm et al., 2022). Interestingly, my results unveiled that pY53 actin in the neurite intermingles with acetylated MTs, which allows to envision that the post-translation modifications of tubulin and actin might contribute to the crosstalk between actin and tubulin during neuronal polarization. More work is necessary to delineate how pY53 actin and acetylated MT are intertwined during neurite growth.

4. Outlook

The initiation of neuronal polarity is marked by one out of several neurites singled out to acquire axonal identity. This study firstly unveils the instructive role of centrosome-dependent microtubule stabilization for initial axon formation, indicating the Cep120-organized MT acetylation directs the axon formation, together with the internal inhibitory signal of somatic F-actin translocation suppressing neurite growth. Actin tyrosine-53 phosphorylation counteracts somatic F-actin translocation to promote neuronal polarization which is favored by acetylated MT in the neurites.

In addition to the points previously described in the discussion section as future perspectives, the next challenge beyond the scope of this study that is worthy

to be highlighted is to characterize the exact mechanisms of somatic MT acetylation spreading into the growing axon. Given the interaction between F-actin and microtubules, it is possible that the stable pool of MTs is transported from the cell body into growing axons following a motor-dependent sliding model as described before (Guha et al., 2021; He et al., 2005; Kundu et al., 2021; Liu et al., 2010; Rao et al., 2017; Slaughter et al., 1997). My work unveiled that actin phosphorylation at tyrosine-53 is influenced by MT acetylation, ultimately leading to timely neurite growth, first the axon and then the dendrites. Considering that MT acetylation/stabilization is sufficient to induce axons out of differentiated dendrites and the existence of acetylated/stable MTs in the lesioned axon stump promotes axon regrowth upon distal axotomies (Dotti and Banker, 1987; Gomis-Rüth et al., 2008). Therefore, it would be worth exploring the ability of actin-tyrosine-53 phosphorylation in converting a minor neurite into a growing axon or guiding axon regeneration under situations in which the original axon is damaged (axonal lesion), thereby further investigating the role of actin-Y53 phosphorylation in axon formation as well as the relationship between actin-Y53 phosphorylation and MT acetylation. Further identification of potential regulators/kinases for tubulin acetylation/actin phosphorylation will give new insight into the research on neuronal polarity.

5. Material and Method

5.1 Material

5.1.1 Animal

C57BL6/J mice and Wistar HsdCpb:WU rats were utilized for this study. All animals were raised and housed in the Central Animal Facility at University Medical Center Hamburg-Eppendorf (UKE), Hamburg based on the standard regulations. Animal experiments were performed according to the German and European Animal Welfare Act and with the approval of local authorities of the city-state Hamburg (Behörde für Gesundheit und Verbraucherschutz, Fachbereich Veterinärwesen) and the animal care committee of the University Medical Center Hamburg-Eppendorf. For primary cultures, 2-4 months old pregnant rats and mice were used.

5.1.2 Cell lines

Rat primary hippocampal, mouse primary cortical cells and BL21-CodonPlus (De3)-RIL competent cells (Agilent Technologies, cat. # 230280) as well as XL10-Gold* ultracompetent cells (Agilent Technologies, cat. # 200315) were involved in this study.

5.1.3 Recombinant DNAs

Table 1: List of recombinant DNAs

Recombinant DNA	Source	Identifier
CAG-Venus	a gift from Zhigang Xie; de Anda et al., 2010	/
pSilencer2-U6-shControl	Xie et al., 2007	/
pSilencer2-U6-shCep120	Xie et al., 2007	/
pAAV-CAG-tDimer	a gift from Thomas Oertner	/
CMV- Actin-mCherry	a gift from Pirta Hotulainen; Bertling et al., 2016	/
CAG-Farnesylated-GFP	a gift from Annette Gärtner; de Anda et al., 2010	/
pNeuroD-GFP	a gift from Zhigang Xie; de Anda et al., 2010	/
pET-21a	Novagen	Cat# 69740-3
pcDNA3.1-mMaroon1	a gift from Michael Lin	RRID: Addgene_83840

mRuby2-Actin-C-18	a gift from Michael Davidson	RRID: Addgene_55889
PaGFP-UtrCH	a gift from William Bement	RRID: Addgene_26738
mPA-GFP-MyosinIIA-C-18	a gift from Michael Davidson	RRID: Addgene_57149
mCherry- β -wt-actin	a gift from Pirta Hotulainen; Bertling et al 2016	/
mCherry- β -Y53A- β -actin	a gift from Pirta Hotulainen; Bertling et al 2016	/
GFP- β -Y53E- β -actin	a gift from Pirta Hotulainen; Bertling et al 2016	/
pBa-KIF5C 559-tdTomato-FKBP	a gift from Gary Banker & Marvin Bentley	RRID: Addgene_64211

5.1.4 Medium and reagents for primary cell culture

Table 2: List of biological reagents used for primary cell culture.

Reagent	Source	concentration
Primary Neuro Basal Medium	Invitrogen (#21103049)	1x (500 mL)
L- Glutamine 200mM	Invitrogen (# 25030024)	2 mM
B-27 Supplement	Invitrogen (# 17504044)	1X
HBSS (without Ca ²⁺ /Mg ²⁺)	Invitrogen (# 14170088)	0.25% (vol/vol)
DMEM with GlutaMAX	Invitrogen (# 6196526)	1x (500 mL)
Fetal bovine serum (FBS)	Gibco (# 105000649)	10 %
Pen/Strep	Gibco (# 15140122)	1X
Poly-L-Lysine (PLL)	Sigma (# P2636-500mg)	5 μ g/ml
Laminin	Sigma (# L2020)	3-5 μ g/ml
Hibernate™-E Medium	Gibco (# A1247601)	1X
Papain	Sigma (# P5306-25mg)	25 μ g/ml
DNase I	Sigma (# D4263-5VL)	10 μ g/ml
Cytosine-1- β -D-arabinofuranoside (AraC)	Sigma (# C1768-100g)	0.5 μ M
Trypan blue	Invitrogen (# 15090046)	/

5.1.5 Antibodies

Antibodies were stored in aliquots at -20°C, and secondary antibodies were protected from light upon using.

5.1.5.1 Primary antibodies

Table 3: List of primary antibodies used in this study

Antibody name	Source	Application
Mouse anti-acetylated tubulin	Sigma (# T7451)	ICC 1:700 WB 1:500
Mouse anti-polyglutamylated tubulin	Sigma (# T9822)	ICC 1:250 WB 1:500
Rat anti- α -tubulin	SySy (# 302217)	ICC 1:400
Rat anti-tryosinated tubulin (YL1/2)	Abcam (# ab6160)	ICC 1:400 WB 1:1000
Sheep anti-tubulin (total)	Cytoskeleton (# ATN02)	ICC 1:400 WB 1:1000
mouse anti-GAPDH	Santa Cruz (# sc-32233),	WB 1:2500
Mouse anti-Tau-1	Millipore (# MAB3420)	ICC 1:700
Chicken anti-MAP2	SySy (# 188006)	ICC 1:500
Mouse anti-Ankyrin G (463)	Santa Cruz (# sc-12719)	ICC 1:700
Rabbit anti-Phospho-Y53-actin	MyBioSource (# MBS474080)	ICC 1:100
Rabbit anti-Cep120	lab-made, Meka et al., 2022	ICC 1:800
Rabbit anti-Pericentrin	Covance (# PRB-432C)	ICC 1:500

5.1.5.2 Secondary antibodies

Table 4: List of secondary antibodies used in this study

Antibody name	Host	Conjugate	Source	Application
Anti-rabbit IgG	Goat	AF 488	Invitrogen (# A11077)	ICC 1:1000
Anti-rabbit IgG	Donkey	AF 647	Invitrogen (# A31573)	ICC 1:1000
Anti-rat Ig G	Goat	AF 568	Invitrogen (# A11077)	ICC 1:1000
Anti-mouse IgG	Donkey	AF 488	Invitrogen (# A21202)	ICC 1:1000
Anti-mouse IgG	Donkey	AF 647	Invitrogen (# A31571)	ICC 1:1000
Anti-mouse IgG	Goat	AF 405	Invitrogen (# A31553)	ICC 1:1000
Anti-mouse IgG	goat	STAR 580	Abberior (# 2-0002-500-1)	ICC 1:500
Anti-rat IgG	goat	STAR RED	Abberior (# STRED-1007-500UG)	ICC 1:500
Anti-sheep IgG	donkey	STAR RED	Abberior (# STRED-1056-500UG)	ICC 1:500

anti-mouse IgG	goat	HRP	Dianova (#115-035-003)	WB 1:5000
anti-rabbit IgG	goat	HRP	Dianova (#111-035-003)	WB 1:5000
anti-rat IgG	donkey	HRP	Dianova (#DAB-87223)	WB 1:5000
anti-sheep IgG	donkey	HRP	Dianova (#713-035-147)	WB 1:5000

5.1.6 Other Dyes

Table 5: List of other dyes used in this study

Dye name	Conjugate	Source	Application	Function
Acti-Stain 488 Phalloidin	AF 488	Cytoskeleton (# PHDG1)	ICC 1:120	Visualize F-actin
Hoechst (4',6-diamidino-2-phenylindole) (DAPI)	AF 350	Invitrogen (# 33258)	ICC 1:5000	Label nucleus

DAPI was applied together with secondary antibodies, while anti-stain 488 phalloidin was used alone after the incubation of secondary antibodies during immunostaining.

5.1.7 Chemicals

Table 6: List of chemicals used in this study

Chemical	Stock	Solvent	Source
Cytochalasin D	2 mM	DMSO	Sigma (# C2618-200UL)
Taxol	5 μ M	DMSO	Sigma (# T7402 9
Nocodazole	6 mM	DMSO	Sigma (# M1404-10MG)
S-nitro-Blebbistatin	20 mM	DMSO	Cayman chemicals (# 856925-75-2-20 μ M)

5.1.8 Commercial Kits

Table 7: List of commercial kits used in this study

Name	Source	Identifier
EndoFree Plasmid Maxi Kit	Qiagen	Cat# 12326
Amata™ Rat Neuron Nucleofector™ Kit	Lonza	Cat# VPG-1003
TMT10plex™ Reagent Set for Isobar Marking	Thermo Scientific	Cat# 90110
Streptavidin Resin	GenScript	Cat# L00353

5.1.9 Enzymes and DNA markers

Table 8: List of enzymes and DNA markers used in this study

Name	Source	Identifier
PhosSTOP™ phosphatase inhibitor cocktail tablets	Roche	Cat# 4906845001
cOmplete™ protease inhibitor cocktail tablets	Roche	Cat# 04693124001
PageRuler™ Prestained Protein Ladder, 10 to 180 kDa	Thermo Scientific	Cat# 26616

5.1.10 Main equipments

Table 9: List of main equipments used in this study

Device	Source
Nikon EclipseTi2 Confocal spinning disk microscope	Nikon (Tokyo, Japan)
Nikon Eclipse Ti Fluorescence Microscope	Nikon (Tokyo, Japan)
CoolSNAP HQ2camera	Roper Scientific (München, Germany)
Stereo microscope Olympus SZX16	Olympus (Tokyo, Japan)
Stereo microscope Zeiss Stemi 2000	Zeiss (Jena, Germany)
Inverted light microscope TELAVAL 31	Zeiss (Jena, Germany)
KL 1500 LCD SCHOTT	Schott (Mainz, Germany)
CO ₂ Incubator HERACELL VIOS 160i	Thermo Scientific™ (Waltham, USA)
Cryostat Leica CM3050 S	Leica Biosystems (Nußloch, Germany)
Sterile Hood MSC-ADVANTAGE	Thermo Scientific (Waltham, USA)
Freezer -20°C/-80°C	Liebherr (Bieberbach, Germany)
Microcentrifuge SD 220VAC	Carl Roth (Karlsruhe, Germany)
Nanodrop ND-1000 Spectrophotometer	Peqlab (Erlangen, Germany)
Electro Square Porator ECM 830	BTX (Holliston Massachusetts, USA)
Tweezertrodes electrodes	BTX (Holliston Massachusetts, USA)
Pierce™ Centrifugation Columns-Screw Cap 69705	Thermo Scientific™ (Waltham, USA)
Amicon Ultra-0.5 Centrifugal Filter Unit UFC500396	Millipore (Burlington, Massachusetts, USA)

5.2. Method

5.2.1 RNA interference and fluorescent protein constructs

The Venus (pCAGIG), mCherry (pCAGIG), Farnesylated-GFP, pNeuroD-GFP, control shRNA, Cep 120 shRNA, and Cep 120-GFP plasmids have been previously reported (Xuecai Ge et al., 2010; de Anda et al., 2010; de Anda et al., 2016). tDimer (pAAV-CAG-tDimer) was kindly

provided by Thomas Oertner (ZMNH, UKE). pBrain-GFP-shGL2 was a gift from Stephen Royle (Addgene plasmid # 60004; RRID: Addgene_60004 (Booth et al., 2011)). Actin-mCherry plasmid, a gift from Pirta Hotulainen (Minerva Foundation Institute for Medical Research, Helsinki, Finland) (Bertling et al., 2016).

The mMaroon1 (pcDNA3.1-mMaroon1) plasmid was provided by Michael Lin (Addgene plasmid#83840; RRID: Addgene_83840; doi: 10.1038/nmeth.4045.). mRuby2-Actin-C-18 was a gift from Michael Davidson (Addgene plasmid # 55889; RRID: Addgene_55889). PaGFP-UtrCH was a gift from William Bement (Addgene plasmid # 26738; RRID: Addgene_26738; DOI: 10.1002/cm.20226). mPA-GFP-MyosinIIA-C-18 was a gift from Michael Davidson (Addgene plasmid # 57149; RRID: Addgene_57149). pBa-KIF5C 559-tdTomato-FKBP was a gift from Gary Banker & Marvin Bentley (Addgene plasmid # 64211; RRID: Addgene_64211). mCherry- β -actin, mCherry- β -wt-actin, mCherry- β -Y53A- β -actin and GFP- β -Y53E- β -actin constructs were kindly provided by Pirta Hotulainen (Bertling et al 2016). Lifeact-RFP (Addgene plasmid mTagRFP-T-Lifeact-7 #54586) plasmids were kindly provided by F. Bradke (DZNE, Bonn).

5.2.2 Recombinant DNAs preparation

XL10-Gold* ultracompetent cells and BL21-CodonPlus (De3)-RIL, strains of *E.coli* were used to amplify the recombinant DNAs (mentioned in 5.2.1) following a standard protocol. Briefly the *E.coli* bacteria and the recombinant DNAs were mixed well and incubated for 15-20 min on ice followed by a heat-shock at 42°C for 90 sec. After that the mixture was cooled down on ice for a couple of minutes before seeding the transfected *E.coli* bacteria on ampicillin or kanamycin LB plates, depending on the antibiotic resistance gene in the vector, and grown overnight. Afterwards the pre-cultures were prepared by picking a single colony from the culture-plates and adding to LB medium (5 mL) in a sterile glass reaction tube containing ampicillin/kanamycin (final concentration 1:1000), let it grow at 37°C for 5-8 h with shaking. Then, the pre-cultured LB medium were added to a bigger falcon containing LB medium (350-400 mL) mixed with

ampicillin/kanamycin (final concentration 1:1000) and grown for overnight at 37°C with shaking. Then, LB culture was harvested by centrifuging at 6000 x g for 15 min at 4°C.

The recombinant DNAs were purified with the endoFree® Plasmid Maxi Kit following the instruction given by the manufacturer. Shortly, the harvested *E.coli* bacteria pellet was treated with several buffers to lysate the bacteria cells and get the recombinant DNA pellet. As a final step, the recombinant DNA pellet was dissolved in 30-50 µL (depending on the pellet size) TE buffer, which was pre-heated to 70°C, and 1 µL recombinant DNA-solution was diluted in TE buffer (1:10) to measure the final concentration with the Nanodrop, then stored at -20°C until further use.

5.2.3 In utero electroporation (IUE)

Pregnant C57BL/6 mice with E13 or E15 embryos were first administered with pre-operative analgesic, buprenorphine (0.1 mg/kg), by subcutaneous injection. After 30 min, mice were anesthetized with 4% isoflurane in oxygen (0.5-0.8 L/min) for induction and during surgery kept with 2–3% isoflurane in oxygen (0.5-0.8 L/min) for maintenance. Later, the uterine horns were exposed via abdominal incision and plasmids mixed with Fast Green (Sigma) were microinjected into the lateral ventricles of embryos. Five current pulses (50 ms pulse/950 ms interval) at 35 V for E15 were delivered across the heads of embryos via electrodes to direct the DNA constructions entering the ventricular zone to the targeted cortical area (Wang and Mei, 2013). After surgery, mice were kept in a warm environment and were provided with moist food containing post-operative analgesic, meloxicam (0.2-1 mg/kg), until they were euthanized for preparing either primary cortical cultures or cortical slices.

Here in this study, for the cep120-microtubule part, we introduced control or Cep120 shRNA or Cep120-GFP plasmids in combination with tDimer into brain cortices at E15, we used 1.5 mg/mL for shRNA (control or Cep120 shRNA), 1.2 mg/mL Cep120-GFP, 0.5 mg/mL of tDimer (for Figure 2-6).

And in the F-actin part, we included mCherry-β-actin, mCherry-Y53A-β-actin and GFP-Y53E-β-actin plasmids in combination with Venus or tDimer plasmids into brain cortices at E15. We

used 1 $\mu\text{g}/\mu\text{l}$ for the β -actin plasmids constructs and 0.5 $\mu\text{g}/\mu\text{l}$ of tDimer or Venus (for Figure 2-15).

5.2.4 Primary cell culture

5.2.4.1 Preparation of coverslips and chambers

Coverslips (12 mm, Carl Roth) were washed in 65% nitric acid with shaking vigorously in a tightly sealed container under a fume hood for 2 days. Later, the nitric acid was disposed of into a special container and the coverslips were rinsed 3 times in ddH₂O shortly to remove the residual acid. Afterwards, the coverslips were rinsed with shaking thoroughly in ddH₂O at least 5 times each 10 minutes. Following ddH₂O washing, coverslips were washed again with absolute ethanol, then placed on 3mm Whatman paper into a glass petri dish. The whole dish containing coverslips was sterilized at 200°C. Once use, the coverslips were pre-coated overnight with 1mg/ml Poly-L-Lysin (PLL, Sigma #P2636 100 mg) at 37°C in the incubator, the next day, coverslips were washed three times in a 24 well plate with 1x PBS and ready for use.

For dishes/tissue culture chambers (Sarstedt, for live imaging), make sure the cover growth area with enough 0,25 mg/ml PLL, place the dishes/chambers in a bigger Petri dish with an open water chamber (small petri dish) to create a moistened atmosphere and place into the incubator.

5.2.4.2 Rat primary hippocampal cell culture

Pregnant rats were anesthetized with CO₂/O₂, euthanized before taking the E18 embryos out from their uteri. Embryos were then decapitated, skulls were opened, brains were collected in petri dishes with 1xHBSS (free of Ca²⁺ and Mg²⁺, Invitrogen) on ice. Hemispheres were separated, meninges were carefully stripped away, and hippocampi were dissected on ice under a dissecting microscope and digested with Papain and DNase I (Worthington for 10 min at 37°C), then Papain digestion was stopped by adding DMEM + 10% FBS, then with 1xHBSS washed 2 to 3 times. Mechanical trituration was performed thoroughly but gently with a fire-polished Pasteur pipette (about 1mm in diameter) until cells were in suspension. Afterwards, cells were centrifuged down and washed with fresh 1xHBSS and counted with Trypan blue

ready for use. Then hippocampal cells were plated at a density of ~30 to 50 000 cells per coverslip directly onto PLL pre-coated glass coverslips or issue culture chambers (Sarstedt, for live imaging) in Neurobasal/B27 medium (Invitrogen) and were maintained in culture for 24 to 72 h or 7- 8 days at 37°C with 5% CO₂ before use.

5.2.4.3 Rat primary hippocampal cell transfection

Hippocampal cells were prepared as described in 5.2.4.2. Before plating, hippocampal cells were first performed using the Amaxa nucleofector system (Amaxa Kit, Lonza #VPG-1003) following the manufacturer's manual. Here actin-mRuby, mMarron1, PaGFP-UtrCH and PaGFP-MyosinIIA plasmids were applied, the final concentration for the Actin-mRuby, mMarron1, PaGFP-UtrCH and PaGFP-MyosinIIA was 1 µg. Empty pcDNA 3.1 was used to make up to 3 µg of DNA for 5 × 10⁶ cells per each transfection mix as the manufacturer recommendation. After electroporation, cells were plated on poly-L-lysine coated coverslips or tissue culture chambers (Sarstedt, for live imaging) in Neurobasal/B27 medium (Invitrogen) and were maintained in culture for 24 to 72 h or 7- 8 days at 37°C with 5% CO₂ before use. When cells had to be cultured for longer in vitro, 0.5 µM Ara-C was added on the 7th day in vitro (DIV7) to the media maintained up to the day needed to inhibit the growth of the glia cells (for Figure 2-13).

5.2.4.4 Mouse primary cortical culture

For cortical cultures, brain cortices transfected via IUE at E15 with plasmids in combination with tDimer or Venus alone were used (mentioned in 5.2.3). Two days later pregnant mice were anesthetized with CO₂/O₂, euthanized before taking the E17.5 embryos out from their uteri. Embryos were then decapitated, skulls were opened, brains were collected in petri dishes with Hibernate-E medium (Invitrogen) on ice. Hemispheres were separated, meninges were carefully stripped away, and cortices were dissected on ice. Transfected (fluorescent) cortical regions were identified and dissected on ice under a stereo microscope (Olympus SZX16) equipped with a UV light source. The isolated cortical regions were first incubated in HBSS (Invitrogen) with papain and DNase (Worthington) for 10 min at 37°C neurons and then

trituated. The cells were then pelleted and washed with fresh HBSS before they were plated on poly-L-lysine coated coverslips or tissue culture chambers (Sarstedt, for live-imaging) in Neurobasal/B27 medium (Invitrogen), maintained in culture for 48 to 72 h at 37°C with 5% CO₂ before use.

5.2.5 Pharmacological treatment

Refer to the pharmacological manipulation, in the Cep120-microtubule part, rat hippocampal or mouse cortical neurons in culture were treated with CytoD (final concentration 2 mM; Sigma) or Taxol (final concentration 5 nM) either at the time of plating (at 0 h) or ~30 h later. Mouse cortical neurons were treated for 30 min with 6 mM Nocodazole at ~48 h after plating. Afterwards, cells were fixed after 48 or 72 h in culture with 4% PFA (including 4% sucrose) for immunostaining.

As for the somatic F-actin part, CytoD treatment (2 μM): for data shown in Figure 2-19G, H and I, hippocampal cells were treated with at DIV1 (14 to 18 h after plating), for 60 or 90 min, then washed out and fixed later. S-nitro-Blebbistatin treatment (20 μM): for photoactivation experiments shown in Figure 2-10D, E; Figure 2-11B, C and D, DIV1 neurons (14 to 18 h old) were treated for 15 to 75 min; and for neurons shown in Figure 2-14A-D, which were treated at DIV1 (24 h old) and fixed 48 h later (at DIV3). Taxol treatment (5 nM): for data shown in Figure 2-17H and J, neurons were treated at the time of plating (at 0 h), fixed 5 h later; for data shown in Figure 2-17F, G and I, Figure 2-18B and D, neurons were treated at DIV1 (24 h old), fixed at DIV2 (48 h after plating). Nocodazole treatment (6 μM): for data shown in Figure 2-19, DIV1 (24 h old) neurons were treated for 30 min and fixed with 4% PFA for 2 min and with 100% Methanol (pre-chilled at -20°C) for 3 minutes.

5.2.6 Photoactivation experiments

5.2.6.1 Photoactivation setups

Photoactivation experiments of PaGFP-UtrCH and PaGFP-MyosinIIA were performed in the soma of primary rat hippocampal cells using either the iLAS2-Visitron setup (Figure 2-8, Figure 2-10B, D, E and Figure 2-11, described earlier in Meka et al. 2019) or NIKON FRAP setup.

On the iLAS2-Visitron setup the time-lapses were with imaged with a 100x TIRF objective (Nikon, ApoTIRF 100X oil (NA 1.49). Emission light was collected through a quad-band filter (Chroma, 405/488/561/640) followed by a filter wheel with filters for GFP (Chroma, 525/50), RFP (Chroma, 595/50), and Cy5 (Chroma, 700/75). Multichannel images were acquired sequentially with an Orca flash 4.0LT CMOS camera (Hamamatsu) controlled by VisiView software (Visitron Systems GmbH).

On the NIKON FRAP system, images were taken with PLAN APO 60X oil (NA 1.42) objectives on a Nikon EclipseTi2 inverted microscope equipped with a SPECTRA X Light Engine as an LED light source (Lumencor® from AHF analysentechnik AG, Germany), and a digital CMOS camera ORCA-Flash4.0 V3 C13440-20CU (Hamamatsu, Japan) controlled with NIS-Elements software.

During the time-lapse imaging, cells plated on 4 well culture chambers (Sarstedt or Ibidi) were kept in an acrylic chamber at 37°C in 5% CO₂. To identify transfected neurons prior to photoactivation, the cultures used for this experiment were always co-transfected with Actin-mRuby or mMaroon1 together with PaGFP-tagged constructs. To illustrate the neuronal morphology, an image with Actin-mRuby or mMaroon1 signal was captured before the photoactivation with 561 nm or 640 nm lasers, respectively.

Photoactivation was achieved using the 405 nm laser with 50% power (iLAS2 system) or 10% power (NIKON FRAP system). The diameter of 405 nm laser illuminated area for all the cells used for the analysis was either 5.239 µm on iLAS2 system or 5.239 µm on NIKON FRAP system; the 405 nm laser dwell time was 2 ms per pixel (1 pixel = 65 nm) on iLAS2 system or 600 µs per pixel (1 pixel = 73.4 nm) on NIKON FRAP system. Cells were illuminated with 488 nm 5% laser on iLAS2 system or 10% LED power on NIKON FRAP system for 800 ms to record one frame. Three frames were imaged before, and 150 or 200 frames were recorded after the photoactivation.

5.2.6.2 Photoactivation analysis

In every time lapse, photobleaching was checked and, if applicable, corrected with Exponential Bleach (Fiji-ImageJ, NIH). For analysis, the area of photoactivation at either soma was selected as a ROI. Further ROIs were selected in the corresponding compartments (soma, neurite tip). For the soma, we selected at the region of photoactivation, for growth cones/neurite tips we selected an area, which remains within the central region, even during eventual movement. If the growth cone was moving too much, the region was cropped and aligned via ImageJ's template matching plugin to avoid moving artefacts. Background/autofluorescence signal calculated from the average gray values of the first three frames that were imaged before the photoactivation, these values were then subtracted from the gray values after photoactivation to plot the graphs. For plots, 0 was considered as the first frame after photoactivation. Average gray values over time were measured via the Time series Analyzer plugin. Initial gray values in the photoconverted area were normalized to 1; gray values in the "receiving" compartments (neurite tips) were normalized to fractions of initial gray value at the photoconverted area (in the soma). The ratio of the average neurite tip intensity to the average soma intensity was plotted over time for different experimental groups. For the decay of signal in the photoconverted area in the soma $t_{1/2}$ was determined via Graph-Pad's fitted one-phase exponential decay equation.

5.2.7 Mouse cortical slices

Here We introduced Cep120 shRNA or control shRNA or Cep120-GFP plasmids in combination with tDimer plasmid into brain cortices at E15. The brains from E19 embryos were collected as described in 5.2.3. The brains were kept whole and post-fixed in 4% paraformaldehyde (PFA) overnight at 4 °C, then moved into 30% sucrose solution (in 1xPBS) until they were completely sunk. Afterwards the brains were embedded in Tissue Tek® O.C.T compound on dry ice and stored at -80°C until they were sectioned into 60 µm slices using a cryostat and transferred onto slides.

5.2.8 Immunofluorescence

Rat hippocampal or mouse cortical neurons grown on coverslips were fixed either with 4% PFA at 37°C for 10 min or with 4% PFA at 37°C for 2 min, followed by 3 min ice-cold methanol incubation at -20°C. Cells were then permeabilized with 0.5% Triton X-100 for 10 min. Non-specific binding was blocked by incubation with 5% donkey serum in PBS for 60 min at RT (room temperature), followed by the specific primary antibody (mentioned in 5.1.5.1) incubation of 180 min at RT or overnight at 4°C, and then washed with 1x PBS for 3 times per 4 minutes. Afterwards, coverslips were incubated with respective anti-mouse or anti-rabbit Alexa Fluor 488 or 568 or 647 secondary antibodies (mentioned in 5.1.5.2), along with Phalloidin-488 (1:120) to stain F-actin (only on PFA-fixed cells) and/or Hoechst dye (1:10,000) to stain for nuclei for 60 min at RT followed by three washing steps as described above. Coverslips were mounted onto slides using Fluoromount-G® and dried at RT protected from light.

5.2.9 Western blotting

Rat cortical neurons were treated with 2 µM CytoD and 5 nM Taxol either at the time of plating (0 h) or ~30 h later and harvested 18h later, and lysed in RIPA buffer (50 mM Tris-HCl pH 7.4, 150 mM NaCl, 1 mM EGTA, 1% NP-40, 0.25% sodium deoxycholate, supplemented with proteinase inhibitor (Roche Mini Complete EDTA Free, Roche 11836170001) and phosphatase inhibitor (Phospho STOP, Roche 4906845001). Protein concentration in the samples was determined by the Pierce™ BCA Protein Assay Kit (Thermo Fisher Scientific, 23225) according to the manufacturer's instructions. 20 µg protein was resolved on 10-15% sodium dodecyl sulfate (SDS) polyacrylamide Tris-glycine gradient gel at 30 mA/gel. Proteins from the polyacrylamide gel were transferred to a PVDF membrane (Millipore) with wet transfer method (Gels were electrophoresed at 35 V overnight at 4°C). The total amount of protein on the membranes were determined by Revert™ 700 Total ProteinStain for Western blot normalization Licor (926-11010) according to the manufacturer's instructions.

Membranes were blocked in TBS-Tween20 0.1% with 5% BSA, or with 5% skim milk powder according to the antibody's datasheet instructions for 1 h at room temperature (RT), followed

by overnight incubation with primary antibodies on a shaker at 4°C (mentioned in 5.1.5.1). Then membranes were washed for 30 min in 0.1% TBS-Tween20 and incubated for 2 h at RT with the respective horseradish peroxidase conjugated anti-IgG secondary antibodies (mentioned in 5.1.5.2) and then washed for 30 min in TBS-Tween20 0.1%. Afterwards, immunoreactivity signals on the membranes were visualized by enhanced chemiluminescence NTAS, ChemoStar, ECL Imager.

Western blots were analyzed using Fiji software. Proteins of interest were normalized to the total protein loading intensity or to its respective total protein intensity in the same lane after membrane stripping in a buffer containing (62.5 mM Tris-HCl pH 6.8, 2% SDS and 0.1 M 2-b Mercaptoethanol) for 10 min at 50-60°C with gentle shaking under safety hood and redevelopment.

5.2.10 Image acquisition

5.2.10.1 Epifluorescence imaging

Imaging was taken on an inverted Nikon microscope (Eclipse, Ti) with a 60X oil immersion objective (NA 1.4), light intensity of each channel was set at 1, with an exposure time of 100-900 ms for all the fluorophores except for Hoechst dye (5 ms). Images were captured with a CoolSNAP HQ2camera (Roper Scientific) using NIS-Elements AR software (version 4.20.01 from NikonCorporation).

5.2.10.2 STED microscopy and deconvolution

All STED z-stacks were acquired by a Leica TCS SP8 gated STED system (Leica microsystems, Mannheim, Germany) equipped with a pulsed 775 nm depletion laser and a pulsed white light laser (WLL) for excitation. For acquiring images, either a Leica Objective HCAPO CS2 1003/1.40 Oil or a Glycerol objective (*Leica*, HC APO 93x/1.30 GLYC motCORR) were used.

Rat hippocampal neurons co-labelled with Primary antibodies as described in 5.2.8-mouse anti-AcetyTub; rat anti- α -tubulin; mouse anti-PolyGluTub; rat anti-tryosinated tubulin (YL1/2), followed by species specific secondary antibodies, goat anti-mouse IgG STAR 580; goat anti-

rat IgG STAR RED; donkey anti-sheep IgG STAR RED, were embedded in Mowiol or Abberior liquid Mount and activated via the WLL at 640, 561 and 488 nm, respectively. Emission was acquired between 650 and 710 nm for Abberior Star RED and 580–620 nm for Abberior Star 580 and 500-530 nm for AF 488. Abberior Star RED and Star 580 were depleted with 50% and 100% with 775 nm depletion laser, respectively. The detector time gates for both channels were set to 0.5-6 ns. The imaging format for all images was set to 2048 x 2048 and an optical zoom of 3 resulted in a pixel size for oil: x/y 18,9 nm, for glycerol: x/y 20,4 nm. Z spacing was set to 120 nm or 160 nm. Scan speed was set to 600 lines per second and 8-times line averaging was applied. Confocal overview images were acquired with the same objective, same optical settings but less zoom, less averaging and less excitation power.

Deconvolution of STED z-stacks were done with Huygens Professional (Scientific Volume Imaging, Hilversum, The Netherlands). Within the Deconvolution wizard, images were subjected to automatic background correction (lowest value method), Signal-to-noise ratio was set to 15 for both channels and the Optimized iteration mode of the CMLE was applied until the algorithm reached 25 iteration steps.

5.2.10.3 Confocal spinning disk imaging

Images were taken on with 10X and 60X oil (NA 1.42) objective on a Nikon EclipseTi2 inverted spinning disk confocal (X-Light V2 L-FOV from CrestOptics S.p.A. Italy) microscope equipped with a SPECTRA X Light Engine as an LED light source (Lumencor® from AHF analysentechnik AG, Germany), and a digital CMOS camera ORCA-Flash4.0 V3 C13440-20CU (Hamamatsu, Japan) controlled with NIS-Elements software. LED power for 405, 488, 568 and 647 channels were set to 10%, with an exposure time ranging between 100-400 ms for all the fluorophores except for Hoechst dye (10 ms). Optical configuration settings were set the same between the experimental groups that were compared for analysis. For 60X z series images with a step size of 300 nm for primary neurons.

5.2.11 Image analysis

5.2.11.1 Fluorescent intensity measurement

Images acquired on STED or confocal spinning disk microscope were used for analysis. Images were loaded onto Fiji-ImageJ and z-projection (sum slices) for the entire stacks was performed on the images. Using Fiji-ImageJ, soma region was carefully delineated and integrated density in the soma (soma area * mean intensity) was measured. For background correction, mean intensity (background mean intensity) was obtained from the neighboring region (out of the cell). Using the following equation, we obtained the corrected values. $\text{corrected value} = \text{integrated density in the soma} - (\text{background mean intensity} * \text{soma area})$.

5.2.11.2 Fluorescence signal area measurement

STED images were loaded onto Fiji-ImageJ and z-projection (Maximum intensity projections) for the stacks were created and a threshold applied by using the default setting, the min and max values were adjusted to ensure the thresholding of the fluorescent signal in the respective channels to obtain area of fluorescence signal. Soma area is carefully delineated, and area of fluorescence signal was then normalized to the soma area.

5.2.11.4 Axonal phenotype analysis

Epifluorescence 60x oil objective images of Tau1 immunostained rat hippocampal neurons were used. Images were loaded onto Fiji-ImageJ and Tau1 positive gradients were manually quantified (for Figure 2-5).

5.2.11.5 Neurite analysis (intensity, length and number)

The mean intensity value of AcetyTub in the soma for STED images was measured using Fiji-ImageJ software as described above. Mouse cortical neurons transfected with tDimer together with control, Cep120-shRNA, Cep120-GFP, were used for neurite length and terminals analysis.

pY53 actin and AcetyTub intensity measurements in the neurite shaft: neurite shafts were traced with *segmented line* option and saved to the ROI manager in Fiji from which the total

intensity and length measurements were obtained. Ratio of the total intensities to length was performed to obtain normalized intensity values plotted in graphs.

Neurite length and neurite number analysis: neurites were traced with *segmented line* option and saved to the ROI manager in Fiji from which the length measurements were obtained. For each cell, length of all neurites, length of the longest neurite and length of other neurites were plotted. For neurite number analysis, total number of neurites per cell was obtained from the ROIs obtained above.

5.2.12 Quantification and statistical analysis

Statistical analysis was performed using the GraphPad Prism software versions 8 and 9. To compare means of two groups, data were first tested for normal distribution and when the data passed normality test, Student's t-test (two-tailed) was used, otherwise its nonparametric counterpart Mann-Whitney test was used to compare means of two groups. Asterisks *, **, *** and **** represent $P < 0.05$, 0.01 , 0.001 , and 0.0001 , respectively. Error bars in the graphs always represent standard error of mean.

5.2.13 Image processing

Linear adjustment of brightness and contrast was performed on images using Photoshop CS or Fiji - ImageJ.

6. References

- Abbi, S., and Guan, J.L. (2002). Focal adhesion kinase: protein interactions and cellular functions. *Histology and histopathology* *17*, 1163-1171.
- Ahmad, F.J., Joshi, H.C., Centonze, V.E., and Baas, P.W. (1994). Inhibition of microtubule nucleation at the neuronal centrosome compromises axon growth. *Neuron* *12*, 271-280.
- Allen, C., and Borisy, G.G. (1974). Structural polarity and directional growth of microtubules of *Chlamydomonas* flagella. *Journal of molecular biology* *90*, 381-402.
- Andersen, E.F., and Halloran, M.C. (2012). Centrosome movements in vivo correlate with specific neurite formation downstream of LIM homeodomain transcription factor activity. *Development (Cambridge, England)* *139*, 3590-3599.
- Andersen, S.S., and Bi, G.Q. (2000). Axon formation: a molecular model for the generation of neuronal polarity. *BioEssays : news and reviews in molecular, cellular and developmental biology* *22*, 172-179.

- Arimura, N., and Kaibuchi, K. (2007). Neuronal polarity: from extracellular signals to intracellular mechanisms. *Nature reviews Neuroscience* 8, 194-205.
- Audebert, S., Koulakoff, A., Berwald-Netter, Y., Gros, F., Denoulet, P., and Eddé, B. (1994). Developmental regulation of polyglutamylated alpha- and beta-tubulin in mouse brain neurons. *Journal of cell science* 107 (Pt 8), 2313-2322.
- Baas, P.W. (1999). Microtubules and neuronal polarity: lessons from mitosis. *Neuron* 22, 23-31.
- Baas, P.W., Black, M.M., and Banker, G.A. (1989). Changes in microtubule polarity orientation during the development of hippocampal neurons in culture. *The Journal of cell biology* 109, 3085-3094.
- Baas, P.W., Rao, A.N., Matamoros, A.J., and Leo, L. (2016). Stability properties of neuronal microtubules. *Cytoskeleton (Hoboken, NJ)* 73, 442-460.
- Baek, K., Liu, X., Ferron, F., Shu, S., Korn, E.D., and Dominguez, R. (2008). Modulation of actin structure and function by phosphorylation of Tyr-53 and profilin binding. *Proceedings of the National Academy of Sciences of the United States of America* 105, 11748-11753.
- Bahl, S., Ling, H., Acharige, N.P.N., Santos-Barriopedro, I., Pflum, M.K.H., and Seto, E. (2021). EGFR phosphorylates HDAC1 to regulate its expression and anti-apoptotic function. *Cell Death & Disease* 12, 469.
- Baillat, G., Moqrish, A., Castets, F., Baude, A., Bailly, Y., Benmerah, A., and Monneron, A. (2001). Molecular cloning and characterization of phocein, a protein found from the Golgi complex to dendritic spines. *Molecular biology of the cell* 12, 663-673.
- Banker, G. (2018). The Development of Neuronal Polarity: A Retrospective View. *The Journal of neuroscience : the official journal of the Society for Neuroscience* 38, 1867-1873.
- Barnes, A.P., and Polleux, F. (2009). Establishment of axon-dendrite polarity in developing neurons. *Annual review of neuroscience* 32, 347-381.
- Barnes, A.P., Solecki, D., and Polleux, F. (2008). New insights into the molecular mechanisms specifying neuronal polarity in vivo. *Current opinion in neurobiology* 18, 44-52.
- Basto, R., Lau, J., Vinogradova, T., Gardiol, A., Woods, C.G., Khodjakov, A., and Raff, J.W. (2006). Flies without centrioles. *Cell* 125, 1375-1386.
- Bennett, M.V., and Zukin, R.S. (2004). Electrical coupling and neuronal synchronization in the Mammalian brain. *Neuron* 41, 495-511.
- Benson, D.L., Watkins, F.H., Steward, O., and Banker, G. (1994). Characterization of GABAergic neurons in hippocampal cell cultures. *Journal of neurocytology* 23, 279-295.
- Bernstein, B.W., and Bamburg, J.R. (2010). ADF/cofilin: a functional node in cell biology. *Trends in cell biology* 20, 187-195.
- Bertling, E., Englund, J., Minkeviciene, R., Koskinen, M., Segerstråle, M., Castrén, E., Taira, T., and Hotulainen, P. (2016). Actin Tyrosine-53-Phosphorylation in Neuronal Maturation and Synaptic Plasticity. *The Journal of neuroscience : the official journal of the Society for Neuroscience* 36, 5299-5313.

- Betleja, E., Nanjundappa, R., Cheng, T., and Mahjoub, M.R. (2018). A novel Cep120-dependent mechanism inhibits centriole maturation in quiescent cells. *eLife* 7.
- Bito, H., Furuyashiki, T., Ishihara, H., Shibasaki, Y., Ohashi, K., Mizuno, K., Maekawa, M., Ishizaki, T., and Narumiya, S. (2000). A critical role for a Rho-associated kinase, p160ROCK, in determining axon outgrowth in mammalian CNS neurons. *Neuron* 26, 431-441.
- Bonnet, C., Boucher, D., Lazereg, S., Pedrotti, B., Islam, K., Denoulet, P., and Larcher, J.C. (2001). Differential binding regulation of microtubule-associated proteins MAP1A, MAP1B, and MAP2 by tubulin polyglutamylation. *The Journal of biological chemistry* 276, 12839-12848.
- Bornens, M. (2008). Organelle positioning and cell polarity. *Nature reviews Molecular cell biology* 9, 874-886.
- Boucher, D., Larcher, J.C., Gros, F., and Denoulet, P. (1994). Polyglutamylation of tubulin as a progressive regulator of in vitro interactions between the microtubule-associated protein Tau and tubulin. *Biochemistry* 33, 12471-12477.
- Bradke, F., and Dotti, C.G. (1997). Neuronal polarity: vectorial cytoplasmic flow precedes axon formation. *Neuron* 19, 1175-1186.
- Bradke, F., and Dotti, C.G. (1999). The role of local actin instability in axon formation. *Science (New York, NY)* 283, 1931-1934.
- Bradke, F., and Dotti, C.G. (2000a). Changes in membrane trafficking and actin dynamics during axon formation in cultured hippocampal neurons. *Microscopy research and technique* 48, 3-11.
- Bradke, F., and Dotti, C.G. (2000b). Differentiated neurons retain the capacity to generate axons from dendrites. *Current biology : CB* 10, 1467-1470.
- Brankatschk, M., and Dickson, B.J. (2006). Netrins guide *Drosophila* commissural axons at short range. *Nature neuroscience* 9, 188-194.
- Brouhard, G.J., and Rice, L.M. (2018). Microtubule dynamics: an interplay of biochemistry and mechanics. *Nature reviews Molecular cell biology* 19, 451-463.
- Burkel, B.M., von Dassow, G., and Bement, W.M. (2007). Versatile fluorescent probes for actin filaments based on the actin-binding domain of utrophin. *Cell motility and the cytoskeleton* 64, 822-832.
- Calderon de Anda, F., Gärtner, A., Tsai, L.H., and Dotti, C.G. (2008). Pyramidal neuron polarity axis is defined at the bipolar stage. *Journal of cell science* 121, 178-185.
- Camacho Leal Mdel, P., Sciortino, M., Tornillo, G., Colombo, S., Defilippi, P., and Cabodi, S. (2015). p130Cas/BCAR1 scaffold protein in tissue homeostasis and pathogenesis. *Gene* 562, 1-7.
- Cantley, L.C. (2002). The phosphoinositide 3-kinase pathway. *Science (New York, NY)* 296, 1655-1657.

- Cary, L.A., Han, D.C., Polte, T.R., Hanks, S.K., and Guan, J.L. (1998). Identification of p130Cas as a mediator of focal adhesion kinase-promoted cell migration. *The Journal of cell biology* *140*, 211-221.
- Cassimeris, L., and Spittle, C. (2001). Regulation of microtubule-associated proteins. *International review of cytology* *210*, 163-226.
- Catterall, W.A. (2000). From ionic currents to molecular mechanisms: the structure and function of voltage-gated sodium channels. *Neuron* *26*, 13-25.
- Chen, X., and Macara, I.G. (2005). Par-3 controls tight junction assembly through the Rac exchange factor Tiam1. *Nature cell biology* *7*, 262-269.
- Ciani, L., and Salinas, P.C. (2007). c-Jun N-terminal kinase (JNK) cooperates with Gsk3beta to regulate Dishevelled-mediated microtubule stability. *BMC cell biology* *8*, 27.
- Conde, C., and Cáceres, A. (2009). Microtubule assembly, organization and dynamics in axons and dendrites. *Nature reviews Neuroscience* *10*, 319-332.
- Cook, B., Peterson, A., Woldman, W., and Terry, J. (2021). Neural Field Models: historical perspectives and recent advances.
- Costa, A.R., and Sousa, M.M. (2020). Non-Muscle Myosin II in Axonal Cell Biology: From the Growth Cone to the Axon Initial Segment. *Cells* *9*.
- Craig, A.M., and Banker, G. (1994). Neuronal polarity. *Annual review of neuroscience* *17*, 267-310.
- Cunningham, C.C., Leclerc, N., Flanagan, L.A., Lu, M., Janmey, P.A., and Kosik, K.S. (1997). Microtubule-associated protein 2c reorganizes both microtubules and microfilaments into distinct cytological structures in an actin-binding protein-280-deficient melanoma cell line. *The Journal of cell biology* *136*, 845-857.
- da Silva, J.S., and Dotti, C.G. (2002). Breaking the neuronal sphere: regulation of the actin cytoskeleton in neuritogenesis. *Nature reviews Neuroscience* *3*, 694-704.
- Da Silva, J.S., Medina, M., Zuliani, C., Di Nardo, A., Witke, W., and Dotti, C.G. (2003). RhoA/ROCK regulation of neuritogenesis via profilin Ila-mediated control of actin stability. *The Journal of cell biology* *162*, 1267-1279.
- de Anda, F.C., Meletis, K., Ge, X., Rei, D., and Tsai, L.H. (2010). Centrosome motility is essential for initial axon formation in the neocortex. *The Journal of neuroscience : the official journal of the Society for Neuroscience* *30*, 10391-10406.
- de Anda, F.C., Pollarolo, G., Da Silva, J.S., Camoletto, P.G., Feiguin, F., and Dotti, C.G. (2005). Centrosome localization determines neuronal polarity. *Nature* *436*, 704-708.
- Dedigama-Arachchige, P.M., and Pflum, M.K. (2016). K-CLASP: A Tool to Identify Phosphosite Specific Kinases and Interacting Proteins. *ACS chemical biology* *11*, 3251-3255.
- Dehmelt, L., Smart, F.M., Ozer, R.S., and Halpain, S. (2003). The role of microtubule-associated protein 2c in the reorganization of microtubules and lamellipodia during neurite initiation. *The Journal of neuroscience : the official journal of the Society for Neuroscience* *23*, 9479-9490.

- Del Río, J.A., González-Billault, C., Ureña, J.M., Jiménez, E.M., Barallobre, M.J., Pascual, M., Pujadas, L., Simó, S., La Torre, A., Wandosell, F., *et al.* (2004). MAP1B is required for Netrin 1 signaling in neuronal migration and axonal guidance. *Current biology : CB* *14*, 840-850.
- Delcommenne, M., Tan, C., Gray, V., Rue, L., Woodgett, J., and Dedhar, S. (1998). Phosphoinositide-3-OH kinase-dependent regulation of glycogen synthase kinase 3 and protein kinase B/AKT by the integrin-linked kinase. *Proceedings of the National Academy of Sciences of the United States of America* *95*, 11211-11216.
- Distel, M., Hocking, J.C., Volkmann, K., and Köster, R.W. (2010). The centrosome neither persistently leads migration nor determines the site of axonogenesis in migrating neurons in vivo. *The Journal of cell biology* *191*, 875-890.
- Doble, B.W., and Woodgett, J.R. (2003). GSK-3: tricks of the trade for a multi-tasking kinase. *Journal of cell science* *116*, 1175-1186.
- Donahoo, A.L., and Richards, L.J. (2009). Understanding the mechanisms of callosal development through the use of transgenic mouse models. *Seminars in pediatric neurology* *16*, 127-142.
- Dotti, C.G., and Banker, G.A. (1987). Experimentally induced alteration in the polarity of developing neurons. *Nature* *330*, 254-256.
- Dotti, C.G., Sullivan, C.A., and Banker, G.A. (1988). The establishment of polarity by hippocampal neurons in culture. *J Neurosci* *8*, 1454-1468.
- Dupraz, S., Hilton, B.J., Husch, A., Santos, T.E., Coles, C.H., Stern, S., Brakebusch, C., and Bradke, F. (2019). RhoA Controls Axon Extension Independent of Specification in the Developing Brain. *Current biology : CB* *29*, 3874-3886.e3879.
- Ems-McClung, S.C., Emch, M., Zhang, S., Mahnoor, S., Weaver, L.N., and Walczak, C.E. (2020). RanGTP induces an effector gradient of XCTK2 and importin α/β for spindle microtubule cross-linking. *The Journal of cell biology* *219*.
- Erck, C., Peris, L., Andrieux, A., Meissirel, C., Gruber, A.D., Vernet, M., Schweitzer, A., Saoudi, Y., Pointu, H., Bosc, C., *et al.* (2005). A vital role of tubulin-tyrosine-ligase for neuronal organization. *Proceedings of the National Academy of Sciences of the United States of America* *102*, 7853-7858.
- Etienne-Manneville, S., and Hall, A. (2002). Rho GTPases in cell biology. *Nature* *420*, 629-635.
- Etienne-Manneville, S., and Hall, A. (2003). Cdc42 regulates GSK-3 β and adenomatous polyposis coli to control cell polarity. *Nature* *421*, 753-756.
- Evans, L., Mitchison, T., and Kirschner, M. (1985). Influence of the centrosome on the structure of nucleated microtubules. *The Journal of cell biology* *100*, 1185-1191.
- Farina, F., Gaillard, J., Guérin, C., Couté, Y., Sillibourne, J., Blanchoin, L., and Théry, M. (2016). The centrosome is an actin-organizing centre. *Nature cell biology* *18*, 65-75.
- Feng, W., Wu, H., Chan, L.N., and Zhang, M. (2008). Par-3-mediated junctional localization of the lipid phosphatase PTEN is required for cell polarity establishment. *The Journal of biological chemistry* *283*, 23440-23449.

- Fivaz, M., Bandara, S., Inoue, T., and Meyer, T. (2008). Robust neuronal symmetry breaking by Ras-triggered local positive feedback. *Current biology* : CB 18, 44-50.
- Flynn, K.C., HELLAL, F., Neukirchen, D., Jacob, S., Tahirovic, S., Dupraz, S., Stern, S., Garvalov, B.K., Gurniak, C., Shaw, A.E., *et al.* (2012). ADF/cofilin-mediated actin retrograde flow directs neurite formation in the developing brain. *Neuron* 76, 1091-1107.
- Forscher, P., and Smith, S.J. (1988). Actions of cytochalasins on the organization of actin filaments and microtubules in a neuronal growth cone. *The Journal of cell biology* 107, 1505-1516.
- Fukata, Y., Itoh, T.J., Kimura, T., Ménager, C., Nishimura, T., Shiromizu, T., Watanabe, H., Inagaki, N., Iwamatsu, A., Hotani, H., *et al.* (2002). CRMP-2 binds to tubulin heterodimers to promote microtubule assembly. *Nature cell biology* 4, 583-591.
- Gao, F.B. (1998). Messenger RNAs in dendrites: localization, stability, and implications for neuronal function. *BioEssays* : news and reviews in molecular, cellular and developmental biology 20, 70-78.
- Gao, W.Q., and Hatten, M.E. (1993). Neuronal differentiation rescued by implantation of Weaver granule cell precursors into wild-type cerebellar cortex. *Science (New York, NY)* 260, 367-369.
- Garrard, S.M., Capaldo, C.T., Gao, L., Rosen, M.K., Macara, I.G., and Tomchick, D.R. (2003). Structure of Cdc42 in a complex with the GTPase-binding domain of the cell polarity protein, Par6. *The EMBO journal* 22, 1125-1133.
- Gärtner, A., Huang, X., and Hall, A. (2006). Neuronal polarity is regulated by glycogen synthase kinase-3 (GSK-3beta) independently of Akt/PKB serine phosphorylation. *Journal of cell science* 119, 3927-3934.
- Garvalov, B.K., Flynn, K.C., Neukirchen, D., Meyn, L., Teusch, N., Wu, X., Brakebusch, C., Bamberg, J.R., and Bradke, F. (2007). Cdc42 regulates cofilin during the establishment of neuronal polarity. *The Journal of neuroscience* : the official journal of the Society for Neuroscience 27, 13117-13129.
- Gerisch, G., Schroth-Diez, B., Müller-Taubenberger, A., and Ecke, M. (2012). PIP3 waves and PTEN dynamics in the emergence of cell polarity. *Biophysical journal* 103, 1170-1178.
- Goldmann, W.H. (2012). Mechanotransduction and focal adhesions. *Cell biology international* 36, 649-652.
- Goldstein, L.S., and Yang, Z. (2000). Microtubule-based transport systems in neurons: the roles of kinesins and dyneins. *Annual review of neuroscience* 23, 39-71.
- Gomis-Rüth, S., Wierenga, C.J., and Bradke, F. (2008). Plasticity of polarization: changing dendrites into axons in neurons integrated in neuronal circuits. *Current biology* : CB 18, 992-1000.
- Goodwin, P.R., Sasaki, J.M., and Juo, P. (2012). Cyclin-dependent kinase 5 regulates the polarized trafficking of neuropeptide-containing dense-core vesicles in *Caenorhabditis elegans* motor neurons. *The Journal of neuroscience* : the official journal of the Society for Neuroscience 32, 8158-8172.

- Götz, M., and Huttner, W.B. (2005). The cell biology of neurogenesis. *Nature reviews Molecular cell biology* 6, 777-788.
- Govek, E.E., Newey, S.E., and Van Aelst, L. (2005). The role of the Rho GTPases in neuronal development. *Genes & development* 19, 1-49.
- Gu, J., Tamura, M., Pankov, R., Danen, E.H., Takino, T., Matsumoto, K., and Yamada, K.M. (1999). Shc and FAK differentially regulate cell motility and directionality modulated by PTEN. *The Journal of cell biology* 146, 389-403.
- Guha, S., Patil, A., Muralidharan, H., and Baas, P.W. (2021). Mini-review: Microtubule sliding in neurons. *Neuroscience letters* 753, 135867.
- Guo, W., Jiang, H., Gray, V., Dedhar, S., and Rao, Y. (2007). Role of the integrin-linked kinase (ILK) in determining neuronal polarity. *Developmental biology* 306, 457-468.
- Hammond, J.W., Huang, C.F., Kaech, S., Jacobson, C., Banker, G., and Verhey, K.J. (2010). Posttranslational modifications of tubulin and the polarized transport of kinesin-1 in neurons. *Molecular biology of the cell* 21, 572-583.
- Hand, R., Bortone, D., Mattar, P., Nguyen, L., Heng, J.I., Guerrier, S., Boutt, E., Peters, E., Barnes, A.P., Parras, C., *et al.* (2005). Phosphorylation of Neurogenin2 specifies the migration properties and the dendritic morphology of pyramidal neurons in the neocortex. *Neuron* 48, 45-62.
- He, Y., Francis, F., Myers, K.A., Yu, W., Black, M.M., and Baas, P.W. (2005). Role of cytoplasmic dynein in the axonal transport of microtubules and neurofilaments. *The Journal of cell biology* 168, 697-703.
- Henty-Ridilla, J.L., Rankova, A., Eskin, J.A., Kenny, K., and Goode, B.L. (2016). Accelerated actin filament polymerization from microtubule plus ends. *Science (New York, NY)* 352, 1004-1009.
- Hilliard, M.A., and Bargmann, C.I. (2006). Wnt signals and frizzled activity orient anterior-posterior axon outgrowth in *C. elegans*. *Developmental cell* 10, 379-390.
- Hoogenraad, C.C., and Bradke, F. (2009). Control of neuronal polarity and plasticity--a renaissance for microtubules? *Trends in cell biology* 19, 669-676.
- Horiguchi, K., Hanada, T., Fukui, Y., and Chishti, A.H. (2006). Transport of PIP3 by GAKIN, a kinesin-3 family protein, regulates neuronal cell polarity. *The Journal of cell biology* 174, 425-436.
- Horton, A.C., and Ehlers, M.D. (2003). Neuronal polarity and trafficking. *Neuron* 40, 277-295.
- Huang, E.J., and Reichardt, L.F. (2003). Trk receptors: roles in neuronal signal transduction. *Annual review of biochemistry* 72, 609-642.
- Huber, K.M., Kayser, M.S., and Bear, M.F. (2000). Role for rapid dendritic protein synthesis in hippocampal mGluR-dependent long-term depression. *Science (New York, NY)* 288, 1254-1257.

- Huda, S., Soh, S., Pilans, D., Byrska-Bishop, M., Kim, J., Wilk, G., Borisy, G.G., Kandere-Grzybowska, K., and Grzybowski, B.A. (2012). Microtubule guidance tested through controlled cell geometry. *Journal of cell science* *125*, 5790-5799.
- Ikegami, K., Heier, R.L., Taruishi, M., Takagi, H., Mukai, M., Shimma, S., Taira, S., Hatanaka, K., Morone, N., Yao, I., *et al.* (2007). Loss of alpha-tubulin polyglutamylation in ROSA22 mice is associated with abnormal targeting of KIF1A and modulated synaptic function. *Proceedings of the National Academy of Sciences of the United States of America* *104*, 3213-3218.
- Inagaki, N., Chihara, K., Arimura, N., Ménager, C., Kawano, Y., Matsuo, N., Nishimura, T., Amano, M., and Kaibuchi, K. (2001). CRMP-2 induces axons in cultured hippocampal neurons. *Nature neuroscience* *4*, 781-782.
- Ishikawa, R., and Kohama, K. (2007). Actin-binding proteins in nerve cell growth cones. *Journal of pharmacological sciences* *105*, 6-11.
- Jacobs, T., Causeret, F., Nishimura, Y.V., Terao, M., Norman, A., Hoshino, M., and Nikolić, M. (2007). Localized activation of p21-activated kinase controls neuronal polarity and morphology. *The Journal of neuroscience : the official journal of the Society for Neuroscience* *27*, 8604-8615.
- Jacobson, C., Schnapp, B., and Banker, G.A. (2006). A change in the selective translocation of the Kinesin-1 motor domain marks the initial specification of the axon. *Neuron* *49*, 797-804.
- Jaffe, A.B., and Hall, A. (2005). Rho GTPases: biochemistry and biology. *Annual review of cell and developmental biology* *21*, 247-269.
- Jan, Y.N., and Jan, L.Y. (2003). The control of dendrite development. *Neuron* *40*, 229-242.
- Jang, H., Smith, I.N., Eng, C., and Nussinov, R. (2021). The mechanism of full activation of tumor suppressor PTEN at the phosphoinositide-enriched membrane. *iScience* *24*, 102438.
- Jiang, H., Guo, W., Liang, X., and Rao, Y. (2005). Both the establishment and the maintenance of neuronal polarity require active mechanisms: critical roles of GSK-3beta and its upstream regulators. *Cell* *120*, 123-135.
- Joseph, N., Al-Jassar, C., Johnson, C.M., Andreeva, A., Barnabas, D.D., Freund, S.M.V., Gergely, F., and van Breugel, M. (2018). Disease-Associated Mutations in CEP120 Destabilize the Protein and Impair Ciliogenesis. *Cell reports* *23*, 2805-2818.
- Kaech, S., and Banker, G. (2006). Culturing hippocampal neurons. *Nature protocols* *1*, 2406-2415.
- Kaneko, A., and Sankai, Y. (2014). Long-term culture of rat hippocampal neurons at low density in serum-free medium: combination of the sandwich culture technique with the three-dimensional nanofibrous hydrogel PuraMatrix. *PloS one* *9*, e102703.
- Kim, K.Y., Kovács, M., Kawamoto, S., Sellers, J.R., and Adelstein, R.S. (2005). Disease-associated mutations and alternative splicing alter the enzymatic and motile activity of nonmuscle myosins II-B and II-C. *The Journal of biological chemistry* *280*, 22769-22775.
- Kim, Y.T., Hur, E.M., Snider, W.D., and Zhou, F.Q. (2011). Role of GSK3 Signaling in Neuronal Morphogenesis. *Frontiers in molecular neuroscience* *4*, 48.

- Kishi, M., Pan, Y.A., Crump, J.G., and Sanes, J.R. (2005). Mammalian SAD kinases are required for neuronal polarization. *Science (New York, NY)* 307, 929-932.
- Kollins, K.M., Hu, J., Bridgman, P.C., Huang, Y.Q., and Gallo, G. (2009). Myosin-II negatively regulates minor process extension and the temporal development of neuronal polarity. *Developmental neurobiology* 69, 279-298.
- Komarova, Y., De Groot, C.O., Grigoriev, I., Gouveia, S.M., Munteanu, E.L., Schober, J.M., Honnappa, S., Buey, R.M., Hoogenraad, C.C., Dogterom, M., *et al.* (2009). Mammalian end binding proteins control persistent microtubule growth. *The Journal of cell biology* 184, 691-706.
- Konishi, Y., and Setou, M. (2009). Tubulin tyrosination navigates the kinesin-1 motor domain to axons. *Nature neuroscience* 12, 559-567.
- Koukouritaki, S.B., Vardaki, E.A., Papakonstanti, E.A., Lianos, E., Stournaras, C., and Emmanouel, D.S. (1999). TNF-alpha induces actin cytoskeleton reorganization in glomerular epithelial cells involving tyrosine phosphorylation of paxillin and focal adhesion kinase. *Molecular medicine (Cambridge, Mass)* 5, 382-392.
- Kovács, M., Tóth, J., Hetényi, C., Málnási-Csizmadia, A., and Sellers, J.R. (2004). Mechanism of blebbistatin inhibition of myosin II. *The Journal of biological chemistry* 279, 35557-35563.
- Kowalski, R.J., and Williams, R.C., Jr. (1993). Microtubule-associated protein 2 alters the dynamic properties of microtubule assembly and disassembly. *The Journal of biological chemistry* 268, 9847-9855.
- Kubota, K., Seno, T., and Konishi, Y. (2013). A low-density culture method of cerebellar granule neurons with paracrine support applicable for the study of neuronal morphogenesis. *Brain research* 1539, 15-23.
- Kundu, T., Dutta, P., Nagar, D., Maiti, S., and Ghose, A. (2021). Coupling of dynamic microtubules to F-actin by Fmn2 regulates chemotaxis of neuronal growth cones. *Journal of cell science* 134.
- Larcher, J.C., Boucher, D., Lazereg, S., Gros, F., and Denoulet, P. (1996). Interaction of kinesin motor domains with alpha- and beta-tubulin subunits at a tau-independent binding site. Regulation by polyglutamylation. *The Journal of biological chemistry* 271, 22117-22124.
- Lawlor, M.A., and Alessi, D.R. (2001). PKB/Akt: a key mediator of cell proliferation, survival and insulin responses? *Journal of cell science* 114, 2903-2910.
- Lefcort, F., and Bentley, D. (1989). Organization of cytoskeletal elements and organelles preceding growth cone emergence from an identified neuron in situ. *The Journal of cell biology* 108, 1737-1749.
- Li, R., and Gundersen, G.G. (2008). Beyond polymer polarity: how the cytoskeleton builds a polarized cell. *Nature reviews Molecular cell biology* 9, 860-873.
- Lilienberg, J., Hegyi, Z., Szabó, E., Hathy, E., Málnási-Csizmadia, A., Réthelyi, J.M., Apáti, Á., and Homolya, L. (2021). Pharmacological Modulation of Neurite Outgrowth in Human Neural Progenitor Cells by Inhibiting Non-muscle Myosin II. *Frontiers in cell and developmental biology* 9, 719636.

- Limouze, J., Straight, A.F., Mitchison, T., and Sellers, J.R. (2004). Specificity of blebbistatin, an inhibitor of myosin II. *Journal of muscle research and cell motility* 25, 337-341.
- Lin, C.H., Espreafico, E.M., Mooseker, M.S., and Forscher, P. (1996). Myosin drives retrograde F-actin flow in neuronal growth cones. *Neuron* 16, 769-782.
- Lin, Y.N., Wu, C.T., Lin, Y.C., Hsu, W.B., Tang, C.J., Chang, C.W., and Tang, T.K. (2013). CEP120 interacts with CPAP and positively regulates centriole elongation. *The Journal of cell biology* 202, 211-219.
- Liu, M., Nadar, V.C., Kozielski, F., Kozłowska, M., Yu, W., and Baas, P.W. (2010). Kinesin-12, a mitotic microtubule-associated motor protein, impacts axonal growth, navigation, and branching. *The Journal of neuroscience : the official journal of the Society for Neuroscience* 30, 14896-14906.
- Liu, X., Shu, S., Hong, M.S., Levine, R.L., and Korn, E.D. (2006). Phosphorylation of actin Tyr-53 inhibits filament nucleation and elongation and destabilizes filaments. *Proceedings of the National Academy of Sciences of the United States of America* 103, 13694-13699.
- Lowery, L.A., and Van Vactor, D. (2009). The trip of the tip: understanding the growth cone machinery. *Nature reviews Molecular cell biology* 10, 332-343.
- Lüders, J., and Stearns, T. (2007). Microtubule-organizing centres: a re-evaluation. *Nature reviews Molecular cell biology* 8, 161-167.
- Matov, A., Applegate, K., Kumar, P., Thoma, C., Krek, W., Danuser, G., and Wittmann, T. (2010). Analysis of microtubule dynamic instability using a plus-end growth marker. *Nature methods* 7, 761-768.
- Medeiros, N.A., Burnette, D.T., and Forscher, P. (2006). Myosin II functions in actin-bundle turnover in neuronal growth cones. *Nature cell biology* 8, 215-226.
- Meka, D.P., Kobler, O., Hong, S., Friedrich, C.M., Wuesthoff, S., Henis, M., Schwanke, B., Krisp, C., Schmuelling, N., Rueter, R., *et al.* (2022). Centrosome-dependent microtubule modifications set the conditions for axon formation. *Cell reports* 39, 110686.
- Meka, D.P., Scharrenberg, R., Zhao, B., Kobler, O., König, T., Schaefer, I., Schwanke, B., Klykov, S., Richter, M., Eggert, D., *et al.* (2019). Radial somatic F-actin organization affects growth cone dynamics during early neuronal development. *EMBO reports* 20, e47743.
- Ménager, C., Arimura, N., Fukata, Y., and Kaibuchi, K. (2004). PIP3 is involved in neuronal polarization and axon formation. *Journal of neurochemistry* 89, 109-118.
- Millard, T.H., Sharp, S.J., and Machesky, L.M. (2004). Signalling to actin assembly via the WASP (Wiskott-Aldrich syndrome protein)-family proteins and the Arp2/3 complex. *The Biochemical journal* 380, 1-17.
- Mitchison, T., and Kirschner, M. (1984). Dynamic instability of microtubule growth. *Nature* 312, 237-242.
- Moore, S.W., Correia, J.P., Lai Wing Sun, K., Pool, M., Fournier, A.E., and Kennedy, T.E. (2008). Rho inhibition recruits DCC to the neuronal plasma membrane and enhances axon chemoattraction to netrin 1. *Development (Cambridge, England)* 135, 2855-2864.

- Morgan, J.L., Dhingra, A., Vardi, N., and Wong, R.O. (2006). Axons and dendrites originate from neuroepithelial-like processes of retinal bipolar cells. *Nature neuroscience* 9, 85-92.
- Mori, T., Wada, T., Suzuki, T., Kubota, Y., and Inagaki, N. (2007). Singar1, a novel RUN domain-containing protein, suppresses formation of surplus axons for neuronal polarity. *The Journal of biological chemistry* 282, 19884-19893.
- Murthy, K., and Wadsworth, P. (2005). Myosin-II-dependent localization and dynamics of F-actin during cytokinesis. *Current biology : CB* 15, 724-731.
- Nakada, C., Ritchie, K., Oba, Y., Nakamura, M., Hotta, Y., Iino, R., Kasai, R.S., Yamaguchi, K., Fujiwara, T., and Kusumi, A. (2003). Accumulation of anchored proteins forms membrane diffusion barriers during neuronal polarization. *Nature cell biology* 5, 626-632.
- Nakata, T., and Hirokawa, N. (2003). Microtubules provide directional cues for polarized axonal transport through interaction with kinesin motor head. *The Journal of cell biology* 162, 1045-1055.
- Namba, T., Funahashi, Y., Nakamuta, S., Xu, C., Takano, T., and Kaibuchi, K. (2015). Extracellular and Intracellular Signaling for Neuronal Polarity. *Physiological reviews* 95, 995-1024.
- Neukirchen, D., and Bradke, F. (2011). Neuronal polarization and the cytoskeleton. *Seminars in cell & developmental biology* 22, 825-833.
- Nishimura, T., Kato, K., Yamaguchi, T., Fukata, Y., Ohno, S., and Kaibuchi, K. (2004). Role of the PAR-3-KIF3 complex in the establishment of neuronal polarity. *Nature cell biology* 6, 328-334.
- Nishimura, T., Yamaguchi, T., Kato, K., Yoshizawa, M., Nabeshima, Y., Ohno, S., Hoshino, M., and Kaibuchi, K. (2005). PAR-6-PAR-3 mediates Cdc42-induced Rac activation through the Rac GEFs STEF/Tiam1. *Nature cell biology* 7, 270-277.
- Nobes, C.D., and Hall, A. (1995). Rho, rac, and cdc42 GTPases regulate the assembly of multimolecular focal complexes associated with actin stress fibers, lamellipodia, and filopodia. *Cell* 81, 53-62.
- Noctor, S.C., Martinez-Cerdeno, V., Ivic, L., and Kriegstein, A.R. (2004). Cortical neurons arise in symmetric and asymmetric division zones and migrate through specific phases. *Nat Neurosci* 7, 136-144.
- Nogales, E. (2000). Structural insights into microtubule function. *Annual review of biochemistry* 69, 277-302.
- Oinuma, I., Katoh, H., and Negishi, M. (2007). R-Ras controls axon specification upstream of glycogen synthase kinase-3beta through integrin-linked kinase. *The Journal of biological chemistry* 282, 303-318.
- Oliva, A.A., Jr., Atkins, C.M., Copenagle, L., and Banker, G.A. (2006). Activated c-Jun N-terminal kinase is required for axon formation. *The Journal of neuroscience : the official journal of the Society for Neuroscience* 26, 9462-9470.

- Ori-McKenney, K.M., Jan, L.Y., and Jan, Y.N. (2012). Golgi outposts shape dendrite morphology by functioning as sites of acentrosomal microtubule nucleation in neurons. *Neuron* **76**, 921-930.
- Ozer, R.S., and Halpain, S. (2000). Phosphorylation-dependent localization of microtubule-associated protein MAP2c to the actin cytoskeleton. *Molecular biology of the cell* **11**, 3573-3587.
- Pichaud, F., Walther, R.F., and Nunes de Almeida, F. (2019). Regulation of Cdc42 and its effectors in epithelial morphogenesis. *Journal of cell science* **132**.
- Pierce, J.P., Mayer, T., and McCarthy, J.B. (2001). Evidence for a satellite secretory pathway in neuronal dendritic spines. *Current biology : CB* **11**, 351-355.
- Pilo-Boyl, P., Di Nardo, A., Mülle, C., Sassoè-Pognetto, M., Panzanelli, P., Mele, A., Kneussel, M., Costantini, V., Perlas, E., Massimi, M., *et al.* (2007). Profilin2 contributes to synaptic vesicle exocytosis, neuronal excitability, and novelty-seeking behavior. *The EMBO journal* **26**, 2991-3002.
- Pimm, M.L., and Henty-Ridilla, J.L. (2021). New twists in actin-microtubule interactions. *Molecular biology of the cell* **32**, 211-217.
- Pinheiro, E.M., and Gertler, F.B. (2006). Nervous Rac: DOCK7 regulation of axon formation. *Neuron* **51**, 674-676.
- Pollard, T.D., and Borisy, G.G. (2003). Cellular motility driven by assembly and disassembly of actin filaments. *Cell* **112**, 453-465.
- Pollard, T.D., and Cooper, J.A. (1986). Actin and actin-binding proteins. A critical evaluation of mechanisms and functions. *Annual review of biochemistry* **55**, 987-1035.
- Powell, S.K., Rivas, R.J., Rodriguez-Boulan, E., and Hatten, M.E. (1997). Development of polarity in cerebellar granule neurons. *Journal of neurobiology* **32**, 223-236.
- Prasad, B.C., and Clark, S.G. (2006). Wnt signaling establishes anteroposterior neuronal polarity and requires retromer in *C. elegans*. *Development (Cambridge, England)* **133**, 1757-1766.
- Rao, A.N., Falnikar, A., O'Toole, E.T., Morphew, M.K., Hoenger, A., Davidson, M.W., Yuan, X., and Baas, P.W. (2016). Sliding of centrosome-unattached microtubules defines key features of neuronal phenotype. *The Journal of cell biology* **213**, 329-341.
- Rao, A.N., Patil, A., Black, M.M., Craig, E.M., Myers, K.A., Yeung, H.T., and Baas, P.W. (2017). Cytoplasmic Dynein Transports Axonal Microtubules in a Polarity-Sorting Manner. *Cell reports* **19**, 2210-2219.
- Reed, N.A., Cai, D., Blasius, T.L., Jih, G.T., Meyhofer, E., Gaertig, J., and Verhey, K.J. (2006). Microtubule acetylation promotes kinesin-1 binding and transport. *Current biology : CB* **16**, 2166-2172.
- Riedl, J., Crevenna, A.H., Kessenbrock, K., Yu, J.H., Neukirchen, D., Bista, M., Bradke, F., Jenne, D., Holak, T.A., Werb, Z., *et al.* (2008). Lifeact: a versatile marker to visualize F-actin. *Nature methods* **5**, 605-607.

- Sakakibara, A., and Hatanaka, Y. (2015). Neuronal polarization in the developing cerebral cortex. *Frontiers in neuroscience* 9, 116.
- Sakakibara, A., Sato, T., Ando, R., Noguchi, N., Masaoka, M., and Miyata, T. (2014). Dynamics of centrosome translocation and microtubule organization in neocortical neurons during distinct modes of polarization. *Cerebral cortex (New York, NY : 1991)* 24, 1301-1310.
- Sampo, B., Kaech, S., Kunz, S., and Banker, G. (2003). Two distinct mechanisms target membrane proteins to the axonal surface. *Neuron* 37, 611-624.
- Sánchez-Huertas, C., Freixo, F., Viais, R., Lacasa, C., Soriano, E., and Lüders, J. (2016). Non-centrosomal nucleation mediated by augmin organizes microtubules in post-mitotic neurons and controls axonal microtubule polarity. *Nature communications* 7, 12187.
- Sanchez, A.D., and Feldman, J.L. (2017). Microtubule-organizing centers: from the centrosome to non-centrosomal sites. *Current opinion in cell biology* 44, 93-101.
- Schaefer, A.W., Kabir, N., and Forscher, P. (2002). Filopodia and actin arcs guide the assembly and transport of two populations of microtubules with unique dynamic parameters in neuronal growth cones. *The Journal of cell biology* 158, 139-152.
- Schwamborn, J.C., and Püschel, A.W. (2004). The sequential activity of the GTPases Rap1B and Cdc42 determines neuronal polarity. *Nature neuroscience* 7, 923-929.
- Scott, E.K., and Luo, L. (2001). How do dendrites take their shape? *Nature neuroscience* 4, 359-365.
- Seetharaman, S., and Etienne-Manneville, S. (2019). Microtubules at focal adhesions - a double-edged sword. *Journal of cell science* 132.
- Semenov, A., Goldsteins, G., and Castrén, E. (2006). Phosphoproteomic analysis of neurotrophin receptor TrkB signaling pathways in mouse brain. *Cellular and molecular neurobiology* 26, 163-175.
- Shelly, M., Cancedda, L., Heilshorn, S., Sumbre, G., and Poo, M.M. (2007). LKB1/STRAD promotes axon initiation during neuronal polarization. *Cell* 129, 565-577.
- Shelly, M., Cancedda, L., Lim, B.K., Popescu, A.T., Cheng, P.L., Gao, H., and Poo, M.M. (2011). Semaphorin3A regulates neuronal polarization by suppressing axon formation and promoting dendrite growth. *Neuron* 71, 433-446.
- Shelly, M., Lim, B.K., Cancedda, L., Heilshorn, S.C., Gao, H., and Poo, M.M. (2010). Local and long-range reciprocal regulation of cAMP and cGMP in axon/dendrite formation. *Science (New York, NY)* 327, 547-552.
- Shi, S.H., Cheng, T., Jan, L.Y., and Jan, Y.N. (2004). APC and GSK-3beta are involved in mPar3 targeting to the nascent axon and establishment of neuronal polarity. *Current biology : CB* 14, 2025-2032.
- Shi, S.H., Jan, L.Y., and Jan, Y.N. (2003). Hippocampal neuronal polarity specified by spatially localized mPar3/mPar6 and PI 3-kinase activity. *Cell* 112, 63-75.

- Slaughter, T., Wang, J., and Black, M.M. (1997). Microtubule transport from the cell body into the axons of growing neurons. *The Journal of neuroscience : the official journal of the Society for Neuroscience* 17, 5807-5819.
- Song, A.H., Wang, D., Chen, G., Li, Y., Luo, J., Duan, S., and Poo, M.M. (2009). A selective filter for cytoplasmic transport at the axon initial segment. *Cell* 136, 1148-1160.
- Sperber, B.R., Leight, S., Goedert, M., and Lee, V.M. (1995). Glycogen synthase kinase-3 beta phosphorylates tau protein at multiple sites in intact cells. *Neuroscience letters* 197, 149-153.
- Stepanova, T., Slemmer, J., Hoogenraad, C.C., Lansbergen, G., Dortland, B., De Zeeuw, C.I., Grosveld, F., van Cappellen, G., Akhmanova, A., and Galjart, N. (2003). Visualization of microtubule growth in cultured neurons via the use of EB3-GFP (end-binding protein 3-green fluorescent protein). *The Journal of neuroscience : the official journal of the Society for Neuroscience* 23, 2655-2664.
- Steward, O., and Schuman, E.M. (2001). Protein synthesis at synaptic sites on dendrites. *Annual review of neuroscience* 24, 299-325.
- Stiess, M., Maghelli, N., Kapitein, L.C., Gomis-Rüth, S., Wilsch-Bräuninger, M., Hoogenraad, C.C., Tolić-Nørrelykke, I.M., and Bradke, F. (2010). Axon extension occurs independently of centrosomal microtubule nucleation. *Science (New York, NY)* 327, 704-707.
- Stone, M.C., Roegiers, F., and Rolls, M.M. (2008). Microtubules have opposite orientation in axons and dendrites of *Drosophila* neurons. *Molecular biology of the cell* 19, 4122-4129.
- Südhof, T.C. (2008). Neuroligins and neurexins link synaptic function to cognitive disease. *Nature* 455, 903-911.
- Sütterlin, C., and Colanzi, A. (2010). The Golgi and the centrosome: building a functional partnership. *The Journal of cell biology* 188, 621-628.
- Szikora, S., Földi, I., Tóth, K., Migh, E., Vig, A., Bugyi, B., Maléth, J., Hegyi, P., Kaltenecker, P., Sanchez-Soriano, N., *et al.* (2017). The formin DAAM is required for coordination of the actin and microtubule cytoskeleton in axonal growth cones. *Journal of cell science* 130, 2506-2519.
- Tahirovic, S., and Bradke, F. (2009). Neuronal polarity. *Cold Spring Harbor perspectives in biology* 1, a001644.
- Takano, T., Funahashi, Y., and Kaibuchi, K. (2019). Neuronal Polarity: Positive and Negative Feedback Signals. *Frontiers in cell and developmental biology* 7, 69.
- Takano, T., Wu, M., Nakamuta, S., Naoki, H., Ishizawa, N., Namba, T., Watanabe, T., Xu, C., Hamaguchi, T., Yura, Y., *et al.* (2017). Discovery of long-range inhibitory signaling to ensure single axon formation. *Nature communications* 8, 33.
- Takenawa, T., and Miki, H. (2001). WASP and WAVE family proteins: key molecules for rapid rearrangement of cortical actin filaments and cell movement. *Journal of cell science* 114, 1801-1809.
- Tang, J., Yuan, F., Shen, X., Wang, Z., Rao, M., He, Y., Sun, Y., Li, X., Zhang, W., Li, Y., *et al.* (2019). Bridging Biological and Artificial Neural Networks with Emerging Neuromorphic

- Devices: Fundamentals, Progress, and Challenges. *Advanced materials* (Deerfield Beach, Fla) **31**, e1902761.
- Terman, J.R., and Kashina, A. (2013). Post-translational modification and regulation of actin. *Current opinion in cell biology* **25**, 30-38.
- Togo, T., and Steinhardt, R.A. (2004). Nonmuscle myosin IIA and IIB have distinct functions in the exocytosis-dependent process of cell membrane repair. *Molecular biology of the cell* **15**, 688-695.
- Toriyama, M., Kozawa, S., Sakumura, Y., and Inagaki, N. (2013). Conversion of a signal into forces for axon outgrowth through Pak1-mediated shootin1 phosphorylation. *Current biology : CB* **23**, 529-534.
- Toriyama, M., Shimada, T., Kim, K.B., Mitsuba, M., Nomura, E., Katsuta, K., Sakumura, Y., Roepstorff, P., and Inagaki, N. (2006). Shootin1: A protein involved in the organization of an asymmetric signal for neuronal polarization. *The Journal of cell biology* **175**, 147-157.
- Trivedi, N., Marsh, P., Goold, R.G., Wood-Kaczmar, A., and Gordon-Weeks, P.R. (2005). Glycogen synthase kinase-3beta phosphorylation of MAP1B at Ser1260 and Thr1265 is spatially restricted to growing axons. *Journal of cell science* **118**, 993-1005.
- Vicente-Manzanares, M., Ma, X., Adelstein, R.S., and Horwitz, A.R. (2009). Non-muscle myosin II takes centre stage in cell adhesion and migration. *Nature reviews Molecular cell biology* **10**, 778-790.
- von Stein, W., Ramrath, A., Grimm, A., Müller-Borg, M., and Wodarz, A. (2005). Direct association of Bazooka/PAR-3 with the lipid phosphatase PTEN reveals a link between the PAR/aPKC complex and phosphoinositide signaling. *Development (Cambridge, England)* **132**, 1675-1686.
- Votin, V., Nelson, W.J., and Barth, A.I. (2005). Neurite outgrowth involves adenomatous polyposis coli protein and beta-catenin. *Journal of cell science* **118**, 5699-5708.
- Wang, F., Kovacs, M., Hu, A., Limouze, J., Harvey, E.V., and Sellers, J.R. (2003). Kinetic mechanism of non-muscle myosin IIB: functional adaptations for tension generation and maintenance. *The Journal of biological chemistry* **278**, 27439-27448.
- Wells, D.G., Richter, J.D., and Fallon, J.R. (2000). Molecular mechanisms for activity-regulated protein synthesis in the synapto-dendritic compartment. *Current opinion in neurobiology* **10**, 132-137.
- Westermann, S., and Weber, K. (2003). Post-translational modifications regulate microtubule function. *Nature reviews Molecular cell biology* **4**, 938-947.
- Wilkes, O.R., and Moore, A.W. (2020). Distinct Microtubule Organizing Center Mechanisms Combine to Generate Neuron Polarity and Arbor Complexity. *Frontiers in cellular neuroscience* **14**, 594199.
- Wilson, C.A., Tsuchida, M.A., Allen, G.M., Barnhart, E.L., Applegate, K.T., Yam, P.T., Ji, L., Keren, K., Danuser, G., and Theriot, J.A. (2010). Myosin II contributes to cell-scale actin network treadmilling through network disassembly. *Nature* **465**, 373-377.

- Winckler, B., Forscher, P., and Mellman, I. (1999). A diffusion barrier maintains distribution of membrane proteins in polarized neurons. *Nature* *397*, 698-701.
- Witte, H., Neukirchen, D., and Bradke, F. (2008). Microtubule stabilization specifies initial neuronal polarization. *The Journal of cell biology* *180*, 619-632.
- Wloga, D., Joachimiak, E., and Fabczak, H. (2017). Tubulin Post-Translational Modifications and Microtubule Dynamics. *International journal of molecular sciences* *18*.
- Xie, Z., Moy, L.Y., Sanada, K., Zhou, Y., Buchman, J.J., and Tsai, L.H. (2007). Cep120 and TACCs control interkinetic nuclear migration and the neural progenitor pool. *Neuron* *56*, 79-93.
- Xu, R., and Du, S. (2021). Overexpression of Lifeact-GFP Disrupts F-Actin Organization in Cardiomyocytes and Impairs Cardiac Function. *Frontiers in cell and developmental biology* *9*, 746818.
- Yamada, M., and Hayashi, K. (2019). Microtubule nucleation in the cytoplasm of developing cortical neurons and its regulation by brain-derived neurotrophic factor. *Cytoskeleton (Hoboken, NJ)* *76*, 339-345.
- Yap, C.C., Wisco, D., Kujala, P., Lasiecka, Z.M., Cannon, J.T., Chang, M.C., Hirling, H., Klumperman, J., and Winckler, B. (2008). The somatodendritic endosomal regulator NEEP21 facilitates axonal targeting of L1/NgCAM. *The Journal of cell biology* *180*, 827-842.
- Yau, K.W., Schätzle, P., Tortosa, E., Pagès, S., Holtmaat, A., Kapitein, L.C., and Hoogenraad, C.C. (2016). Dendrites In Vitro and In Vivo Contain Microtubules of Opposite Polarity and Axon Formation Correlates with Uniform Plus-End-Out Microtubule Orientation. *The Journal of neuroscience : the official journal of the Society for Neuroscience* *36*, 1071-1085.
- Yoshimura, T., Arimura, N., Kawano, Y., Kawabata, S., Wang, S., and Kaibuchi, K. (2006). Ras regulates neuronal polarity via the PI3-kinase/Akt/GSK-3beta/CRMP-2 pathway. *Biochemical and biophysical research communications* *340*, 62-68.
- Yoshimura, T., Kawano, Y., Arimura, N., Kawabata, S., Kikuchi, A., and Kaibuchi, K. (2005). GSK-3beta regulates phosphorylation of CRMP-2 and neuronal polarity. *Cell* *120*, 137-149.
- Yu, P., Santiago, L.Y., Katagiri, Y., and Geller, H.M. (2012). Myosin II activity regulates neurite outgrowth and guidance in response to chondroitin sulfate proteoglycans. *Journal of neurochemistry* *120*, 1117-1128.
- Zhang, X.F., Schaefer, A.W., Burnette, D.T., Schoonderwoert, V.T., and Forscher, P. (2003). Rho-dependent contractile responses in the neuronal growth cone are independent of classical peripheral retrograde actin flow. *Neuron* *40*, 931-944.
- Zhao, B., Meka, D.P., Scharrenberg, R., König, T., Schwanke, B., Kobler, O., Windhorst, S., Kreutz, M.R., Mikhaylova, M., and Calderon de Anda, F. (2017). Microtubules Modulate F-actin Dynamics during Neuronal Polarization. *Scientific reports* *7*, 9583.
- Zheng, M., and Wang, P. (2021). Role of insulin receptor substance-1 modulating PI3K/Akt insulin signaling pathway in Alzheimer's disease. *3 Biotech* *11*, 179.

- Zhou, F.Q., Zhou, J., Dedhar, S., Wu, Y.H., and Snider, W.D. (2004). NGF-induced axon growth is mediated by localized inactivation of GSK-3beta and functions of the microtubule plus end binding protein APC. *Neuron* *42*, 897-912.
- Zmuda, J.F., and Rivas, R.J. (1998). The Golgi apparatus and the centrosome are localized to the sites of newly emerging axons in cerebellar granule neurons in vitro. *Cell motility and the cytoskeleton* *41*, 18-38.
- Zolessi, F.R., Poggi, L., Wilkinson, C.J., Chien, C.B., and Harris, W.A. (2006). Polarization and orientation of retinal ganglion cells in vivo. *Neural development* *1*, 2.
- Zoughlami, Y., van Stalborgh, A.M., van Hennik, P.B., and Hordijk, P.L. (2013). Nucleophosmin1 is a negative regulator of the small GTPase Rac1. *PloS one* *8*, e68477.
- Zumbrunn, J., Kinoshita, K., Hyman, A.A., and Näthke, I.S. (2001). Binding of the adenomatous polyposis coli protein to microtubules increases microtubule stability and is regulated by GSK3 beta phosphorylation. *Current biology : CB* *11*, 44-49.
- Zwetsloot, A.J., Tut, G., and Straube, A. (2018). Measuring microtubule dynamics. *Essays in biochemistry* *62*, 725-735.

7. Appendix








7.1 List of Abbreviation

RHCs:	Rat hippocampal cells
PNs:	Pyramidal neurons
RGCs:	Retinal ganglion cells
CGNs:	Cerebellar granule neurons
VZ:	Ventricular zone
SVZ:	Subventricular zone
IZ:	Intermediate zone
PSPs:	Postsynaptic potentials
CP:	Cortical plate
PI3K:	Phosphatidylinositol 3-kinase
PIP3:	Phosphatidylinositol-(3,4,5)-trisphosphate
PTEN:	Phosphatase and Tensin Homologue Deleted on Chromosome 10
PDK1:	Phosphoinositide 3-dependent protein kinase 1
ILK:	Integrin-linked kinase
PKB:	Protein kinase B
GSK3β:	Glycogen Synthase Kinase 3 β
CRMP2:	Collapsin-response mediator protein 2
APC:	Adenomatous polyposis coli
PAR3/6:	Partitioning defective 3/6
aPKC:	atypical protein kinase C
GTP:	Guanosine-5'-triphosphate
GDP:	Guanosine diphosphate
RhoA:	Ras homolog family member A
GAPs:	GTPase activating proteins
GEFs:	Guanine nucleotide-exchange
GDI:	Guanine nucleotide-dissociation
Cdc42:	Cell division cycle 42

Rac1:	Ras-related C3 botulinum toxin substrate 1
ROCK:	Rho-Associated Kinase
PAK:	p21-activated kinase
WASP:	Wiskott–Aldrich Syndrome protein
WAVE:	WASP-family verprolin-homologous protein
cAMP:	Cyclic adenosine monophosphate
cGMP:	Cyclic guanosine monophosphate
LKB1:	Liver kinase B1
DCC:	Colorectal cancer suppressor
UNC-6:	Laminin-related protein 6
BDNF:	Brain-derived neurotrophic factor
Sema3A:	Semaphorin 3A
Tiam1:	T-lymphoma and metastasis 1
F-actin:	Actin filaments
G-actin:	Globular actin
ATP:	Adenosine triphosphate
ADP:	Adenosine diphosphate
Arp2/3:	Actin-related protein 2/3
SADK:	Synapses of amphids defective kinase
ADF:	Actin depolymerizing factor
KIF3A:	Kinesin family member 3A
MT:	Microtubule
MTOC:	Microtubule organizing center
ncMTOCs:	Non-centrosome MTOCs
γTuRC:	γ-tubulin ring complex
MAPs:	Microtubule-associated proteins
PCM:	Pericentriolar material
PTMs:	Post-translational modifications

PolyGluTub:	Polyglutamylated tubulin
AcetyTub:	Acetylated tubulin
CytoD:	Cytochalasin D
STED:	Stimulated emission depletion microscopy
DMSO:	Dimethyl sulfoxide
EB3:	End-binding protein 3
TACC3:	Transforming Acidic Coiled-Coil Containing Protein 3
MLCK:	Myosin light chain kinase
PaGFP:	Photoactivatable green fluorescent protein
Y53:	Tyrosine-53
TrkB:	Tyrosine receptor kinase B
RLCs:	Regulatory light chains
ELCs:	Essential light chains
SUMO:	Small ubiquitin-like modifier
FAK:	Focal adhesion kinase
MS:	Mass spectrometry

7.2 List of hazardous substances

Substance	GHS symbol	Hazardous statements	Precautionary statements
Dimethyl sulfoxide (DMSO)	none	H227	none
Paraformaldehyde (PFA)		H228, H302 + H332, H315, H317, H318, H335, H351, H402	P210, P261, P280, P305 + P351 + P338
Ethanol		H225, H319	P210, P233, P240, P241, P242, P243, P264, P280, P303 + P361 + P353, P305 + P351 + P338, P337 + P313, P370 + P378, P403 + P235, P501
Nocodazole		H341, H361d	P281
Taxol (Paclitaxel)		H303, H315, H317, H318, H334, H335, H341, H361, H370	P260, P280, P305 + P351 + P338, P307 + P311
Cytochalasin D		H300, H361	P203, P264, P270, P280, P301+P316, P318, P321, P330, P405, P501
S-nitro-Blebbistatin	none	none	none
Triton X-100		H302, H313, H315, H318, H401, H410	P264, P270, P273, P280, P301 + P312 + P330, P302 + P352, P305 + P351 + P338 + P310, P312, P332 + P313, P391, P501
HEPES	none	none	none
Papain		H303, H315, H319, H334, H335	P261, P305 + P351 + P338, P342 + P311

7.3 List of Publications

Shuai Hong^{1#}, Durga Praveen Meka^{1##}, Oliver Kobler², Robin Scharrenberg¹, Carina Meta Friedrich¹, Birgit Schwanke¹, Melanie Richter¹ and Froylan Calderon de Anda^{1*\$}. **Actin Y53 Phosphorylation Regulates Somatic F-actin Radial Translocation to Promote Neuronal Polarization** (bioRxiv-preprint).

Melad Henis^{1*}, Tabitha Rücker¹, Robin Scharrenberg¹, Melanie Richter¹, Lucas Baltussen², **Shuai Hong**¹, Durga Praveen Meka¹, Birgit Schwanke¹, Nagammal Neelagandan^{3, 8}, Danie Daaboul², Nadeem Murtaza^{4, 6}, Christoph Krisp⁷, Sönke Harder⁷, Hartmut Schlüter⁷, Matthias Kneussel⁹, Irm Hermans-Borgmeyer¹⁰, Joris de Wit², Karun K. Singh^{4, 5}, Kent E. Duncan^{3, 11*} and Froylan Calderón de Anda ^{1*}. **The autism susceptibility kinase, TAOK2, phosphorylates eEF2 and modulates translation**. *Sciences Advances*, 2023.

Durga Praveen Meka¹, Oliver Kobler^{2#}, **Shuai Hong**^{1#}, Carina Meta Friedrich¹, Souhaila Wuesthoff¹, Melad Henis³, Birgit Schwanke¹, Christoph Krisp⁴, Nessa Schmuelling¹, René Rueter¹, Tabitha Ruecker¹, Ewelina Betleja⁵, Tao Cheng⁵, Moe R Mahjoub⁵, Peter Soba⁶, Hartmut Schlüter⁴, Eugenio F Fornasiero⁷, Froylan Calderon de Anda⁸. **Centrosome-dependent microtubule modifications set the conditions for axon formation**. *Cell Reports*, 2022.

Nadeem Murtaza¹, Annie A Cheng², Chad O Brown¹, Durga Praveen Meka³, **Shuai Hong**³, Jarryll A Uy⁴, Joelle El-Hajjar⁵, Neta Pipko⁵, Brianna K Unda², Birgit Schwanke³, Sansi Xing⁵, Bhooma Thiruvahindrapuram⁶, Worrawat Engchuan⁶, Brett Trost⁶, Eric Deneault⁷, Froylan Calderon de Anda³, Bradley W Doble⁸, James Ellis⁹, Evdokia Anagnostou¹⁰, Gary D Bader¹¹, Stephen W Scherer⁹, Yu Lu⁵, Karun K Singh¹². **Neuron-specific protein network mapping of autism risk genes identifies shared biological mechanisms and disease-relevant pathologies**. *Cell Reports*, 2022.

Shared authorship

Acknowledgement

First, I would like to express my sincere appreciation to my **direct supervisor Dr. Froylan Calderon de Anda** for giving me the opportunity to join his great group “Neuronal Development, ZMNH, UKE”, guiding me how to conceive and tackle scientific questions to “work smart”, despite the challenges the pandemic brought along. Great thanks to **Dr. Durga Praveen Meka**, the closest work partner, for his guidance and supervision, efforts in the STED imaging and somatic F-actin photoactivation work. Thanks to both who directed and enabled me to grow professionally.

I would like to thank my supervisor **Prof. Dr. rer. nat. Hartmut Schlüter** for the supervision and directions for this project. Sincere thanks for my thesis committee members.

I would like to express my gratitude and thanks to all members who help in this project, especially Dr. Melanie Richter for taking care of the mouse lines. Many thanks to Birgit Schwanke for all cell cultures and in the utero electroporation. Big thanks to Carina Meta Friedrich for working in actin-mutants part. Great thanks to Dr. Peter Soba and his team for the feedback and discussions we had in our meetings. Thanks to Tabitha Rücker for her help in productive conversations for the project and graduation. Thanks to Dr. Melad Henis for sharing his knowledge in western blots, Thanks to all members of the ZMNH, UKE and the members of the Ph.D. Program in the chemistry department of Hamburg University.

Of course, many thanks to the collaborators: Oliver Kobler for assisting STED imaging for this project. I would like to give my heartfelt thanks to Ole Johanns and Souhaila Wüsthoffand for helping me out especially at the beginning when I joined the group, for helping me settle down in the lab and in Hamburg.

Thanks so much to all my friends for your kindness and support. Special thanks to my family in China: **my parents, my brother** to whom I dedicate this thesis. Your love, encouragement, and support make this journey possible and enjoyable. You are always a big motivation that keeps me moving forward!

Declaration on oath

Hiermit versichere ich an Eides statt, die vorliegende Dissertation selbst verfasst und keine anderen als die angegebenen Hilfsmittel benutzt zu haben. Die eingereichte schriftliche Fassung entspricht der auf dem elektronischen Speichermedium. Ich versichere, dass diese Dissertation nicht in einem früheren Promotionsverfahren eingereicht wurde.

Ort, Datum: Hamburg, 20.12.2023

Unterschrift: Hong, Shuai